VERIFICATION AND VALIDATION OF THE MAXIMUM ENTROPY METHOD OF MOMENT RECONSTRUCTION OF ENERGY DEPENDENT NEUTRON FLUX

by

Douglas Spencer Crawford

A dissertation submitted to the faculty of
The University of Utah
in partial fulfillment of the requirements for the degree of

Doctor of Philosophy

in

Nuclear Engineering

Department of Civil and Environmental Engineering

The University of Utah

December 2012

The University of Utah Graduate School

STATEMENT OF DISSERTATION APPROVAL

The dissertation of **Douglas Spencer Crawford**

has been approved by the following supervisory committee members:

Terry A. Ring	, Chair	**27 April 2012** Date Approved
Dong-Ok Choe	, Member	**27 April 2012** Date Approved
Philip J. Smith	, Member	**27 April 2012** Date Approved
Sivaraman Guruswamy	, Member	**27 April 2012** Date Approved
Raj Rajamani	, Member	**27 April 2012** Date Approved

and by **Paul Tikalsky**, Chair of

the Department of **Civil and Environmental Engieering**

and by Charles A. Wight, Dean of The Graduate School.

ABSTRACT

The method of moments in conjunction with the maximum entropy method of reconstructing density distributions is applied to the energy dependent neutron diffusion equation to solve for neutron flux within a critical assembly. The energy dependent neutron diffusion equation (EDNDE) is converted into a moment equation which is solved analytically for a bare spherical critical assembly of pure ^{235}U in the radial direction. The normalized energy dependent neutron diffusion moments (NEDNDM) generated analytically is verified to NEDNDM, as calculated by Monte Carlo N Particle 5 version 1.40 (MCNP5) and Attila-7.1.0-beta version (Attila). The normalized NEDNDM are validated with the bare spherical critical assembly experiment, named GODIVA. The NEDNDM are then put into the maximum entropy method to solve for neutron flux within the two critical assemblies (100% ^{235}U and GODIVA) and the neutron flux is verified with MCNP5 and Attila and validated with GODIVA.

The analytic NEDNDM values fall between the NEDNDM from MCNP5 (lower bound) and Attila (upper bound). The error is taken to be relative to the Monte Carlo simulation. The error range is from 0% to 14%. The error range of the NEDNDM compared to NEDNDM from GODIVA is 0% to 24%. The verification and validation error of the maximum entropy method is 12% to 25% where MCNP5 is taken to be the comparison standard. The error range of the reconstructed flux validated with GODIVA is 0% to 10%. The error range of the neutron flux spectrum from MCNP5 compared to

GODIVA is 0%-20% and the Attila error range compared to the GODIVA is 0%-35%. The method of moments coupled with the maximum entropy method for reconstructing flux is shown to be a fast reliable method, compared to either Monte Carlo methods (MCNP5) or 30 multienergy group methods (Attila) and to GODIVA the bare sphere critical assembly experiment.

To my wife, Sherrie and my children, Dalton, Joseph, Sophia and Jennie, miracles still happen

TABLE OF CONTENTS

LIST OF TABLES

LIST OF FIGURES

ACKNOWLEDGMENTS

Great patience and encouragement were given through the last years of this educational process from my wife, Sherrie, and my children Dalton, Joseph, Sophia and Jennie. They have earned the reward education provides along with me. I would also like to acknowledge Dr Terry Ring for his guidance, time and service, especially when the process was filled with thorns. The research was enhanced by the donation of the software Attila-7.1.0 from Transpire INC and special thanks goes to them for this donation. I appreciate the help and explanation Tony Saad provided on the maximum entropy method. I would also like to thank the supervisory committee for their time serving as committee members.

CHAPTER 1

INTRODUCTION

Neutron transport phenomenon is challenging because of the complicated physics of neutron-isotope interactions called cross sections. Solving neutron transport phenomenon requires solving the neutron transport equation (NTE), which is a mathematical statement of the balance of neutrons in a given system subject to these cross sections. Orchestrating the cross sections in the NTE gives rise to two different viewpoints and methods to solve the neutron transport equation. The two general methods or viewpoints are; stochastic (statistic/probabilistic) and deterministic. The two methods have different qualities that are unique and appear to be opposing philosophies to each other, yet each method is effective and the two methods are supplementary to each other. Either viewpoint taken to solve the NTE leads to a valid solution. The main difference between the two is less solution fidelity and fast simulations (deterministic) or very long computational simulation times and a more accurate solution (stochastic). Even though there is a vast amount of complexity to solve the NTE by either method, amazingly the simplest and least sophisticated method to solve the NTE (one-speed neutron diffusion theory) provides insight into neutron transport phenomena (Duderstadt & Hamilton, 1976).

One-speed neutron diffusion theory is solvable analytically which makes it

attractive. Analytic solutions provide an equation to work with to understand the phenomena instead of a list of numbers with inherent numeric error. Analytic solutions to the neutron transport equation are very limited and can only be applied to a few cases (Lewis & Miller, 1993). The rest of the situations where the neutron transport equation must be solved require numerical methods. Some of the numerical methods that have become widely used to solve the NTE are: Monte Carlo, collision probability in lattice codes (the stochastic or probabilistic numerical methods) and the deterministic numerical methods which can be any combination of; S_N, P_N, method of characteristics and neutron diffusion theory. There are other numerical methods used to solve the NTE and this is not meant to be an exhaustive list of the numerical methods applied to neutron transport phenomena. The numerical methods are also broken down further into another broad classification; a continuous or discontinuous treatment of the energy variable. The discontinuous treatment of the energy variable is called multienergy group method or multigroup method, where the cross sections are broken into discrete energy groups and an energy dependent neutron diffusion equation (EDNDE) is written for each group carefully balancing the sources and sink terms to parallel a continuous treatment of the energy variable.

Limits to multigroup methods come from an assumed neutron spectrum that is used to solve for the group averaged cross sections and due to the discretization of the energy variable the solution does not capture the entire energy spectrum unless there is an enormous number of energy groups. The multigroup method requires tens to thousands of energy groups for accurate solutions and to increase fidelity in the solution one must increase the number of equations to solve simultaneously. The continuous Monte Carlo

methods overcome any deficiencies in the lack of fidelity in a multigroup approach but at a computational price, long computational times for accurate answers, even on today's computational platforms. Continuous Monte Carlo methods are not readily able to incorporate other physics effects where deterministic methods have been able to be fully coupled with other physics effects. Multiphysics methods can be fully implemented with deterministic neutron flux calculations to solve a much broader set of problems in reactor physics analysis.

The method of moments in conjunction with the maximum entropy method for reconstructing density distributions applied to the energy dependent neutron diffusion equation (EDNDE) is a blend of the two broad methods mentioned (stochastic and deterministic) as well as a continuous energy solution that could be quickly implemented into a multiphysics calculation. The simple cases modeled in the research, allow for moments 0-5 to be solved analytically which provide an equation to work with to reconstruct the neutron flux. The moments of a population density distribution provide averaged information, the mean number of neutrons and the mean energy of the neutrons, the variance of the distribution, etc. For most reactor physics analysis the neutron flux spectrum is needed, not the moments of a distribution, to determine nuclear reaction rates. The neutron flux can be treated as a distribution where the moments of the distribution, (probabilistic parameters) are solved for with a deterministic equation, EDNDE and then the neutron flux (the distribution) is reconstructed by the maximum entropy method.

Chapters 2 and 3 detail the theory of the method of moments and how the method of moments is verified and validated for the EDNDE by comparing normalized energy

dependent neutron moments (NEDNM) or moments to NEDNM from standard neutronics codes. The two standard codes are Monte Carlo N-Particle version 5 (MCNP5) (A General Monte Carlo N-Particle Transport Code-Version 5, 2008), a continuous energy stochastic method and Attila-7.1.0 beta version (Attila), a S_N, P_N and 30-energy group deterministic code. Chapter 4 explains the maximum entropy method and outlines the details for the validation and verification of the reconstructed neutron flux.

CHAPTER 2

VERIFICATION OF ANALYTIC ENERGY MOMENTS FOR THE ONE-DIMENTIONAL ENERGY DEPENDENT NEUTRON DIFFUSION EQUATION WITH MCNP5 AND ATTILA-7.1.0

Introduction

Solving for neutron energy distributions in nuclear reactors is complex and has been studied with various methods, mostly numeric in nature (Cho, February 2008). The main difficulty in solving for neutron distributions lies in solving the neutron transport equation, (Duderstadt & Hamilton, 1976, p. 114). The complexities and difficulties in trying to solve the transport equation arise because it depends on seven variables: energy of the neutrons (E), angle of neutron travel (θ and ϕ), space (x, y and z) and time (t). Simplifications are made to create a more easily solvable equation, but numerical methods are still necessary to solve for neutron fluxes and populations (Lewis & Miller, 1993).

The success of quadrature method of moments (QMOM) for particles is encouraging and has motivated the work presented here. QMOM has been shown to be an excellent method to solve partial integro-differential equations for particle population balances (Marchisio, Pikturna, & Fox, May 2003), aerosols (McGraw, 1997), and suspended particles in a fluid within computational fluid dynamics codes

(Bin-Wan & Ring, October 2006), (Marchisio, Virgil, & O., August 2003). The particle equations in question are similar mathematically to the EDNDE. The EDNDE is shown in equation 2.1. This is the first attempt to verify the method of moments as an accurate solution to EDNDE. Once the method of moments is proven successful, QMOM may be used to drastically reduce the computational burden in multiphysics problems that include neutron transport.

$$\frac{1}{v}\frac{\partial\phi(\vec{r},E,t)}{\partial t} - \nabla D(\vec{r},E)\nabla\phi(\vec{r},E,t) + \Sigma_t(\vec{r},E)\phi(\vec{r},E,t) = \int_0^\infty \Sigma_s(\vec{r},E\rightarrow \acute{E})\phi(\vec{r},\acute{E},t)\,d\acute{E} + \chi(E)\int_0^\infty \nu(\acute{E})\Sigma_f(\vec{r},\acute{E})\phi(\vec{r},\acute{E},t)\,d\acute{E} \quad \text{Equation 2.1}$$

The method of moments (MOM) approach solves for the moments of a distribution instead of the distribution itself. MOM can be considered to be a deterministic method to find stochastic parameters. The neutron flux can be treated as a probability density function (PDF), where the normalized moments provide the mean, variance, skewness and kurtosis (Kenny, 1947) of the flux so once the moments are solved for they can be put into the correct PDF to reproduce the flux. Mathematically the mean, variance, skewness and kurtosis (Casella & Berger, 2002) for the energy variable of the neutron flux are represented here where ϕ in equations 2.2-2.5 represents the energy dependent neutron flux $\phi(\vec{r},E,t)$:

$$mean = \frac{\int_0^\infty E*\phi dE}{\int_0^\infty \phi dE} \quad \text{Equation 2.2}$$

$$variance = \frac{\int_0^\infty E^2*\phi dE}{\int_0^\infty \phi dE} \quad \text{Equation 2.3}$$

$$skewness = \frac{\int_0^\infty E^3*\phi dE}{\int_0^\infty \phi dE} \quad \text{Equation 2.4}$$

$$kurtosis = \frac{\int_0^\infty E^4*\phi dE}{\int_0^\infty \phi dE} \quad \text{Equation 2.5}$$

The starting point for the analysis is the EDNDE, we have assumed diffusion theory is applicable and consider only the 1-D analytic case for a bare sphere. The same analysis can be applied to an infinite slab as well with similar results. Neutron diffusion theory is well documented in literature; (Duderstadt 1976, Foster 1977, Lamarsh 2001, Lewis1993 and Weinberg 1958) and is not discussed in detail here. An average angle of scatter for the neutrons (μ) is also assumed. This method does not assume any distribution to develop the cross sections or a specific spectrum for fission as a weighting value per energy group, which makes this method very unique. The method of moment's analysis does cut off at 10MeV since this value captures 100% of the fission spectrum and the neutron flux above that energy is very small and assumed to be negligible.

This paper is focused on deriving and comparing analytic moments from the energy dependent neutron diffusion equation (EDNDE) equation 2.1, with energy moments generated from MCNP5 (MCNP) and Attila 7.1.0-beta (Attila), which both are full neutron transport codes. This seems like an apples and oranges comparison, since this is a comparison between transport and analytic EDNDE moments, but it is necessary because the Monte Carlo method used in Los Alamos National Lab's MCNP (A General Monte Carlo N-Particle Transport Code-Version 5, 2008) software is widely accepted and respected among nuclear engineers and scientists for determining neutron multiplication factors, reaction rates and for benchmarking criticality calculations (INL NEA/NSC DOC(95)03, September 2009). Comparison of moments with Attila is important also because it is a multigroup transport code where 30 energy groups were used in the reported calculations. Table 2.1 shows the energy groups in the Attila 30 group library.

Table 2.1 Energy Group Structure for Attila-7.1.0-beta

Group #	Energy range MeV		Group #	Energy range MeV		Group #	Energy range MeV	
1	20	17	11	7.79	6.87	21	8.21E-1	2.35E-1
2	17	16	12	6.87	6.07	22	2.35E-1	6.74E-2
3	16	15	13	6.07	5.35	23	6.74E-2	1.93E-2
4	15	13.9	14	5.35	4.72	24	1.93E-2	5.53E-3
5	13.9	13.0	15	4.72	3.68	25	5.53E-3	3.54E-4
6	13.0	12.0	16	3.68	2.87	26	3.54E-4	2.26E-5
7	12.0	11.0	17	2.87	2.23	27	2.26E-5	3.47E-6
8	11.0	10.0	18	2.23	1.74	28	3.47E-6	6.25E-7
9	10.0	8.82	19	1.74	1.19	29	6.25E-7	1.24E-8
10	8.82	7.79	20	1.19	8.21E-1	30	1.24E-8	1.0E-11

Simplification of Energy Dependent Neutron Diffusion Equation

The starting point for formulation of an expression for analytical moments is equation 2.1. Equation 2.2.1is solved over the entire fission spectrum; which is well approximated to be from 0 to 10 MeV (Lamarsh, Introduction to Nuclear Reactor Theory, 1966). This analysis assumes steady state so the time dependent term, $\frac{1}{v}\frac{\partial\phi(\vec{r},E)}{\partial t}$ is set equal to zero. The system is homogenous so the energy dependent cross sections and diffusion coefficient depend on energy only. The EDNDE, after the assumptions are applied has the following form in equation 2.6.

$$-D(E)\nabla^2\phi(\vec{r},E)+\Sigma_t(E)\phi(\vec{r},E)=$$

$$\int_0^\infty \Sigma_s\left(E\rightarrow \acute{E}\right)\phi\left(\vec{r},\acute{E},t\right)d\acute{E}+\chi(E)\int_0^\infty \nu\left(\acute{E}\right)\Sigma\left(\acute{E}\right)\phi\left(\vec{r},\acute{E}\right)d\acute{E} \qquad \text{Equation 2.6}$$

The differential scattering cross section Σ_s (E'->E), is defined so that integrating from 0 to ∞, the probability of scattering into E is unity and yields Σ_s (E) as the result (Duderstadt & Hamilton, 1976). The entire population of neutrons is treated as one large energy group E, from 0 to 10MeV. The two assumptions change equation 2.6 into

equation 2.7. Equation 2.7 looks like the one-speed theory equation (Duderstadt & Hamilton, 1976, p. 295), except this equation retains the energy dependence of the cross sections over the range of interest, 0 to 10MeV where an overall energy dependent function F(E) will be derived for and then transformed into the moment form of the EDNDE.

$$-D(E)\nabla^2\phi(\vec{r},E)+\Sigma_a(E)\phi(\vec{r},E)=\nu(E)\Sigma_f(E)\phi(\vec{r},E) \qquad \text{Equation 2.7}$$

Derivation of F(E) for Energy Moments

An appropriate approximation to the energy dependency of the macroscopic cross sections and the diffusion coefficient is vital for any flux calculation; so a set of functions and constants have been carefully chosen so the energy dependent functionality is retained as much as possible and allow an analytic solution to be found. The macroscopic cross sections may generally be divided into three distinct regions: thermal, resonance and fast, and in this analysis the authors consider a 4^{th} region called the transition region and it spans from 2300eV to 0.9MeV. The reason for this subdivision is explained in more detail below.

The 1/v or $1/E^{1/2}$ law is a good approximation to the thermal region of many isotopes and found to be mathematically viable in foil activation (Morry & Williams, 1972). The cross section data referred to and in use for this paper are from the evaluated nuclear data files, ENDF information is found on the web at http://atom.kaeri.re.kr/ (Institute, 2000) and http://t2.lanl.gov/data/neutron7.html) (Lab, ENDF/B-VII Incident-Neutron Data, 2000). A summation of Breit-Wigner single level resonance formulas will be used to generate a function for the resonance region to capture the complicated energy

dependence. The functional piece that dominates the Breit-Wigner formulas in general is the $\frac{\text{Constant}_1}{(E-E_r)^2+\text{Constant}_2}$ term (Lamarsh, Introduction to Nuclear Reactor Theory, 1966, pp. 43-64). The transition to the fast region of the cross sections generally has a 1/E drop off rate (Weinberg & Wigner, 1958, p. 57) and the fast region (0.1MeV to 10MeV) has a $1/E^{5/2}$ with some broad resonances, which makes the fast region appear somewhat like a series of stair steps for $^{235}U\ \Sigma_f\ (E)$.

It is very difficult to fit an analytic function to the resonance region, and the number of resonance peaks makes writing a function for each peak even more daunting, but with patience a single level Breit-Wigner can be written for each peak and has been for this work. A summation of these single level Breit-Wigner resonance functions was assembled to provide a functional form, that when integrated over the function would provide correct values when compared to the resonance values from The Chart of the Nuclides and Isotopes 16th Edition (Lockheed Martin/ Knolls Atomic Power Laboratory, 2002). The simple functional approximations for the energy dependent cross sections are somewhat crude but "if we choose the group constants properly, even one-speed diffusion theory could give an accurate description of nuclear reactor behavior" (Duderstadt & Hamilton, 1976, p. 295).

The general functional relationships for D(E), $\nu(E)$, $\Sigma_f(E)$, $\Sigma_T(E)$, $\Sigma_S(E)$ and $\Sigma_a(E)$ with energy are incorporated into one function of energy F(E). The first step is to put all of the energy dependent functions together as one function of energy, labeled F(E), see equation 2.8. The second step is to take F(E) (equation 2.9) and determine the functional shapes of F(E) by using the ENDF-VII values arranged the same as F(E), called ENDF-F(E). This work only shows curve fits of F(E) for 100% ^{235}U. The third step is to curve fit

ENDF-F(E) with the appropriate function fit for the different energy ranges. The result of the curve fit of ENDF-F(E) is equation 2.16.

$$\nabla^2\phi(\vec{r},\mathrm{E}) + \left(\frac{\nu(\mathrm{E})\Sigma_\mathrm{f}(\mathrm{E})-\Sigma_\mathrm{a}(\mathrm{E})}{\mathrm{D(E)}}\right)\phi(\vec{r},\mathrm{E}) = 0 \qquad \text{Equation 2.8}$$

$$\mathrm{F(E)} = \frac{\nu(\mathrm{E})\Sigma_\mathrm{f}(\mathrm{E})-\Sigma_\mathrm{a}(\mathrm{E})}{\mathrm{D(E)}} = 3(\nu(E)\Sigma_\mathrm{f}(\mathrm{E}) - \Sigma_\mathrm{a}(\mathrm{E}))(\Sigma_\mathrm{t}(\mathrm{E}) - \bar{\mu}\Sigma_\mathrm{s}(\mathrm{E})) \qquad \text{Equation 2.9}$$

It is assumed the total macroscopic cross section, the transport cross section, the function ν(E) (the number of neutrons released in fission by an incident neutron of energy E), the neutron diffusion coefficient and the average angle of scatter are:

$$\Sigma_\mathrm{t}(\mathrm{E}) = \Sigma_\mathrm{a}(\mathrm{E}) + \Sigma_\mathrm{s}(\mathrm{E}) \qquad \text{Equation 2.10}$$

$$\Sigma(\mathrm{E})_\mathrm{tr} = \Sigma_\mathrm{t}(\mathrm{E}) - \bar{\mu}_o\Sigma_\mathrm{s}(\mathrm{E}) \qquad \text{Equation 2.11}$$

$$D_i(E) = \frac{1}{3\Sigma_{\mathrm{i,tr}}(\mathrm{E})} = \frac{1}{3\left(\Sigma_{\mathrm{i,tr}}(\mathrm{E})-\bar{\mu}_\mathrm{i}\Sigma_{\mathrm{i,s}}(\mathrm{E})\right)} \qquad \text{Equation 2.12}$$

$$\nu(\mathrm{E}) = \nu_s\mathrm{E} + \upsilon_{s0} \text{ for } 0 \le \mathrm{E} \le 1\mathrm{MeV} \qquad \text{Equation 2.13}$$

$$\nu(E) = \nu_f E + \upsilon_{f0} for\ E > 1MeV \qquad \text{Equation 2.14}$$

$$\bar{\mu}_\mathrm{o} = \frac{2}{3\mathrm{A}} \qquad \text{Equation 2.15}$$

A is the atomic mass number of isotope, (i). Equation 2.15 is a decent approximation for the average angel of scatter for large atoms i.e. A>16. The function ν(E) is for ^{235}U where $\nu_s = 0.066$, $\upsilon_{s0} = 2.432$, $\nu_f = 0.15$ and $\upsilon_{f0} = 2.349$ (Duderstadt & Hamilton, 1976, p. 61) if the energy variable is in units of MeV. The result of the function fit of ENDF-F(E) is equation 2.16. Figures 2.1 through 2.5 show comparisons of equation 2.16 with the ENDF-F(E).

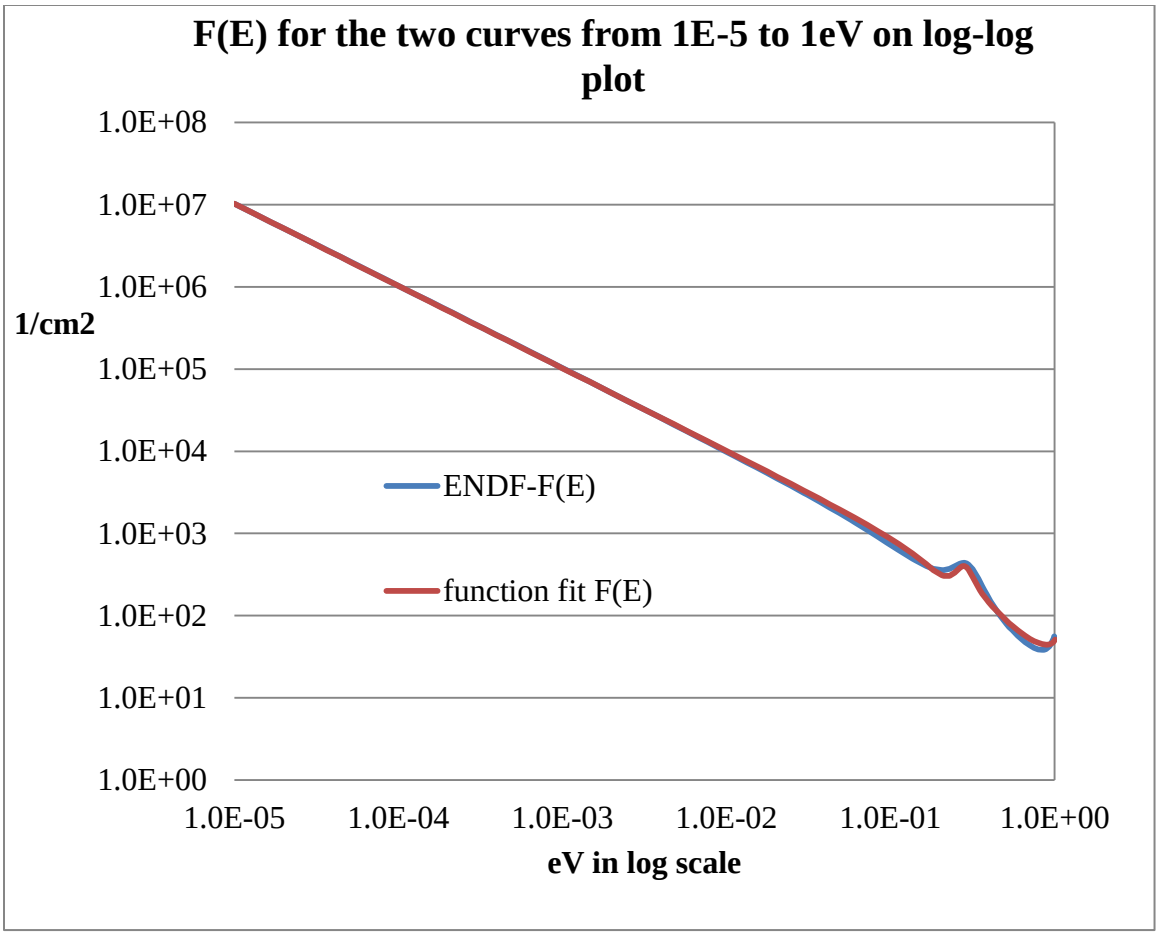

Figure 2.1 Log-log plot of F(E) from 1E-5eV to 1eV

Figure 2.1 shows the thermal region from 1E-5eV to 1eV on a log-log plot. The first term in equation 2.16 is the dominate feature in figure 2.1. The first resonance in the F(E) of pure ^{235}U is also seen in figure 2.1. Figures 2.2-2.5 are not put on a log-log plot format to point out the negative regions that show up from $\nu(E)\Sigma(\mathrm{E})_{\mathrm{f}}-\Sigma(\mathrm{E})_{\mathrm{a}}$ term in F(E), where the absorption cross section is greater than the product of $\nu(E)\Sigma(\mathrm{E})_{\mathrm{f}}$. Figure 2.4 is explicitly included to show the comparison and difference between the two, ENDF-F(E) and equation 2.16, for ^{235}U. Figure 2.4 demonstrates how the "tails" of the resonance peaks overlap and. equation 2.16 is not as sharp as the ENDF-F(E) in the overlap spaces between each resonance peak.

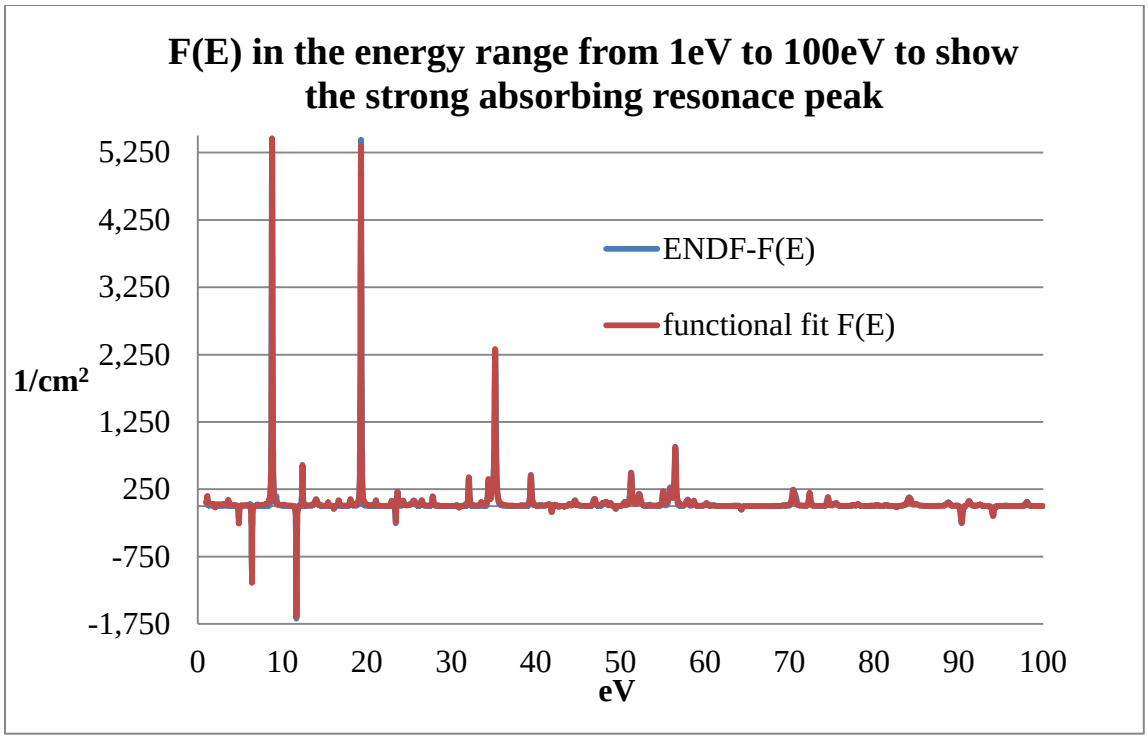

Figure 2.2 Plot of F(E) from 1eV to 100eV

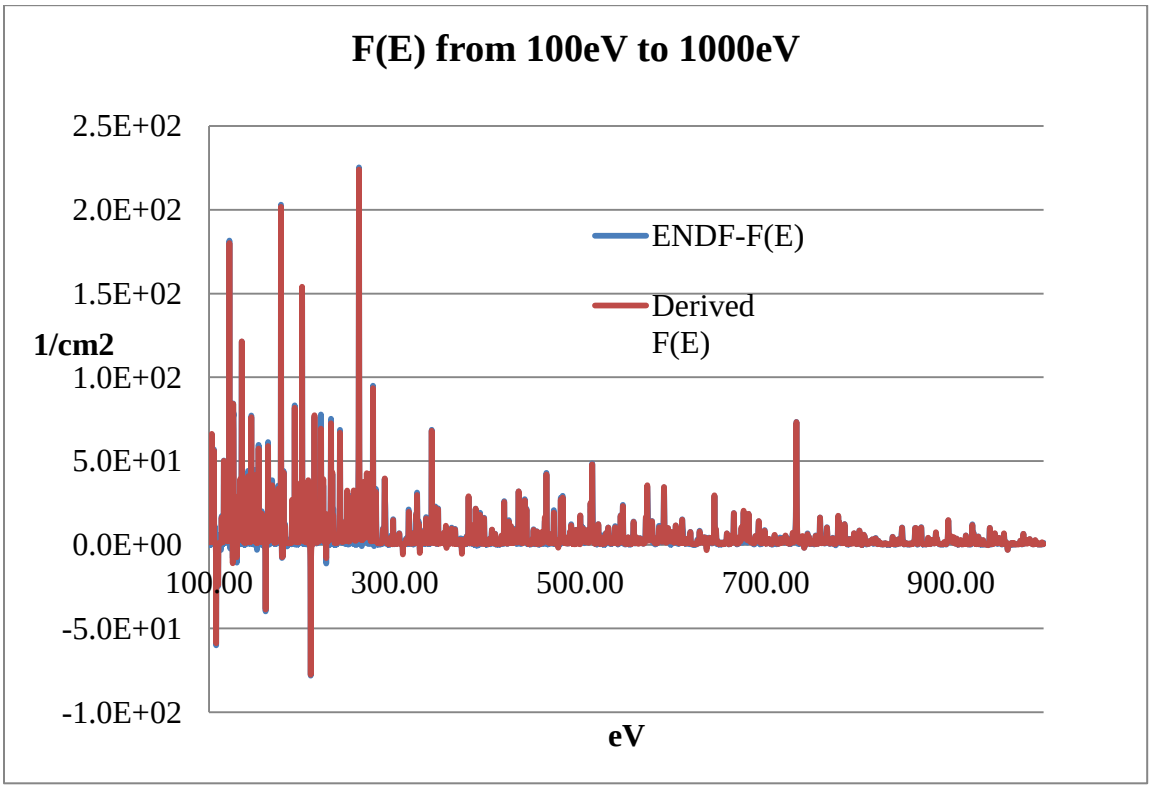

Figure 2.3 Plot of F(E) from 100eV to 1000eV

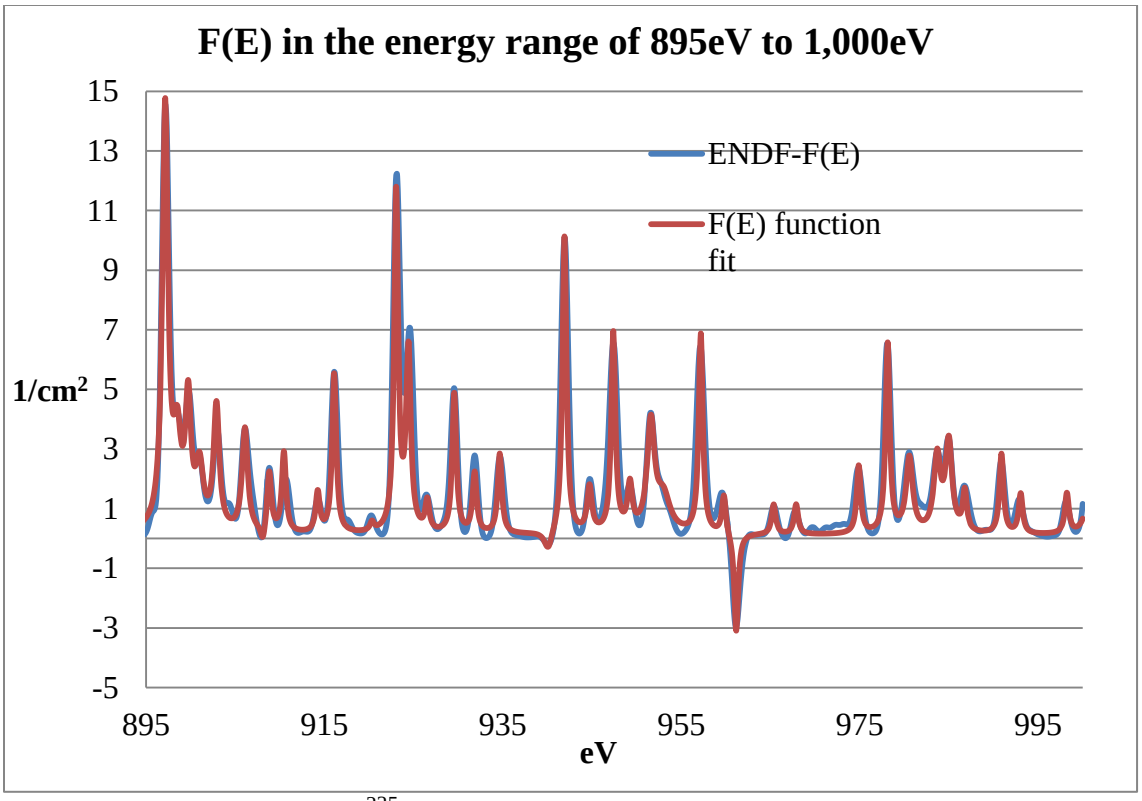

Figure 2.4 F(E) for pure ^{235}U from 895eV to 1000eV to show a closer view of the comparison of the two F(E) functions

Some of the minor peaks throughout the resonance region were not modeled because the peak height is less than 0.2cm^{-2} (see figure 2.4). A second reason for leaving out some of the extremely small peaks is because the resonance integral value from The Chart of the Nuclides and Isotopes 16th Edition matched the resonance integral value from equation 2.16. Figure 2.5 shows the end of the resonance region and the beginning of the transition region. Figure 2.6 shows the transition region and the fast region up to 10MeV.

$$F(E) = \frac{Rp_0}{E} + \sum_{l=1}^{N} \frac{Rp_l}{(E-Er_l)^2+w_l} + \sum_{m=1}^{N_{TRANS}} \frac{Rp_m \cdot (v_s E + v_{s0})_{2300eV\ to\ 1MeV}}{(E-Er_m)^2+w_m} + \sum_{n=1}^{N_{FAST}} \frac{Rp_n \cdot (v_f E + v_{f0})_{E>1MeV}}{(E-Er_n)^4+w_n \cdot E}$$

Equation 2.16

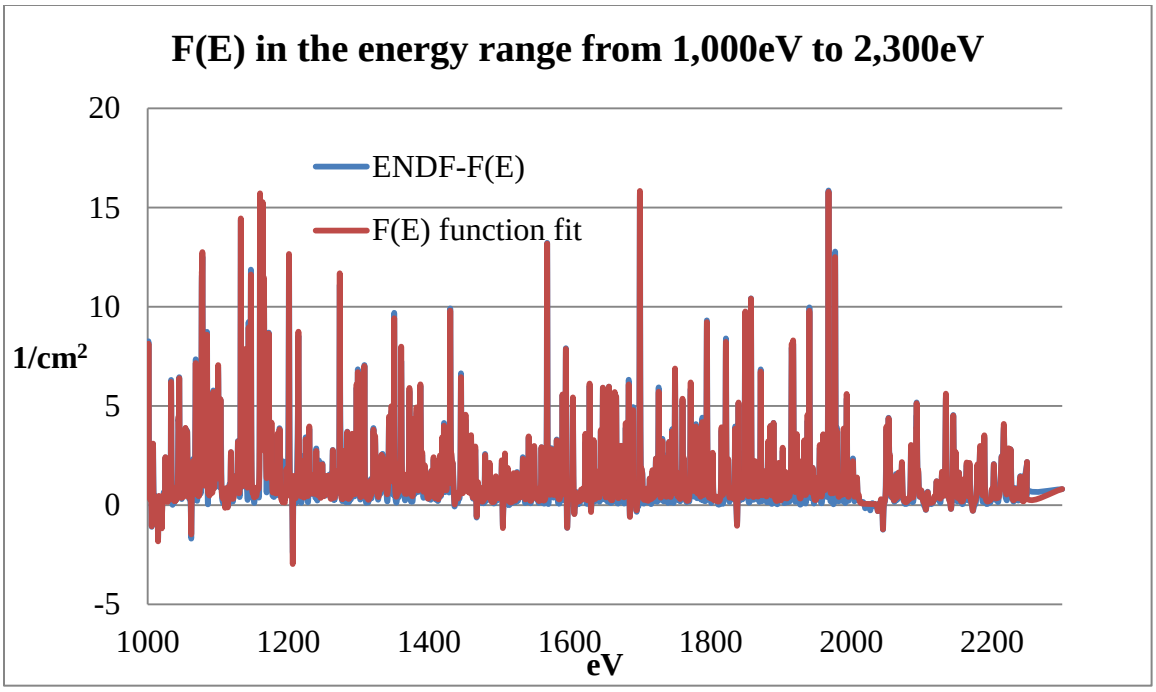

Figure 2.5 Comparison plot of derived F(E) to ENDF-F(E) in the energy range of 1000eV to 2300Ev

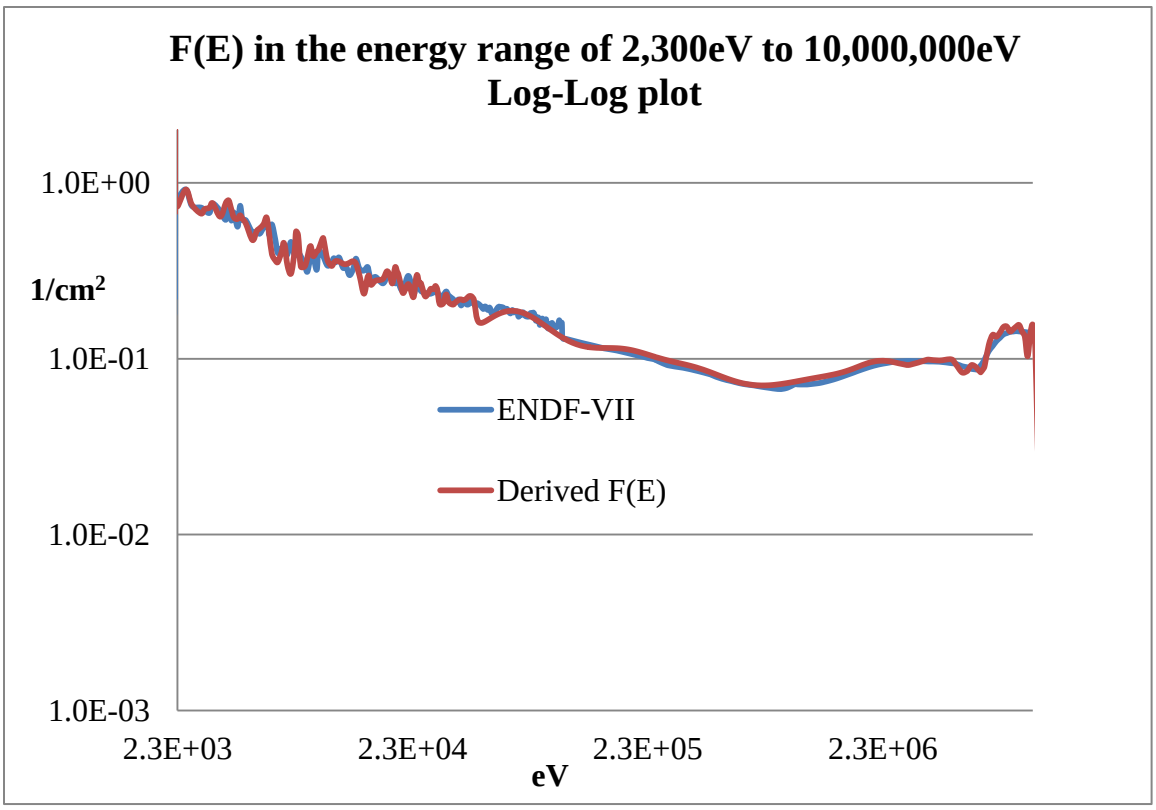

Figure 2.6 Comparison of the two F(E) functions from 2300ev to 10MeV

The constants from equation 2.16 are:

$Rp_0[=]\frac{Energy}{cm^2}$, $Rp_{l,m}'s[=]\frac{Energy^2}{cm^2}$, $Er_{l,m,n}'s[=]Energy$, $w_{l,m}'s[=]Energy^2$, $Rp_n\ 's[=]\frac{Energy^4}{cm^2}$, $w_n's[=]Energy^3$, ν_s & $\nu_f[=]\frac{neutrons}{Energy}$ and υ_{s0} & $\upsilon_{f0}[=]neutrons$, where N, N_{TRANS} and N_{FAST} are the number of terms included in each sum with indices l, m and n. The $Rp_{l,m}'s$ can be positive or negative because in some energy ranges $(-\Sigma_a(E))$is greater than $(\nu(E)\Sigma_f(E))$ in equation 2.9. The data for each constant is in Appendix A. 774 individual terms, $\left(\frac{Rp_l}{(E-Er_l)^2+w_l}\right)$ are accounted for in the first summation, 104 terms $\left(\frac{Rp_m\cdot(\nu_s E+\upsilon_{s0})_{2300eV\ to\ 1MeV}}{(E-Er_m)^2+w_m}\right)$ in the second summation and 9 individual terms $\left(\frac{Rp_n\cdot(\nu_f E+\upsilon_{f0})_{E>1MeV}}{(E-Er_n)^4+w_n\cdot E}\right)$ are accounted for in the third summation of equation 2.16.

The first term $\frac{Rp_0}{E}$ and the first summation term $\sum_{l=1}^{N}\frac{Rp_l}{(E-Er_l)^2+w_l}$ in equation 2.16 were observable by visual inspection of the ENDF-F(E) plot. The first term comes from the 1/v portions of the cross sections multiplied together and the first summation term captured ENFD-F(E) in the energy range of 1eV to 2250eV. This range remained visually similar to the resonance region of $^{235}U\ \Sigma(E)_t$ except for the few negative regions and the height and width of the each resonance peak which is specific to ENDF-F(E) resonance peaks. The height and width of each ENDF-F(E) peak can be matched by equation 2.16 by adjusting Rp_l and w_l respectively.

The second and third summation terms in equation 2.16 account for the linear effect of $\nu(E)$ on F(E). The first and second terms of equation 2.16 are not affected by $\nu(E)$ because the slope is so small, just the constant affects F(E) and it is absorbed into

Rp_0 and the $Rp_l's$. The slope of ν(E)does not change the value of ν(E) until roughly 46keV and only from 2.43 to 2.44 neutrons produced per incident neutron. It is included in the energy range at 2300eV because of the shape of ENDF-F(E) from 2300eV to 0.9MeV is a rough 1/E function, which $\frac{Rp_m\cdot(\nu_s E+\upsilon_{s0})_{2300eV\ to\ 1MeV}}{(E-Er_m)^2+w_m}$ is approximately a 1/E function. A summation of these terms $\frac{Rp_m\cdot(\nu_s E+\upsilon_{s0})_{2300eV\ to\ 1MeV}}{(E-Er_m)^2+w_m}$ provided a few useful qualities to fit the ENDF-F(E) from 2300eV to 0.9MeV. The first is an ability to shift a 1/E function to this energy range at various places without the sharp discontinuity from these two $\frac{1}{(E-Er_m)}$ or $\frac{(\nu_s E+\upsilon_{s0})}{(E-Er_m)}$ functions or any similar function with an odd order in the denominator i.e. a term $\frac{1}{(E-Er_m)^{2n+1}}$ where n=0…∞. The second reason this function is chosen is because it produced a smooth curve (see figure 6 from 0.1MeV to 0.9MeV) with a long forward tail which is the 1/E shape desired in this region without the sharp discontinuity. The third reason for this function is small resonance peaks are in this energy range. The small peaks could be modeled with this function because it can be easily tuned by adjusting Rp_m and $w_m$to have a peak at the resonance energy Er_m.

The energy range 0.9 to 10MeV yielded a different shape. In this energy range ENDF-F(E) increased in a stair step shape (broad resonance) similar to the ^{235}U fission cross section shape from 0.9 to 10MeV. The slope of ν(E) in this energy range is larger and the effect from this linear function is greater. The term inside the third summation, $\frac{Rp_n\cdot(\nu_f E+\upsilon_{f0})_{E>1MeV}}{(E-Er_n)^4+w_n\cdot E}$ is used for similar reasons already mentioned: a smooth curve without sharp discontinuities (no odd ordered denominators), an ability to add an increase or "peak" at a specific energy(Er_n). The denominator $((E-Er_n)^4+w_n\cdot E)$ allowed for a much broader peak and a sharper drop off creating the level stair effect that corresponds

to the broad width of the peak. The $w_n \cdot E$ in the denominator along with the 4th order term $(E - Er_n)^4$ restricted any long forward or backward tail that is seen with this these denominator choices $((E - Er_n)^2 + E \cdot w_n)$ and $((E - Er_m)^2 + w_m)$. The elimination of the long tails in this energy region was necessary to get the correct overlap between resonances; the other function choices investigated could not provide this effect in this energy region and consequently did not match the ENDF-F(E). Overall the functions included into equation 2.16 allowed for analytic analysis and the development of analytic moments to be created.

Derivation of Energy Dependent Neutron Moments

The set of analytical energy dependent neutron moments are found from transforming equation 2.8 with the definition of a raw moment. The mathematical definition of a raw moment is $m_k = \int_0^\infty E^k \, \phi(\vec{r}, \mathrm{E}) \mathrm{dE}$ where k = 0, 1, 2, 3 … N (Casella & Berger, 2002) and N is the total number of moments desired. Transformation of equation 8 into moment form requires placing F(E) into equation 8, multiply by E^k, then apply the definition of a moment i.e. integrate from 0 to infinity; the result is equation 2.17. The constant $\mathrm{B_{Ek}}^2$ in equation 2.17 is based on the diffusion boundary conditions that must be satisfied and is explained in the neutron diffusion boundary section of this paper.

$$\int_0^\infty E^k \nabla^2 \phi(\vec{r}, \mathrm{E}) \mathrm{dE} + \int_0^\infty E^k \mathrm{F(E)} \phi(\vec{r}, \mathrm{E}) \mathrm{dE} + \int_0^\infty E^k \mathrm{B_{Ek}}^2 \phi(\vec{r}, \mathrm{E}) \mathrm{dE} = 0 \qquad \text{Equation 2.17}$$

The Laplace operator in equation 2.17 depends only on position so it comes through the energy integral, recognize the moment definition for two of the terms in equation 2.17 and equation 2.18 is the 1 dimensional EDNDE in moment form

$$\nabla^2 m_k + \mathrm{B_{Ek}}^2 \cdot m_k + \int_0^\infty E^k \mathrm{F(E)}\phi(\vec{\mathrm{r}}, \mathrm{E})\mathrm{dE} = 0 \qquad \text{Equation 2.18}$$

This new partial-integro differential equation, equation 2.18 needs to be simplified further to solve analytically. The term $E^k \mathrm{F(E)}$ can be simplified as follows.

$$E^k \cdot F(E) =$$

$$Rp_0 E^{k-1} + \sum_{l=1}^{N_{resonance}} \frac{E^k \cdot Rp_i}{E^2 - 2Er_l E + {Er_l}^2 + w_l} + \sum_{m=1}^{N_{TRANS}} \frac{E^k \cdot Rp_m \cdot (\nu_s E + \upsilon_{s0})_{0.1MeV\ to\ 1MeV}}{(E - Er_m)^2 + w_m} +$$

$$\sum_{n=1}^{N_{FAST}} \frac{E^k \cdot Rp_n \cdot (\nu_f E + \upsilon_{f0})_{E>1MeV}}{(E - Er_n)^4 + w_n \cdot E} \qquad \text{Equation 2.19}$$

The summations can be broken down into the various k[th] components by polynomial long division. This is an example of polynomial long division, $\frac{\mathrm{c_1 u^k}}{\mathrm{b_1} u^2 + \mathrm{b_2} u^1 + \mathrm{b_3}} = \frac{\mathrm{c_1}}{\mathrm{b_1}} \mathrm{u^{k-2}} +$

$\frac{\mathrm{c_1 b_2}}{{\mathrm{b_1}}^2} \mathrm{u^{k-3}} + \frac{\mathrm{c_1}({\mathrm{b_2}}^2 - \mathrm{b_1})}{{\mathrm{b_1}}^3} \mathrm{u^{k-4}} + \frac{\mathrm{c_1}({\mathrm{b_2}}^3 - \mathrm{b_1 b_2})}{{\mathrm{b_1}}^3} \mathrm{u^{k-5}} \ldots +$ higher order terms.

In general, $E^k \cdot F(E)$ can now be written as $E^k \cdot F(E) = C_{E1} E^{k-1} + C_{E2} E^{k-2} +$

$C_{E3} E^{k-3} + C_{E4} \mathrm{E^{k-4}} + C_{E5} \mathrm{E^{k-5}} + \cdots +$ higher order terms

The constants $(C_E{}'s)$ for moment 1-5 and the units associated with them are shown in Table 2.2. The constants from the polynomial long division are listed specifically in equations 2.20 through 2.24. Polynomial long division allows an analytical treatment of the integral term in equation 2.18 which is unique to any neutron transport or diffusion method.

Table 2.2 Constants from Polynomial Long Division of F(E)

Constant	Value	Units
CE1	0.0615	MeV/cm^2
CE2	0.0842	MeV^2/cm^2
CE3	0.3551	MeV^3/cm^2
CE4	2.1254	MeV^4/cm^2
CE5	13.5917	MeV^5/cm^2

$$C_{E1} = Rp_0 + \sum_{m=1}^{N_{TRANS}} \nu_s Rp_m \quad \text{Equation 2.20}$$

$$C_{E2} = \sum_{l=1}^{N} Rp_l + \sum_{m=1}^{NR_{TRANS}} (2Rp_m \nu_s Er_m + Rp_m \nu_{s0}) \quad \text{Equation 2.21}$$

$$C_{E3} = \sum_{l=1}^{N} 2Rp_l Er_l + \sum_{m=1}^{NR_{TRANS}} \left(3Rp_m \nu_s {Er_m}^2 + 2Er_m Rp_m \nu_0 - Rp_m \nu_s w_m\right) + \sum_{n=1}^{NR_{FAST}} Rp_n \nu_f \quad \text{Equation 2.22}$$

$$C_{E4} = \sum_{l=1}^{N} \left(3Rp_l {Er_l}^2 - Rp_l w_l\right) + \sum_{m=1}^{N_{TRANS}} \left(4Rp_m \nu_s {Er_m}^3 + 3Rp_m {Er_m}^2 \nu_{s0} - 4Rp_m Er_m \nu_s w_m - Rp_m w_m \nu_{s0}\right) + \sum_{n=1}^{N_{FAST}} \left(4Rp_n Er_n \nu_f + Rp_n \nu_{f0}\right) \quad \text{Equation 2.23}$$

$$C_{E5} = \sum_{l=1}^{N} 4Rp_l {Er_l}^3 + \sum_{m=1}^{N_{TRANS}} \left(5Rp_m \nu_s {Er_m}^4 + 4Rp_m {Er_m}^3 \nu_{s0} - 10Rp_m {Er_m}^2 \nu_s w_m - 4Er_m Rp_m w_m \nu_{s0} + Rp_m \nu_s {w_m}^2\right) + \sum_{n=1}^{N_{FAST}} \left(10Rp_n \nu_f {Er_n}^2 + 4Rp_n Er_n \nu_{f0}\right) \quad \text{Equation 2.24}$$

The higher order moments (k > 5) can be derived from dividing F(E) further, but the 5th energy moment is sufficient to show how the moments from MCNP and Attila compare to the derived neutron diffusion moments. It has been shown that five moments is enough to reconstruct a particle population (Marchisio, Pikturna, & Fox, May 2003), but for neutron fluxes that still needs to be researched and sorted out.

Equation 2.18 becomes equation 2.25 by recognizing the terms in moment form in the integral of $E^k \cdot F(E)$.

$$\nabla^2 m_k + {B_{Ek}}^2 m_k + C_{E1} m_{k-1} + C_{E2} m_{k-2} + C_{E3} m_{k-3} + C_{E4} m_{k-4} + C_{E5} m_{k-5} = 0 \quad \text{Equation 2.25}$$

Equation 2.25 is a set of partial differential equations, PDEs where the total number of equations is N. This analysis set N equal to 5. This set of PDE's can be turned into a set of ordinary differential equations (ODEs) by making the assumption that the moments only depend on one dimension, r in this case. Each individual ODE moment equation is shown below and the set of moments work together as a system of equations.

$$\nabla^2 m_0 + {B_{E0}}^2 m_0 = -C_{E1} m_{-1} - C_{E2} m_{-2} - C_{E3} m_{-3} - C_{E4} m_{-4} - C_{E5} m_{-5} \quad \text{Equation 2.26}$$

$$\nabla^2 m_1 + {B_{E1}}^2 m_1 = -C_{E1} m_0 - C_{E2} m_{-1} - C_{E3} m_{-2} - C_{E4} m_{-3} - C_{E5} m_{-4} \quad \text{Equation 2.27}$$

$$\nabla^2 m_2 + {B_{E2}}^2 m_2 = -C_{E1} m_1 - C_{E2} m_0 - C_{E3} m_{-1} - C_{E4} m_{-2} - C_{E5} m_{-3} \quad \text{Equation 2.28}$$

$$\nabla^2 m_3 + {B_{E3}}^2 m_3 = -C_{E1} m_2 - C_{E2} m_1 - C_{E3} m_0 - C_{E4} m_{-1} - C_{E5} m_{-2} \quad \text{Equation 2.29}$$

$$\nabla^2 m_4 + {B_{E4}}^2 m_4 = -C_{E1} m_3 - C_{E2} m_2 - C_{E3} m_1 - C_{E4} m_0 - C_{E5} m_{-1} \quad \text{Equation 2.30}$$

$$\nabla^2 m_5 + {B_{E5}}^2 m_5 = -C_{E1} m_4 - C_{E2} m_3 - C_{E3} m_2 - C_{E4} m_1 - C_{E5} m_0 \quad \text{Equation 2.31}$$

Solution to the raw moment set come from setting the negative moments (k=-1, -2, -3 etc…) equal to zero. The reason for this is these moments are not in the set by definition; k ≡ 0, 1, 2, 3…N.

The set of ODEs is now

$$\nabla^2 m_0 + {B_{E0}}^2 m_0 = 0 \quad \text{Equation 2.32}$$

$$\nabla^2 m_1 + {B_{E1}}^2 m_1 = -C_{E1} m_0 \quad \text{Equation 2.33}$$

$$\nabla^2 m_2 + {B_{E2}}^2 m_2 = -C_{E1} m_1 - C_{E2} m_0 \quad \text{Equation 2.34}$$

$$\nabla^2 m_3 + {B_{E3}}^2 m_3 = -C_{E1} m_2 - C_{E2} m_1 - C_{E3} m_0 \quad \text{Equation 2.35}$$

$$\nabla^2 m_4 + {B_{E4}}^2 m_4 = -C_{E1} m_3 - C_{E2} m_2 - C_{E3} m_1 - C_{E4} m_0 \quad \text{Equation 2.36}$$

$$\nabla^2 m_5 + {B_{E5}}^2 m_5 = -C_{E1} m_4 - C_{E2} m_3 - C_{E3} m_2 - C_{E4} m_1 - C_{E5} m_0 \quad \text{Equation 2.37}$$

Each k^{th} moment can now be solved analytically beginning with the $zero^{th}$ raw moment. The rest of the raw moments can be solved analytically with the method of undetermined coefficients (Edwards & Penney, 2001). The solution to equation 2.32 for a one dimensional case turns out to be mathematically the same as the solution to the one-speed diffusion equation, which is comforting because this matches expectations and the flux shape from MCNP and Attila. The particular and homogeneous solutions to the ODE

set with the corresponding constants for the raw energy dependent neutron diffusion moments are listed below in equations 2.38-2.58.

$$m_0 = a_0 \frac{sin(B_{E0} \cdot r)}{r}$$ Equation 2.38

$$m_1 = a_1 \frac{sin(B_{E1} \cdot r)}{r} + b_1 \cdot r \cdot cos(B_{E1} \cdot r)$$ Equation 2.39

where

$$b_1 = \frac{a_0 C_{E1}}{2B_{E1}}$$ Equation 2.40

$$m_2 = a_2 \frac{sin(B_{E2} \cdot r)}{r} + b_2\, cos(B_{E2} \cdot r) \;\; + c_2\, r\, sin(B_{E2} \cdot r)$$ Equation 2.41

where

$$b_2 = \frac{a_1 C_{E1} + a_0 C_{E2} + 2\, c_2}{2B_{E2}}$$ Equation 2.42

$$\mathrm{c}_2 = -\frac{b_1 C_{E1}}{4B_{E2}}$$ Equation 2.43

$$m_3 = a_3 \frac{sin(B_{E3} \cdot r)}{r} + b_3\, cos(B_{E3} \cdot r) \;\; + c_3 r\, sin(B_{E3} \cdot r) + d_3 r^2 cos(B_{E3} \cdot r)$$

Equation 2.44

where

$$b_3 = \frac{a_2 C_{E1} + a_1 C_{E2} + a_0 C_{E3} + 2\, c_3}{2B_{E3}},$$ Equation 2.45

$$\mathrm{c}_3 = -\frac{b_2 C_{E1} + b_1 C_{E2} + 6\, d_3}{4B_{E3}}$$ Equation 2.46

$$\mathrm{d}_3 = \frac{\mathrm{c}_2 C_{E1}}{6B_{E3}}$$ Equation 2.47

$$m_4 = a_4 \frac{\sin(B_{E4} \cdot r)}{r} + b_4 \cos(B_{E4} \cdot \mathrm{r}) \;\; + \mathrm{c}_4 \mathrm{r} \sin(B_{E4} \cdot \mathrm{r}) + \mathrm{d}_4\, \mathrm{r}^2 \cos(B_{E4} \cdot \mathrm{r}) +$$

$$\mathrm{e}_4\, \mathrm{r}^3 \sin(B_{E4} \cdot \mathrm{r})$$ Equation 2.48

where

$$b_4 = \frac{a_3 C_{E1} + a_2 C_{E2} + a_1 C_{E3} + a_0 C_{E4} + 2\, c_4}{2B_{E4}}, \quad \text{Equation 2.49}$$

$$c_4 = -\frac{b_3 C_{E1} + b_2 C_{E2} + b_1 C_{E3} + 6 d_4}{4B_{E4}}, \quad \text{Equation 2.50}$$

$$d_4 = \frac{c_3 C_{E1} + c_2 C_{E2} + 12\, e_4}{6B_{E4}} \quad \text{Equation 2.51}$$

$$e_4 = -\frac{d_3 C_{E1}}{8B_{E4}} \quad \text{Equation 2.52}$$

$$m_5 = a_5 \frac{sin(B_{E5} \cdot r)}{r} + b_5 \cos(B_{E5} \cdot r) + c_5 r \sin(B_{E5} \cdot r) + d_5\, r^2 \cos(B_{E5} \cdot r) +$$

$$e_5\, r^3 \sin(B_{E5} \cdot r) + f_5\, r^4 \cos(B_{E5} \cdot r) \quad \text{Equation 2.53}$$

where

$$b_5 = \frac{a_4 C_{E1} + a_3 C_{E2} + a_2 C_{E3} + a_1 C_{E4} + a_0 C_{E5} + 2\, c_5}{2B_{E5}}, \quad \text{Equation 2.54}$$

$$c_5 = -\frac{b_4 C_{E1} + b_3 C_{E2} + b_2 C_{E3} + b_1 C_{E4} + 6 d_5}{4B_{E5}}, \quad \text{Equation 2.55}$$

$$d_5 = \frac{c_4 C_{E1} + c_3 C_{E2} + c_2 C_{E3} + 12 e_5}{6B_{E5}}, \quad \text{Equation 2.56}$$

$$e_5 = -\frac{d_4 C_{E1} + d_3 C_{E2} + 20\, f_5}{8B_{E5}} \quad \text{Equation 2.57}$$

$$f_5 = \frac{e_4 C_{E1}}{10B_{E5}} \quad \text{Equation 2.58}$$

The unknown coefficients of the raw moments, a_k's and B_{Ek}'s are determined from the two neutron diffusion theory boundary conditions, after they are put in moment form.

Neutron Diffusion Boundary Conditions in Energy Moment Form

The first boundary condition that must be satisfied, is that the flux must be finite everywhere so the moments must be finite everywhere also. This condition is enforced by

setting the amplitude constants in the $C_k \cdot \cos(B_{Ek}r)\ /r$ terms (which come from the homogeneous portion of the solution for each moment) equal to zero. The reason C_k is set to zero is; as the radius approaches zero, $C_k * \cos(B_{Ek}r)\ /r$ approaches infinity, so the C_k's are set to zero.

The second boundary condition is that the flux is zero at the transport corrected extrapolated boundary. The transport corrected extrapolated boundary is, $\tilde{R} = R + r_o$, and $r_o = 2.13 \cdot D(E)$ where r_o is the extrapolated correction distance. For one group or one speed theory, D(E) is the diffusion value for one energy value, i.e., a 1MeV neutron traveling through ^{235}U, D(1MeV) ≈ 1cm (Foster & Wright, 1977, p. 250). For the purposes of having the correct boundary for each moment, D(E) needs to ensure that at the appropriate extrapolated distance in moment form the neutron flux is zero. The boundary condition is satisfied and represented by the following relationship $m_k(\tilde{R}) = \int_0^\infty E^k \phi\left(r = \tilde{R}_k, E\right) dE = 0$. The boundary condition at the extrapolated distance in moment form is $\int_0^\infty \tilde{R} E^k \phi(\vec{r}, E) dE = \int_0^\infty R E^k \phi(\vec{r}, E) dE + 2.13 * \int_0^\infty E^k \phi(\vec{r}, E) D(E) dE$.

Simplify the moment form of the extrapolated distance with the approximation that $\phi(\vec{r}, E) = \phi(E)\phi(\vec{r})$, since this treatment is only at the boundary so the position dependence can be separated out R and $\tilde{R}$ can be treated as constants. Divide by the raw moment definition on each side of the expression and the spatial dependence $\phi(\vec{r})$ come through the integrals, $\tilde{R} \frac{\phi(\vec{r}) \int_0^\infty E^k \phi(E) dE}{\phi(\vec{r}) \int_0^\infty E^k \phi(E) dE} = R \frac{\phi(\vec{r}) \int_0^\infty E^k \phi(E) dE}{\phi(\vec{r}) \int_0^\infty E^k \phi(E) dE} +$

$2.13 \frac{\phi(\vec{r}) \int_0^\infty E^k D(E) \phi(E) dE}{\phi(\vec{r}) \int_0^\infty E^k \phi(E) dE}$ see 2.59. Table 2.3 shows the extrapolated boundaries.

$$\tilde{R}_k = R + 2.13 \cdot \frac{\int_0^\infty E^k D(E) \phi(E) dE}{\int_0^\infty E^k \phi(E) dE} \qquad \text{Equation 2.59}$$

Table 2.3 The Extrapolated Boundaries for Moment 0-5

$\tilde{R}_0$	$\tilde{R}_1$	$\tilde{R}_2$	$\tilde{R}_3$	$\tilde{R}_4$	$\tilde{R}_5$
10.24cm	10.25cm	10.37cm	10.38cm	10.40cm	10.40cm

Values for $\tilde{R}_k$ are found with the energy dependent diffusion coefficient, $\left(D_i(E) = \frac{1}{3\Sigma_{\mathrm{i,tr}}} = \frac{1}{3\left(\Sigma_{\mathrm{i,t}} - \bar{\mu}_{\mathrm{i}}\Sigma_{\mathrm{i,s}}\right)}\right)$ the ENDF values for the cross sections and the assumption that $\phi(E)$ is represented by equation 2.60 from 1eV to 10MeV (Duderstadt & Hamilton, 1976, p. 330). Below 1eV the neutron flux is assumed to be a Maxwell-Boltzmann distribution at some temperature T (298K) (Duderstadt & Hamilton, 1976). Equation 2.61 represents (ξ) the average increase in lethargy per collision (Lamarsh, 1966, pp. 175-176).

$$\phi(E) = \frac{\mathrm{S}}{\xi \cdot \Sigma(\mathrm{E})_{\mathrm{S}} \cdot \mathrm{E}} \qquad \text{Equation 2.60}$$

$$\xi = \frac{2}{A + \frac{2}{3}} \qquad \text{Equation 2.61}$$

This method allowed the extrapolated boundary to be found for each moment and maintain the entire energy range of interest in a nuclear reactor by numerically integrating (Chapra & Canale, 2002) this term $\frac{\int_0^\infty E^k D(E)\phi(E)dE}{\int_0^\infty E^k \phi(E)dE}$ from equation 2.59.

For the second boundary condition to be true, either $a_k = b_k = c_k = d_k = e_k = f_k = 0$, the null answer or B_{Ek} for each moment must satisfy the boundary condition. For the 0th moment, B_{E0} satisfies the second boundary condition by taking on the value of $\frac{\pi}{\tilde{R}_0}$, just like one speed theory and a_0 the other unknown coefficient is found by, the power equation, equation 2.72 in the next section. The rest of the moments, k =1-5, the 2nd boundary condition is satisfied as follows, see equations 2.62-2.66.

$$\frac{a_1}{\tilde{R}_1} sin\left(B_{E1} \cdot \tilde{R}_1\right) = -b_1 \, cos\left(B_{E1} \cdot \tilde{R}_1\right) \quad \text{Equation 2.62}$$

$$\left(\frac{a_2}{\tilde{R}_2} + c_2 \, \tilde{R}_2\right) sin\left(B_{E2} \cdot \tilde{R}_2\right) = -b_2 \, cos\left(B_{E2} \cdot \tilde{R}_2\right) \quad \text{Equation 2.63}$$

$$\left(\frac{a_3}{\tilde{R}_3} + c_3 \tilde{R}_3\right) sin\left(B_{E3} \cdot \tilde{R}_3\right) = -\left(b_3 + d_3 \tilde{R}_3{}^2\right) cos\left(B_{E3} \cdot \tilde{R}_3\right) \quad \text{Equation 2.64}$$

$$\left(\frac{a_4}{\tilde{R}_4} + \mathrm{c}_4 \tilde{R}_4 + \mathrm{e}_4 \, \tilde{R}_4{}^3\right) \sin\left(B_{E4} \cdot \tilde{R}_4\right) = -\left(b_4 + \mathrm{d}_4 \, \tilde{R}_4{}^2\right) \cos\left(B_{E4} \cdot \tilde{R}_4\right) \quad \text{Equation 2.65}$$

$$\left(\frac{a_5}{\tilde{R}_5} + \mathrm{c}_5 \tilde{R}_5 + \mathrm{e}_5 \, \tilde{R}_5{}^3\right) \sin\left(B_{E5} \cdot \tilde{R}_5\right) = -\left(b_5 + \mathrm{d}_5 \, \tilde{R}_5{}^2 + \mathrm{f}_5 \, \tilde{R}_5{}^4\right) \cos\left(B_{E5} \cdot \tilde{R}_5\right)$$

Equation 2.66

It turns out the only way for these equations to be equal and have positive amplitudes (the $a_k's$), and positive moments is for the sine and cosine terms to be equal and opposite at $\tilde{R}_k$. Sine and cosine have equal and opposite values when the B_{Ek} values equal $\frac{3\pi}{4\tilde{R}_k}$, so the set of equations become the following because $sin\left(\frac{3\pi}{4\tilde{R}_k} \cdot \tilde{R}_k\right) = -\cos\left(\frac{3\pi}{4\tilde{R}_k} \cdot \tilde{R}_k\right)$ and the remaining unknown coefficients, $a_k's$ follow from working through the algebra of this set of expressions and the amplitudes are positive.

$$a_1 = \tilde{R}_1 b_1 \quad \text{Equation 2.67}$$

$$a_2 = \tilde{R}_2\left(b_2 - c_2 \, \tilde{R}_2\right) \quad \text{Equation 2.68}$$

$$a_3 = \tilde{R}_3\left(b_3 - c_3 \tilde{R}_3 + d_3 \tilde{R}_3{}^2\right) \quad \text{Equation 2.69}$$

$$a_4 = \tilde{R}_4\left(b_4 - \mathrm{c}_4 \tilde{R}_4 + \mathrm{d}_4 \, \tilde{R}_4{}^2 - \mathrm{e}_4 \, \tilde{R}_4{}^3\right) \quad \text{Equation 2.70}$$

$$a_5 = \tilde{R}_5\left(b_5 - \mathrm{c}_5 \tilde{R}_5 + \mathrm{d}_5 \, \tilde{R}_5{}^2 - \mathrm{e}_5 \, \tilde{R}_5{}^3 + \mathrm{f}_5 \, \tilde{R}_5{}^4\right) \quad \text{Equation 2.71}$$

The Power Equation in Energy Moment Form, Finding a_0

For any nuclear reactor, the power is a design choice and a known quantity. Power is proportional to the fission rate multiplied by a conversion factor and averaged over the volume of the fueled region of the nuclear reactor. The power equation below is general and is applicable to any reactor (Lamarsh, 1966, pp. 257-258). C_{fp} is a conversion factor to convert from fissions to Joules.

$$power = \frac{C_{fp} M_f N_A}{MW_f V} \int_0^\infty \sigma_F(E) \bar{\phi}(E)\, dE \qquad \text{Equation 2.72}$$

The constants and parameters in equation 2.72 are:

$V = volume\ of\ the\ fueled\ region$, $C_{fp} = 3.2 \times 10^{-11} \frac{joules}{fission}$,

$M_f = mass\ of\ the\ fuel$, $MW_f = molecular\ weight\ of\ the\ fuel$,

$N_A = Avogadro's\ number$,

$\sigma_F(E) =$ energy dependent microscopic fission cross section and

$$\bar{\phi}(E) = \frac{1}{V}\int_V \phi(r,E) dV = volume\ averaged\ flux \qquad \text{Equation 2.73}$$

The volume averaged flux can be isolated and transformed into moment form by multiplying by E^0 inside the volume integral since this is the only part of the expression that has position dependence shown below.

$$\frac{1}{V}\int_V \int_0^\infty E^0 \phi(r,E)\, dE dV = \frac{1}{V}\int_V m_0 dV \qquad \text{Equation 2.74}$$

The moment form of the volume average flux is the zeroth moment integrated over the volume

$$\bar{\phi}(E)_k = \frac{1}{V}\int_V m_0 dV \qquad \text{Equation 2.75}$$

The Power equation in moment form becomes equation 2.76

$$Power = \frac{C_{fp}M_f N_A}{MW_f V}\int_0^\infty \sigma_F(E)\int_V m_0 dV \, dV \qquad \text{Equation 2.76}$$

The Power equation can be numerically integrated by multiplying the ENDF-VII values with the results of the integrated volume averaged moments$\left(\bar{\phi}(E)\right)$, where the differential volume for the sphere is $4\pi r^2 dr$.

$$\int_V m_0 dV = 4\pi A_0 \int_0^R \frac{sin(\sqrt{C_{E0}}\cdot r)}{r} r^2 dr = 4\pi A_0 \left(\frac{\sin(B_{E0}\cdot R)}{{B_{E0}}^2} - \frac{R\cdot cos(B_{E0}\cdot R)}{B_{E0}}\right) \qquad \text{Equation 2.77}$$

If $\widetilde{R}_0 \approx R$ then equation 2.77 becomes equation 2.78

$$\int_V m_0 dV = \frac{4\pi a_0 R}{B_{E0}} = 4a_0 R^2 \qquad \text{Equation 2.78}$$

The power equation becomes equation 2.79.

$$Power_0 = \frac{C_{fp}M_f N_A}{MW_f}\int_0^\infty \sigma_F(E) 4a_0 R^2 \, dE \qquad \text{Equation 2.79}$$

Now a_0 is shown in equation 2.80.

$$a_0 = \frac{Power_0 MW_f}{4R^2 C_{fp}M_f N_A \int_0^\infty \sigma_F(E) dE} \qquad \text{Equation 2.80}$$

Each of the constants a_k's, b_k's, c_k's etc…has a_0 in the numerator so when these constants are normalized a_0 is divided out, for the purposes of this paper power can be set is such a way that a_0 is 1.

Normalized Energy Dependent Neutron Diffusion Moments

The set of moments that are plotted for comparison are the normalized moments. The moments m_k = 1, 2, 3, 4, 5 are normalized by the 0^{th} moment, m_0. The normalized moments provide information about the population density function i.e. mean energy (m_1/m_0), variance of the energy (m_2/m_0), skewness (m_3/m_0) and kurtosis (m_4/m_0). The

normalized energy dependent neutron diffusion moments (NEDNDM) are seen in equation 2.81-2.86, where $a_0 = 1$. The set of normalized moments, m_k/m_0:

$$\frac{m_0}{m_0} = \frac{a_0\frac{sin(B_{E0}\cdot r)}{r}}{a_0\frac{sin(B_{E0}\cdot r)}{r}} \equiv 1 \qquad \text{Equation 2.81}$$

$$\frac{m_1}{m_0} = \frac{a_1 \sin(B_{E1}\cdot r)}{a_0 \sin(B_{E0}\cdot r)} + \frac{b_1\cdot r\cdot cos(B_{E1}\cdot r)}{a_0 \sin(B_{E0}\cdot r)} \qquad \text{Equation 2.82}$$

$$\frac{m_2}{m_0} = \frac{a_2 sin(B_{E2}\cdot r)}{a_0 sin(B_{E0}\cdot r)} + \frac{b_2 r\, cos(B_{E2}\cdot r)}{a_0 sin(B_{E0}\cdot r)} + \frac{c_2\, r^2 sin(B_{E2}\cdot r)}{a_0 sin(B_{E0}\cdot r)} \qquad \text{Equation 2.83}$$

$$\frac{m_3}{m_0} = \frac{a_3 sin(B_{E3}\cdot r)}{a_0 sin(B_{E0}\cdot r)} + \frac{b_3 r\, cos(B_{E3}\cdot r)}{a_0 sin(B_{E0}\cdot r)} + \frac{c_3 r^2 sin(B_{E3}\cdot r)}{a_0 sin(B_{E0}\cdot r)} + \frac{d_3 r^3 cos(B_{E3}\cdot r)}{a_0 sin(B_{E0}\cdot r)} \qquad \text{Equation 2.84}$$

$$\frac{m_4}{m_0} = \frac{a_4 sin(B_{E4}\cdot r)}{a_0 sin(B_{E0}\cdot r)} + \frac{b_4 r\, cos(B_{E4}\cdot r)}{a_0 sin(B_{E0}\cdot r)} + \frac{c_4\, r^2 sin(B_{E4}\cdot r)}{a_0 sin(B_{E0}\cdot r)} + \frac{d_4\, r^3\, cos(B_{E4}\cdot r)}{a_0 sin(B_{E0}\cdot r)} + \frac{e_4\, r^4 sin(B_{E4}\cdot r)}{a_0 sin(B_{E0}\cdot r)}$$

Equation 2.85

$$\frac{m_5}{m_0} = \frac{a_5 sin(B_{E5}\cdot r)}{a_0 sin(B_{E0}\cdot r)} + \frac{b_5 r\, cos(B_{E5}\cdot r)}{a_0 sin(B_{E0}\cdot r)} + \frac{c_5 r^2 sin(B_{E5}\cdot r)}{a_0 sin(B_{E0}\cdot r)} + \frac{d_5\, r^3\, cos(B_{E5}\cdot r)}{a_0 sin(B_{E0}\cdot r)} + \frac{e_5\, r^4 sin(B_{E5}\cdot r)}{a_0 sin(B_{E0}\cdot r)} +$$

$$\frac{f_5\, r^5\, cos(B_{E5}\cdot r)}{a_0 sin(B_{E0}\cdot r)} \qquad \text{Equation 2.86}$$

The normalized moments or simply called moments for the rest of the paper are displayed in the Results and Discussion section of the paper.

Results and Discussion

Moments for Attila and MCNP5 were created by modeling concentric spheres in 1 cm radial increments away from each other. Nine spheres in all were modeled, a sphere at 1cm, 2cm,…8cm and 8.35cm to model the entire critical spherical assembly. To make the moments in MCNP5 f2 tallies are taken at each sphere surface and each tally was broken into 1000 evenly spaced energy bins up to 10MeV. Energy bins from 10MeV to 20 MeV showed large relative errors > 20% and were omitted due to limits in computer power the authors have access to, a 64-bit laptop with a hex core processor and 6

gigabytes of RAM. To get relative errors below 5% for energy bins from 1E-11 to 10MeV 6million particles are tracked in the MCNP model. The f2 tally data in each energy bin is put in an excel spreadsheet and the various moments were computed numerically based on the definitions for the mean, variance, skewness, kurtosis and higher order moments.

Attila moments are created from the 30 group cross section file radion5 created by Transpire Inc. (energy bins are in Table 2.1). The data to create energy moments from Attila are from a custom report created in Attila where a line edit was made to collect the flux in each energy group at approximately 1cm increments up to the system edge to match the MCNP5 sphere surface tallies. The points along the line edit from Attila are not exactly 1cm apart because each point lined up on a mesh point. The flux data in each energy group are also calculated according to the definitions for the mean, variance, skewness, kurtosis and higher order moments. Figures 2.7-2.11 show the comparison of the moments from the three methods (MCNP5, Attila and Analytic). There are three curves in Figures 2.7-2.11: in blue the MCNP moment, in red the Attila moment and in green the analytic moment.

The most striking feature of the moment comparison is that the Attila moments are numerically greater than the MCNP and analytic moments. The reason the Attila moments are larger is because they are tuned to the fission spectrum which should give an expected mean energy of about 1.98MeV (Lamarsh & Baratta, 2001, p. 87). Researchers (Sevast'yanov, Koshelev, & Maslov, 2000) claim that the fission spectrum for ^{235}U has an average energy value of 1.475MeV+/- 3.77%. If the researchers' spectrum was used then Attila moments would line up more with MCNP5.

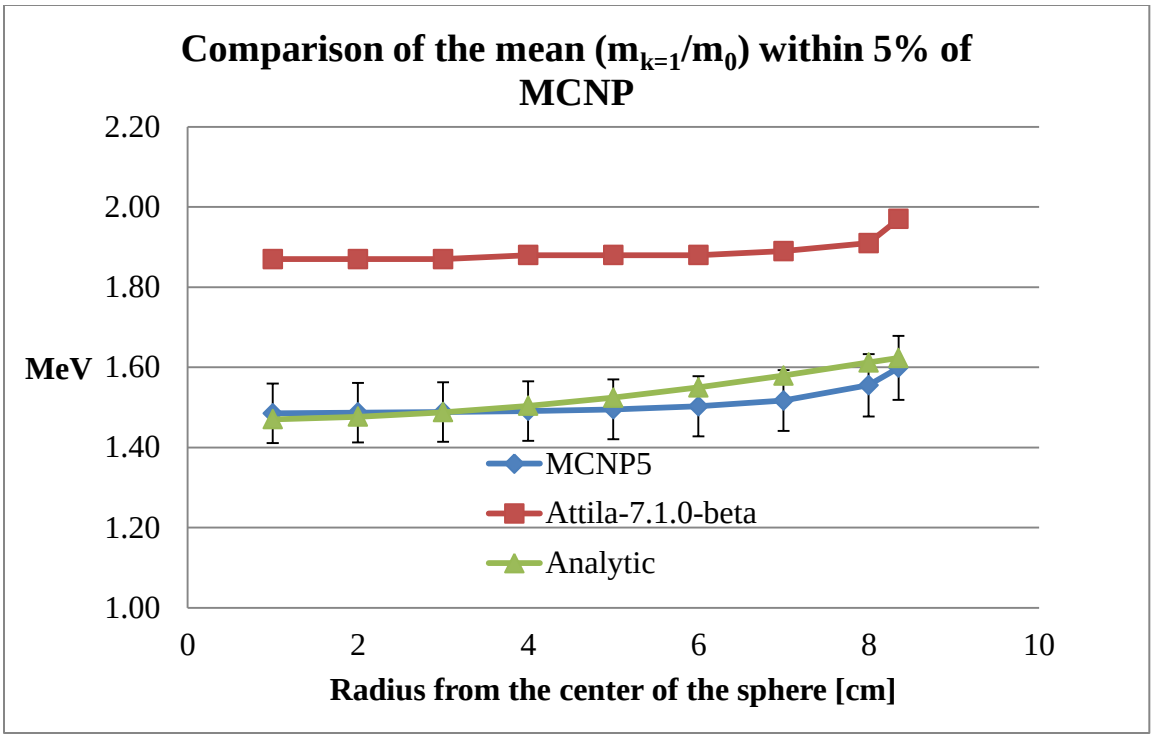

Figure 2.7 Comparison plot of the mean energy for the three computational methods

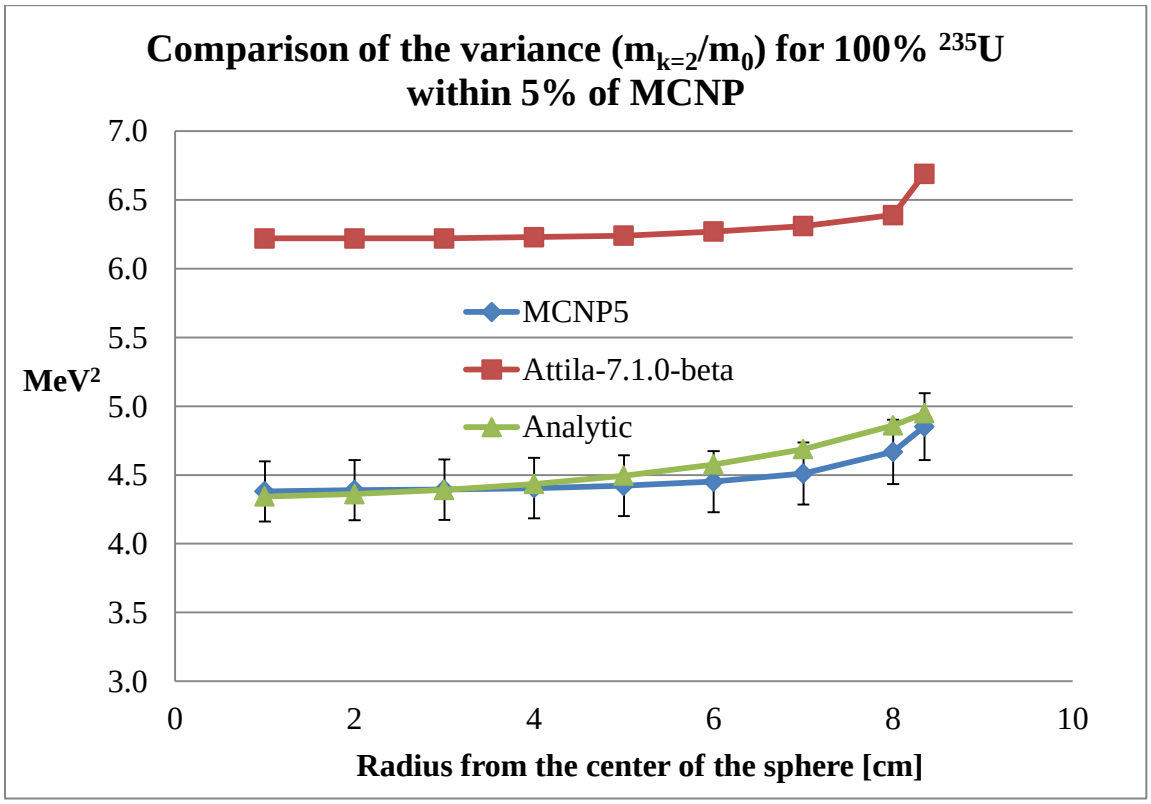

Figure 2.8 Comparison of the variance of energy for the three computational methods

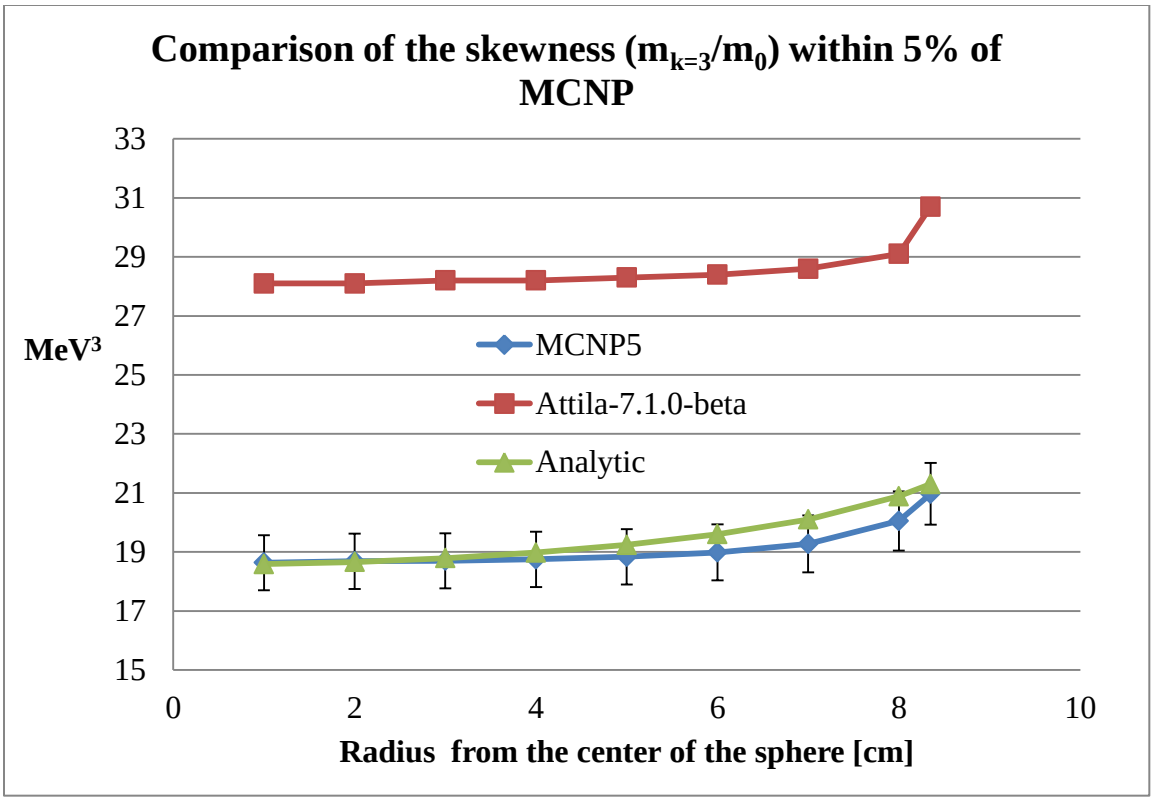

Figure 2.9 Comparison of the skewness of energy for the three computational methods

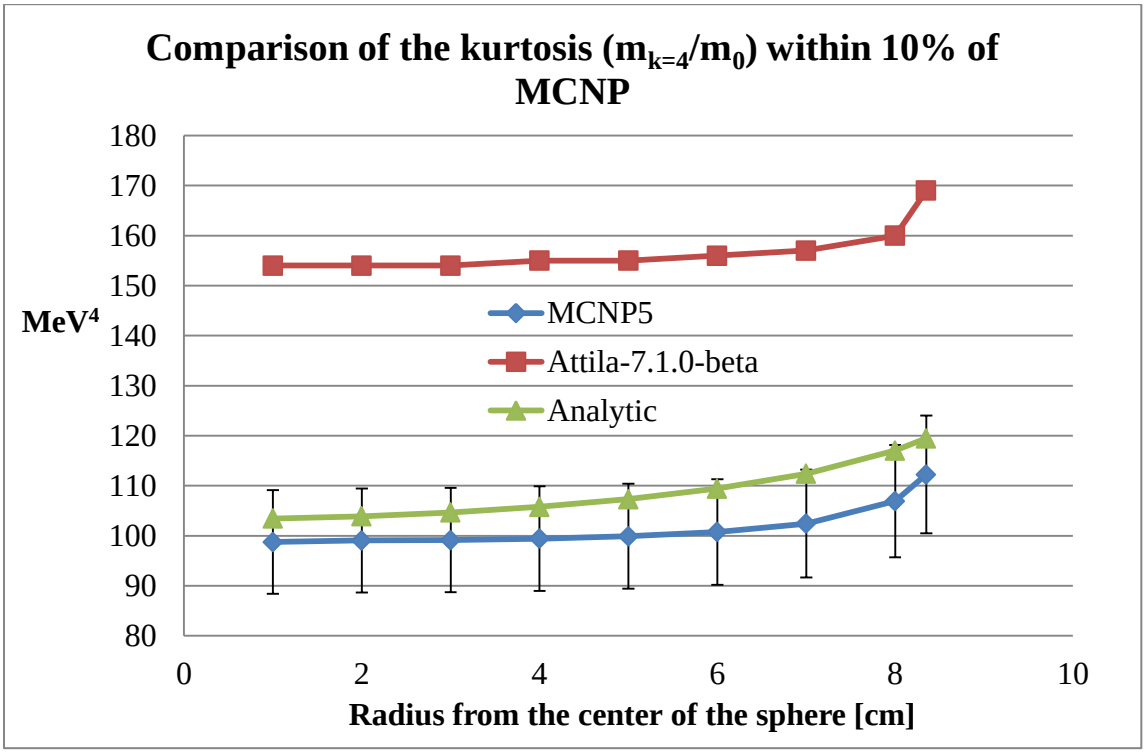

Figure 2.10 Comparison of the kurtosis of energy for the three computational methods

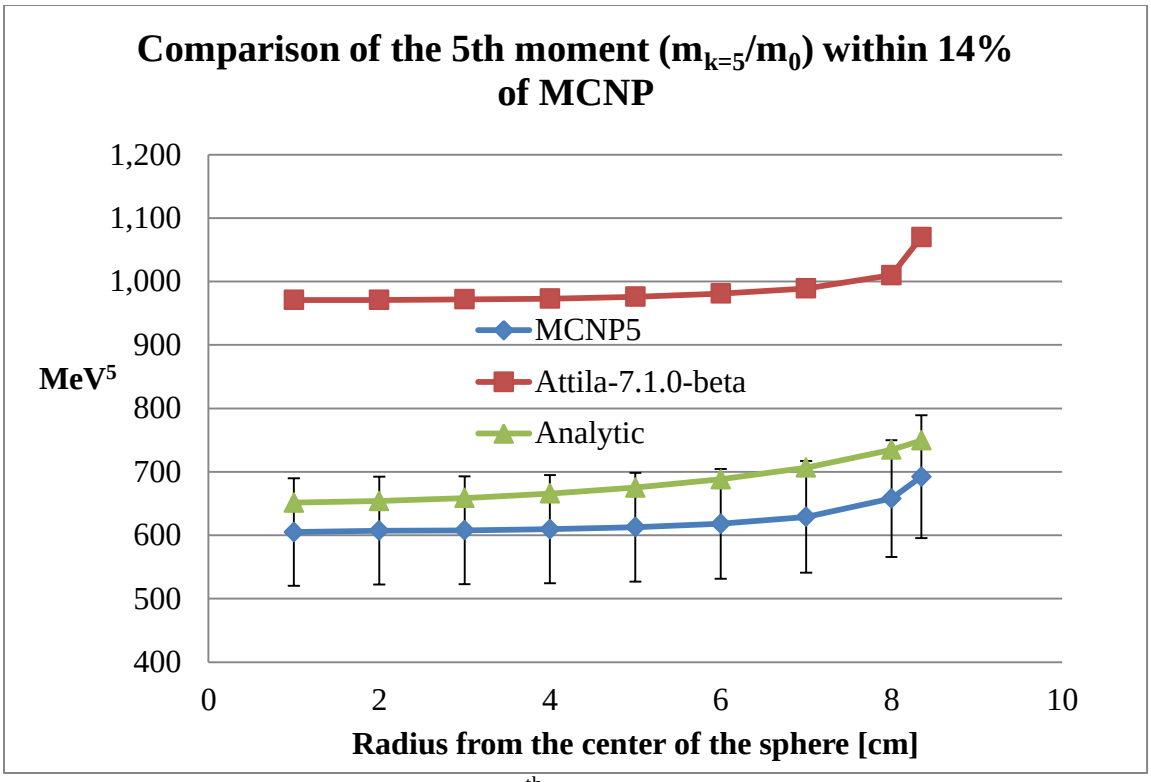

Figure 2.11 Comparison plot of the 5th energy moment for the three computational methods

The method of neutron energy moments does not assume a fission spectrum so the values of the moments are not shifted to that spectrum. Even though the method of neutron energy moments is diffusion based the comparison plots show a good agreement with the transport codes in general. The faster neutrons populate the edges of the system which is seen by the slightly higher average energy. The upturn seen in each moment in Figure 2.7 match physical expectations, the fast neutrons have a longer diffusion length which is the streaming effect seen for high energy neutrons.

Computing times for the three methods differed greatly: MCNP5 calculations were roughly a day, 26.3 hours, Attila computation times were 3-4 hours for a normal mesh of 0.01cm which gave about 100,000 mesh nodes and the method of moments is

analytic so the time frame is seconds to compute. The reason for the day time frame for MCNP was due to the high number of energy bins and particle histories needed to get in the 5% error range for the 1000 bins in the MCNP case. Extremely quick computational time frames are attractive especially when a multiphysics calculation is needed, so seconds compared to hours and days is a huge advantage for the method of moments.

The interesting thing about the analytic moments is that they start to peel away from the MCNP moments right around 3 mean free paths from the boundary of the sphere, about 5 cm (if 1.1cm is taken to be the average mean free path) and then correct back to the boundary value, due to the transport correction factor, r_o. Diffusion theory is valid in finite media at points that are more than a few mean free paths near the edge of the medium (Lamarsh, Introduction to Nuclear Reactor Theory, 1966, p. 129). The limitation of diffusion theory near the boundary of a source is noted and is not valid near the boundary which why it is transport corrected (Glasstone & Sesonke, 1967, p. 112). Even though diffusion theory has its limits the results agree very well with MCNP, the industry gold standard. For multiphysics-engineering type calculations having a continuous energy solution quickly only14% off in the highest moment that is within engineering limits, i.e., 20% is an excellent benefit that can be very useful to see multiphysics effects on nuclear reactors.

The shape of the functions for MCNP and Attila are very similar, the Attila moment functions have a sharper up turn and less of a parabolic shape which the analytic and MCNP moments have. The reason for this could be the group structure of the radion5 neutron cross section file. The authors are thankful for the use of the code from Transpire Inc and the corresponding cross section file. In general the cross section files for Attila

can be custom made for any neutronics problem. The authors felt that the radion5 file was appropriately suited to a fast spectrum critical assembly like the 100% ^{235}U sphere modeled in this work.

The dominate functional shapes that form the constants, CE's for the moments are from the last two summation terms in F(E), see equation 2.16. If the resonance region was not included it would not have changed the value of the analytic moments much for this case, because the contribution from the resonance summation was much smaller than the transition and fast region summations in equation 2.16. This makes sense for a fast reactor such as the theoretical sphere analyzed in this paper. The summation over index l from equation 2.16 does not contribute to the average energy (moment 1) at all and little to moments 2 to 5. A different functional shape might be more suited to fit the data better in this energy range, but the fit of F(E) to the ENDF-F(E) is good and the moments compare very well, so it might be that the fast reactor analyzed in this paper does not depend on the resonance region, so it would not affect the moment values. More work still needs to be done to see how reliable the method is for a broader set of reactor types.

Overall the analytic moments compare well with the two computational platforms; Monte Carlo and the 30-energy group, S_N order, P_N order, finite element code Attila. The higher moments tend to drift away from the MCNP moments and the error bars shows this, where the error range is 5% for the 1^{st} moment to 14% in the 5^{th} moment and no surprises the normalized 0^{th} moment is 1 for all three cases with 0% error, there is not a figure showing this.

The difficulty in finding continuous energy solutions with the multigroup method is the number of group equations to achieve an accurate solution which can be as high as

1000 (Duderstadt & Hamilton, 1976, p. 292). Continually iterating over the integrals of the neutron flux multiplied by the cross section until convergence is reached can be computationally expensive and Monte Carlo methods are very time intensive as well, although accurate. The method of neutron energy moments shown here is computationally cheap comparatively, only six equations to solve and diffusion equations which are relatively quick to solve computationally (Chapra & Canale, 2002) for many numerical methods.

Conclusions and Future Work

The EDNDE has been reformulated in terms of a moment equation and solved analytically for a 1-D sphere. The analytic moment solution to the EDNDE agrees quite with (MCNP5 and Attila) in terms of showing that the higher energy or faster neutrons populate the outer radius of the sphere where they leak out of the system. This leakage is seen by the upturn of all of the moments for all three solution methods at the outer radii of the sphere. The analytical moment results fall within the error bars associated with MCNP5 results for all moments (0 to 5) calculated. The analytical moment results are much more accurate than the 30 energy group Attila simulation because of the reasons stated in the Results and Discussion section of this paper.

Appendix: Constants for 100% ^{235}U F(E)

This appendix is the list of constants for each functional piece in the summations that make up F(E), equation 2.16. The energies, $Er_{l, m, n}$'s are listed in eV. The $Rp_{l, m}$'s are

listed in eV/cm^2. The Rp_n's are listed in eV^4/cm^2. The $w_{l,m}$'s are listed in eV^2. The w_n's are listed in eV^3. Table 2.4-2.6 shows the constants.

Table 2.4 list of the Rp_l's, Er_l's and w_l's for 100% ^{235}U

Rp_l's	Er_l's	w_l's	Rp_l's	Er_l's	w_l's	Rp_l's	Er_l's	w_l's
-1	0.206	8.0E-03	3.4	590.59	0.1	0.75	1308	0.11
0.5	0.2819	2.1E-03	0.4	594.94	0.05	0.2	1311.8	0.23
-70.25	0.25	5.5E-01	3	596.16	0.5	0.05	1315.05	0.2
9.521	8.78	1.8E-03	0.675	598.9	0.1	0.2	1317.07	0.2
-1.15	6.39	1.0E-03	0.35	600.3	0.1	0.1	1318.9	0.2
-0.55	4.85	2.0E-03	1	603.22	0.1	0.7	1320.87	0.2
0.175	1.12	1.5E-03	2	604.4	0.3	0.8	1323.3	0.25
-0.125	2.04	2.5E-03	0.3	608.46	0.1	0.3	1326.05	0.2
0.01	3.14	1.5E-03	1.45	610.21	0.1	0.4	1329.83	0.2
0.1025	3.6	1.5E-03	0.3	612.9	0.1	0.4	1332.23	0.2
-1.65	11.67	1.0E-03	0.3	615.43	0.1	0.8	1333.8	0.4
0.48	12.38	8.0E-04	0.3	616.89	0.1	0.2	1335.5	0.5
8	19.3	1.5E-03	0.725	619.02	0.1	0.5	1336.99	0.3
0.4	23.41	1.5E-03	0.2	626.6	0.1	0.25	1338.75	0.2
0.11	21.07	1.5E-03	0.75	628.99	0.1	1.2	1343.01	0.3
0.13	22.94	1.8E-03	0.3	630.8	0.1	4	1346.56	0.85
0.2	24.29	2.7E-03	0.3	631.69	0.1	0.9	1350.41	0.1
1	23.62	4.8E-03	0.4	633.64	0.1	0.35	1355.6	0.3
1.425	13.99	1.5E-02	0.4	635.41	0.1	0.65	1358.8	0.5
0.075	15.4	1.5E-03	-0.4	636.5	0.1	1.5	1360.37	0.2
-0.075	16.09	1.5E-03	0.7	639.14	0.2	0.6	1363.28	0.75
3.175	25.55	4.2E-02	0.7	641.17	0.2	0.6	1364.07	0.95
0.375	26.49	4.5E-03	2.9	644.96	0.1	0.4	1367.66	0.35
0.115	16.67	1.5E-03	0.8	646.65	0.1	2	1372.05	0.35
0.13	18.05	1.4E-03	0.025	648.83	0.02	0.05	1375.13	0.3
0.625	27.79	4.5E-03	0.1	653.07	0.1	0.4	1378.2	0.1
1.75	32.06	4.2E-03	0.35	656.4	0.3	0.35	1380.7	0.25
-0.15	30.89	5.2E-03	0.65	658.38	0.1	1.35	1382.1	0.3
0.25	33.55	5.2E-03	0.5	663.6	0.1	3.5	1387.6	0.6
1.675	34.38	4.5E-03	1.85	665.92	0.1	0.5	1390.26	0.25
15	35.18	6.5E-03	0.4	672.13	0.1	0.5	1393.8	0.35
1.75	34.87	7.5E-03	0.9	674.11	0.1	1	1395.3	0.8
3.15	39.4	7.0E-03	3.5	676.42	0.2	0.01	1396.16	0.15
-0.675	41.86	6.5E-03	8	678.07	0.6	0.3	1400.75	0.4
1	41.51	3.5E-02	1.75	681.79	0.1	0.3	1403.45	0.2
0.8	42.25	4.0E-02	0.15	683.82	0.1	0.5	1406.4	0.23
-0.3	42.7	3.0E-02	0.6	685.53	0.5	0.4	1410.5	0.22

Table 2.4 list of the Rp_l's, Er_l's and w_l's for 100% 235U continued

Rp_l's	Er_l's	w_l's	Rp_l's	Er_l's	w_l's	Rp_l's	Er_l's	w_l's
-0.07	43.36	6.0E-03	0.45	689.12	0.1	0.4	1415.29	0.18
0.65	189.5	2.5E-02	0.4	690.45	0.1	0.55	1418.47	0.18
1.01	192.32	1.3E-02	2.75	692.75	0.2	0.65	1421.17	0.18
0.6	194.18	2.5E-02	0.3	696.87	0.1	0.275	1423.63	0.2
2.65	198.5	7.5E-02	0.8	699.1	0.1	0.28	1425.77	0.2
3.05	200.28	2.0E-02	0.3	702.55	0.1	0.5	1427.2	0.4
1	203.73	4.5E-02	0.3	703.83	0.1	1.5	1430.07	0.17
0.95	206.99	2.5E-02	4	709.88	0.7	1.525	1433.53	1
-1.65	209.6	2.1E-02	0.3	715.75	0.1	-0.2	1436.27	0.5
1.15	213.65	1.5E-02	0.3	717.13	0.1	0.2	1439.5	0.5
0.25	217.105	2.1E-02	0.3	718.9	0.1	0.1	1442.53	0.5
5	220.62	7.5E-02	0.3	719.92	0.1	1.575	1431.75	1
2.5	221.69	1.0E-01	0.5	721.59	0.1	1.25	1445.29	0.2
0.55	223.16	1.5E-02	0.6	723.53	0.2	0.85	1449.75	0.28
-0.255	226.32	2.1E-02	0.2	727.41	0.1	1.25	1451.81	0.3
0.65	226.74	3.5E-02	0.65	729.38	0.1	0.25	1454.09	0.3
0.65	229.09	6.5E-02	7.3	733.36	0.1	0.4	1456.41	0.4
3.2	231.45	4.5E-02	0.4	737.69	0.1	1	1459.68	0.3
1	232.89	2.5E-02	0.5	739.95	0.1	0.1	1463.74	0.4
1	233.83	6.5E-02	-0.65	741.74	0.28	0.95	1465.65	0.34
4.3	241.16	6.5E-02	0.6	745.35	0.1	-0.2	1467.57	0.2
0.75	245.44	6.5E-02	0.4	747.06	0.1	0.2	1469.52	0.2
0.75	247.91	6.5E-02	0.2	750	0.1	0.3	1472.37	0.4
2	248.94	6.5E-02	0.2	751.22	0.1	0.6	1479.7	0.25
4	253.5	1.5E-01	0.5	754.05	0.1	0.25	1483.01	0.25
2	255.95	6.5E-02	1.6	758.84	0.1	0.5	1486.02	0.25
0.55	259.92	6.5E-02	0.25	761.71	0.1	0.4	1494.8	0.3
14.5	261.65	6.5E-02	0.25	762.87	0.1	0.35	1498.06	0.3
1.25	266.35	3.5E-02	2.5	766.31	0.25	0.2	1500.95	0.3
1	268.2	9.5E-02	0.1	767.99	0.1	0.45	1503.3	0.2
3.5	270.01	8.5E-02	0.3	770.88	0.1	-0.3	1504.85	0.2
3.5	272.78	8.5E-02	0.35	772.63	0.1	0.5	1507.83	0.2
1.85	276.78	2.0E-02	1.5	778.46	0.1	0.025	1509.93	0.2
2	279.84	6.5E-02	2.35	779.41	0.2	0.35	1511.82	0.2
0.35	287.38	4.5E-02	0.25	782.38	0.1	0.3	1520.17	0.2
4	289.46	1.0E-01	1.2	785.3	0.1	0.45	1524.9	0.3
0.15	295.93	4.0E-02	0.3	790.32	0.1	0.2	1527.7	0.3
0.075	298.5	5.3E-03	0.3	792.61	0.1	0.25	1530.29	0.3
0.15	302.79	4.0E-02	0.5	795.5	0.08	0.65	1533.32	0.3
0.2	43.96	7.5E-03	0.3	796.28	0.08	0.15	1535.37	0.3
1	44.61	1.3E-02	1.65	801.33	0.2	0.15	1538.43	0.15
1	46.93	9.8E-03	0.9	806.01	0.2	0.5	1541.51	0.15
1	47.93	2.6E-02	1.6	806.95	0.4	0.1	1546.39	0.5

Table 2.4 list of the Rp_l's, Er_l's and w_l's for 100% 235U continued

Rp_l's	Er_l's	w_l's	Rp_l's	Er_l's	w_l's	Rp_l's	Er_l's	w_l's
1.4	48.3	2.6E-02	0.05	810.11	0.08	1	1549.41	0.35
0.2	48.8	5.5E-03	0.55	812.757	0.3	0.05	1551.61	0.2
0.255	49.43	5.5E-03	1.45	815.11	0.5	0.2	1553.94	0.3
0.3	50.48	5.5E-03	0.25	817.9	0.1	0.7	1559.77	0.25
3.65	51.26	7.5E-03	0.65	818.9	0.2	1.5	1567.81	0.12
3.5	52.21	2.0E-02	0.15	821.86	0.08	0.2	1570.94	0.2
1.58	55.04	7.5E-03	0.05	823.55	0.08	0.5	1573.8	0.2
6	55.88	2.5E-02	0.05	825.51	0.08	0.5	1575.55	0.75
6.45	56.48	7.5E-03	0.05	828.5	0.08	0.7	1579.2	0.3
1.7	57.95	2.0E-02	0.05	830.13	0.08	0.9	1581.44	0.3
0.55	58.66	7.5E-03	0.675	837.15	0.15	0.3	1587.27	0.9
0.85	60.18	2.0E-02	0.9	843.03	0.3	1.075	1589.71	0.2
-0.55	64.3	1.0E-02	1.5	847.2	0.15	1.575	1594.4	0.2
6	70.43	2.5E-02	0.1	851.29	0.15	-0.7	1596.31	0.4
0.95	72.36	5.0E-03	0.05	852.8	0.1	0.4	1598.54	0.5
0.65	74.54	5.0E-03	0.05	854.9	0.1	0.05	1600.54	0.5
1.25	75.49	3.0E-02	0.1	858.3	0.1	1.35	1604.4	0.25
-0.2	82.63	1.0E-02	0.7	861.36	0.08	-0.35	1606.4	0.4
5.15	84.15	4.0E-02	0.7	862.68	0.08	0.1	1609.25	0.2
0.65	84.99	3.0E-02	0.3	866.17	0.08	0.05	1612.53	0.2
1.6	88.75	3.0E-02	0.75	867.95	0.08	0.4	1616.18	0.6
-1.5	94.07	1.0E-02	0.025	871.5	0.08	0.2	1619.7	0.3
-2.55	90.35	1.0E-02	0.3	875.45	0.08	0.5	1622.2	0.15
0.5	89.77	3.5E-02	0.4	879.06	0.15	0.875	1628.13	0.15
2.65	91.24	3.5E-02	0.4	881	0.15	-0.1	1630.18	0.15
0.75	92.52	3.5E-02	0.5	883.81	0.08	0.55	1633.9	0.18
1.5	98.07	2.5E-02	0.95	884.94	0.3	0.2	1637.74	0.6
0.35	77.5	2.0E-02	0.1	886.84	0.3	0.45	1639.98	0.3
0.5	78.08	2.0E-02	0.1	892.69	0.08	0.62	1644.06	0.18
0.5	80.34	3.0E-02	-0.4	803.71	0.4	1	1647	0.18
0.5	81.42	3.0E-02	2.05	897.16	0.15	0.3	1650	0.25
0.65	102.91	1.0E-02	0.6	899.73	0.15	0.1	1652.5	0.5
0.55	105.21	1.0E-02	0.6	902.9	0.15	0.875	1655.64	0.15
-0.6	107.62	1.0E-02	0.5	906.09	0.15	1.2	1663.81	0.23
0.25	305.06	4.0E-02	0.15	908.82	0.08	1.2	1665.9	0.24
-0.25	308.95	4.0E-02	0.2	910.46	0.08	0.3	1671.24	0.24
0.1	312.52	4.0E-02	-0.05	908.1	0.09	0.4	1672.77	0.15
0.075	313.55	4.0E-02	0.1	914.25	0.08	0.375	1675.12	0.2
1.25	315.35	6.5E-02	0.4	916.1	0.08	0.685	1679.47	0.18
0.25	319.66	4.0E-02	0.02	920.34	0.07	0.685	1681.55	0.22
1	323.56	6.5E-02	0.85	923.05	0.08	1.25	1683.76	0.21
1.5	324.28	5.5E-02	0.6	924.42	0.1	-0.475	1685.43	0.4
1	325.97	8.5E-02	0.075	926.53	0.08	0.7	1690.01	0.15

Table 2.4 list of the Rp_l's, Er_l's and w_l's for 100% 235U continued

Rp_l's	Er_l's	w_l's	Rp_l's	Er_l's	w_l's	Rp_l's	Er_l's	w_l's
-0.25	327.21	4.0E-02	0.35	929.56	0.08	-0.2	1695	0.4
0.25	329.27	4.0E-02	0.15	931.84	0.08	2.35	1699.63	0.15
0.1	330.6	4.0E-02	0.2	934.66	0.08	0.4	1701.95	0.35
0.3	332.44	4.0E-02	-0.2	940.09	0.3	0.25	1702.96	0.25
0.25	334.05	1.7E-02	0.75	941.91	0.08	0.075	1706.86	0.25
0.225	336.63	1.7E-02	0.15	944.72	0.1	0.17	1709.31	0.25
0.1	338.71	4.0E-02	0.5	947.39	0.08	0.3	1713.64	0.25
1.25	340.07	1.9E-02	0.15	949.25	0.1	0.4	1717.47	0.25
0.125	342.23	4.0E-02	0.9	951.6	0.25	0.1	1720.12	0.3
0.325	343.95	1.5E-02	0.5	957.19	0.08	0.65	1722.5	0.3
0.31	346.98	1.5E-02	0.1	959.78	0.08	1.25	1726.36	0.23
0.1	349.37	4.0E-02	-0.25	961.17	0.08	0.65	1731.66	0.22
0.1	350.73	4.0E-02	0.075	965.36	0.08	0.65	1735.01	0.3
0.2	351.65	4.0E-02	0.075	967.88	0.08	0.2	1738.22	0.4
0.25	353.14	3.8E-02	0.17	974.9	0.08	0.6	1741.22	0.2
0.25	355.33	2.3E-02	0.475	978.14	0.08	0.7	1745.56	0.2
-0.12	356.06	4.0E-02	0.5	980.58	0.2	1.32	1749.6	0.2
0.1	359.66	4.0E-02	0.5	983.69	0.2	0.6	1751.58	0.5
0.1	360.51	4.0E-02	0.6	984.99	0.2	0.2	1755.03	0.35
0.275	361.6	3.0E-02	0.1	986.79	0.08	1	1760.23	0.2
0.7	365.28	8.0E-02	0.2	990.9	0.08	1	1762.1	0.5
0.1	370.38	4.0E-02	0.1	993.05	0.08	1.2	1771.82	0.2
0.1	371.31	4.0E-02	0.1	998.23	0.08	0.3	1774.44	0.15
-0.25	372.6	4.0E-02	0.7	898.5	0.25	0.8	1777.28	0.25
0.125	373.14	4.0E-02	0.5	901	0.25	0.9	1779.3	0.25
0.165	377.72	4.0E-02	1	953	0.85	0.9	1783.3	0.3
1	379.81	3.5E-02	0.6	1001.05	0.08	1	1788.37	0.25
0.6	383.34	5.4E-02	0.1	1004.42	0.08	0.1	1791.43	0.2
0.85	387.48	4.0E-02	-0.1	1005.67	0.08	2	1794.88	0.22
-0.5	109.79	2.0E-02	0.225	1007.5	0.08	0.175	1799.53	0.4
0.15	113.55	1.0E-02	0.03	1010.49	0.08	0.5	1803.07	0.2
0.75	115.94	1.5E-02	-0.1	1011.24	0.15	0.3	1808.12	1
1.75	118.23	4.5E-02	-0.15	1014.7	0.08	0.75	1815.7	0.2
1.25	121.92	7.0E-03	0.12	1015.91	0.25	0.5	1819.56	0.3
0.45	124.75	3.5E-02	-0.1	1017.62	0.08	2	1821.9	0.25
5.5	125.98	7.5E-02	0.05	1019.08	0.25	0.4	1825.24	0.2
2	126.35	5.0E-02	-0.1	1020.1	0.08	0.3	1829.04	0.5
-0.5	125.5	1.5E-02	0.1	1022.77	0.25	0.3	1830.74	0.75
-0.15	129.9	1.5E-02	0.175	1025.15	0.08	0.75	1835	0.2
0.25	128.05	2.0E-02	0.1	1030.53	0.08	-0.8	1837.8	0.5
1	131.29	4.0E-02	0.455	1033.27	0.08	1.55	1839.86	0.3
1.4	132.08	7.5E-02	0.05	1036.5	0.08	0.2	1843.17	0.5
1.1	132.7	5.0E-02	1.1	1043.75	0.3	4	1849.52	0.42

Table 2.4 list of the Rp_l's, Er_l's and w_l's for 100% 235U continued

Rp_l's	Er_l's	w_l's	Rp_l's	Er_l's	w_l's	Rp_l's	Er_l's	w_l's
0.35	133.54	1.0E-02	0.825	1044.82	0.15	2.05	1857.55	0.2
3	135.25	2.5E-02	0.2	1049.66	0.08	0	1860.42	0.1
1.2	141.99	3.0E-02	0.9	1053.64	0.25	0.6	1863.3	0.3
0.75	145.54	1.0E-02	0.85	1056.08	0.25	0.3	1865.9	0.3
0.3	147.26	2.0E-02	0.15	1059.8	0.15	0.1	1868.3	0.3
1.2	149.06	3.0E-02	-0.138	1061.87	0.08	1.15	1871.36	0.18
0.35	149.88	3.0E-02	0.6	1064.03	0.3	0.295	1875.05	0.2
0.285	153.38	5.0E-03	1.25	1068.19	0.18	0.5	1877.8	0.6
0.25	154.83	3.0E-02	0.05	1071.4	0.06	0.9	1881.95	0.3
0.35	156.75	2.0E-02	0.05	1074.62	0.1	0.75	1885.1	0.2
0.55	158.51	5.0E-02	2.15	1076.83	0.23	1.2	1889.61	0.3
0.55	159.12	5.0E-02	2.1	1077.74	0.2	0	1893.33	0.5
-0.8	160.94	2.0E-02	0.1	1080.06	0.08	0.4	1897.04	0.2
1.45	163.6	2.5E-02	1	1082.56	0.3	0.55	1902.6	0.2
1.55	166.25	7.5E-02	0.6	1084.2	0.08	0.45	1906.65	0.3
0.85	168.02	2.5E-02	0.05	1086.75	0.08	0.2	1910.42	0.3
0.35	169.33	2.5E-02	0.8	1089.92	0.4	2.25	1915.5	0.3
2.75	174.48	8.5E-02	0.4	1093.28	0.08	2.3	1917.54	0.3
0.45	176.54	2.5E-02	0.4	1095.59	0.23	0.95	1922.7	0.3
3.75	177.54	1.9E-02	0.75	1097.5	0.3	0.7	1924.5	0.4
-0.3	178.54	2.5E-02	2	1100.16	0.3	0.6	1930.37	0.3
-0.25	179.42	2.5E-02	1.5	1103.44	0.3	0.6	1933.32	0.2
1.05	180.31	2.5E-02	0.075	1108.42	0.2	1.25	1937.95	0.3
0.65	181.99	6.5E-02	-0.04	1110	0.1	1.85	1940.64	0.2
0.7	392.17	4.0E-02	0.07	1111.2	0.1	1	1945.2	0.6
0.1	356.7	4.0E-02	-0.1	1113.62	0.3	0.4	1952.2	0.35
0.5	396.55	3.3E-02	0.1	1116.08	0.15	0.85	1955.3	0.3
0.1	402.18	3.5E-02	0.75	1118.3	0.3	1	1960.3	0.3
1.752	405.1	2.0E-01	0.35	1123.6	0.3	0.7	1963.67	0.3
0.3	408.45	5.0E-02	0.535	1126.11	0.5	3.2	1967.8	0.21
0.1	414.37	4.0E-02	0.425	1128.2	0.15	0.5	1972.71	1
0.25	415.34	5.0E-02	1.345	1132.3	0.1	2.2	1977.16	0.18
0.75	418.26	3.0E-02	0.15	1134.39	0.2	0.9	1979.7	0.28
0.35	419.83	4.0E-02	0.6	1136.48	0.35	0.2	1983.8	0.8
0.535	423.25	4.0E-02	2.645	1139.08	0.35	0.3	1985.8	0.5
0.425	425.46	4.0E-02	0.85	1143.43	0.1	1.1	1989.29	0.3
0.215	427.42	4.0E-02	1.7	1146.66	0.15	1.1	1993.6	0.2
0.15	428.83	4.0E-02	0.075	1149.9	0.15	0.3	1997.85	0.7
0.75	430.66	9.0E-02	0.1	1152.79	0.2	0.6	1999.84	0.7
1.2	433.81	4.0E-02	0.5	1156.1	1	1	2002.45	0.5
2	434.88	2.0E-01	1.1	1159.65	0.08	0.3	2006.36	0.5
0.3	439.14	4.0E-02	1.9	1161.5	0.28	0.6	2008.22	0.5
1.025	440.4	4.0E-02	3.8	1163.3	0.28	0.1	2010.9	0.3

Table 2.4 list of the Rp_l's, Er_l's and w_l's for 100% 235U continued

Rp_l's	Er_l's	w_l's	Rp_l's	Er_l's	w_l's	Rp_l's	Er_l's	w_l's
0.81	442.26	4.0E-02	2.5	1165.23	0.25	-0.18	2037.9	0.5
0.1	448.5	4.0E-02	1	1167.55	0.2	-0.27	2045.17	0.2
0.85	449.94	1.0E-01	0.6	1170.27	0.1	0.1	2042.43	0.4
0.3	453.7	4.0E-02	0.8	1172	0.1	0.75	2050.17	0.2
0.7	458.7	1.0E-01	0.5	1174	0.2	0.7	2053.18	0.19
1.5	462.02	1.0E-01	0.75	1175.99	0.2	2	2054.84	0.9
3.5	463.8	8.5E-02	0.1	1178.6	0.25	0.2	2058.85	0.6
0.05	466.53	2.0E-02	0.5	1180.7	0.3	0.4	2063.75	0.3
0.6	468.93	1.0E-01	1	1184.41	0.3	0.5	2067.31	0.35
0.75	471.77	4.0E-02	0.9	1187.46	0.25	0.4	2069.75	0.35
-0.1	476.53	4.0E-02	0.1	1190.1	0.08	1	2072.1	0.5
0.1	477.16	4.0E-02	0.1	1192.67	0.08	0.2	2081.23	1
1	479.23	3.8E-02	0.1	1194.18	0.08	0.75	2085.12	0.26
1.05	481.33	3.8E-02	0.4	1197.2	0.25	1	2090.43	0.6
0.2	483.51	5.5E-02	1.25	1200.8	0.1	2	2093.07	0.42
0.1	485.29	4.0E-02	0.3	1204.56	0.3	0.5	2095.29	0.4
0.2	487.1	4.8E-02	-0.35	1206.15	0.1	1	2099.65	1.65
0.4	489.46	5.5E-02	0.5	1207.49	0.35	-0.5	2106.22	1.25
0.6	490.47	5.5E-02	3	1214.2	0.35	0.5	2108.78	0.8
0.425	495.64	5.0E-02	0.175	1216.1	0.25	0.2	2118.2	0.7
1.65	500.28	1.0E-01	0.4	1220.19	0.2	0.75	2121.42	0.7
2	502.1	2.5E-01	0.6	1224.59	0.2	0.3	2124.65	0.5
2	503.36	2.5E-01	0.25	1225.88	0.2	0.75	2129.05	0.5
0.4	506.01	1.0E-01	0.75	1229.7	0.2	2.75	2134.61	0.5
0.4	507.89	5.0E-02	0.5	1232.86	0.4	0.2	2137.75	0.35
2.4	511.4	1.0E-01	0.4	1235.6	0.4	-0.35	2141.9	0.7
2.35	513.16	5.0E-02	0.1	1237.34	0.1	1.75	2145.14	0.4
1.2	519.76	1.0E-01	0.5	1239.65	0.2	0.85	2148.5	0.35
0.2	524.29	5.0E-02	0.75	1243.2	0.4	0.6	2153.21	0.4
0.3	528.03	5.0E-02	0.75	1248.2	0.4	0.4	2160.8	0.35
4	530.51	4.0E-01	0.3	1251.71	0.25	1	2164.15	0.5
0.3	535.33	9.0E-02	0.3	1254.05	0.25	0.7	2168.27	0.35
1	537.81	1.0E-01	0.2	1255.81	0.25	-0.45	2172.9	1
0.1	539.84	5.0E-02	0.45	1258.17	0.35	0.7	2179.37	0.4
0.23	542.15	5.0E-02	0.65	1263.12	0.25	4	2183.35	1.4
0.85	543.81	5.0E-02	0.15	1267.02	0.2	0.75	2189.31	0.23
1.15	546.19	5.0E-02	0.4	1268.31	0.3	0.1	2196.33	1
0.625	551.91	1.5E-01	0.4	1270	0.3	0.45	2199.99	0.75
2	557.77	1.5E-01	1.15	1272.95	0.1	0.75	2202.8	0.4
0.4	561.01	1.0E-01	0.25	1278.46	0.1	0.25	2207.17	0.7
0.3	564.73	9.0E-02	0.25	1280.37	0.1	4	2213.88	2
0.35	566.7	2.0E-01	0.35	1283.72	0.1	3.65	2216.99	1
0.75	570.98	5.0E-02	0.2	1287.5	0.5	1.15	2223.71	0.45

Table 2.4 list of the Rp_l's, Er_l's and w_l's for 100% 235U continued

Rp_l's	Er_l's	w_l's	Rp_l's	Er_l's	w_l's	Rp_l's	Er_l's	w_l's
3	572.56	8.5E-02	0.3	1290.61	0.1	1.15	2226.61	0.45
2	575.83	2.0E-01	1	1291.89	0.8	0.3	2233.24	0.45
3.9	577.64	3.0E-01	1.375	1296.89	0.25	0.3	2236.21	0.75
0.05	579.6	2.0E-02	1.375	1298.63	0.23	1.2	2240.52	0.9
3	585.5	3.0E-01	0.1	1300.78	0.1	0.5	2247.9	0.35
0.3	587.5	5.0E-02	1	1305.59	0.21	0.2	2250	0.1

Table 2.5 list of the Rp_m's, Er_m's and w_m's for 100% ^{235}U

Rp_m's	Er_m's	w_m's	Rp_m's	Er_m's	w_m's	Rp_m's	Er_m's	w_m's
2.5E-5	2.3E+3	8.0E+3	5.0E-6	8.0E+3	2.0E+4	1.0E-5	2.1E+4	1.6E+5
6.0E-5	2.5E+3	1.5E+4	5.0E-6	8.2E+3	2.0E+4	1.0E-5	2.2E+4	1.0E+5
1.5E-5	2.7E+3	8.5E+3	5.0E-6	8.4E+3	2.0E+4	1.0E-5	2.3E+4	2.6E+5
1.5E-5	2.9E+3	1.0E+4	5.0E-6	8.5E+3	2.0E+4	1.0E-5	2.4E+4	2.6E+5
1.5E-5	3.0E+3	1.0E+4	5.0E-6	8.7E+3	2.0E+4	1.0E-5	2.4E+4	2.6E+5
9.0E-6	3.2E+3	8.0E+3	5.0E-6	9.0E+3	2.0E+4	1.0E-5	2.4E+4	2.6E+5
2.0E-5	3.3E+3	1.0E+4	5.0E-6	9.2E+3	2.0E+4	1.0E-5	2.5E+4	5.0E+5
1.5E-5	3.5E+3	1.0E+4	5.0E-6	9.5E+3	2.0E+4	1.0E-5	2.5E+4	2.0E+5
1.5E-5	3.7E+3	1.0E+4	5.0E-6	9.6E+3	2.0E+4	1.0E-5	2.6E+4	3.0E+5
1.2E-5	3.8E+3	1.0E+4	7.0E-6	1.0E+4	5.0E+4	1.0E-5	2.6E+4	3.0E+5
8.0E-6	3.9E+3	1.0E+4	1.0E-4	1.0E+4	1.0E+6	1.0E-5	2.7E+4	3.0E+5
8.0E-6	4.0E+3	1.0E+4	1.0E-4	1.1E+4	1.0E+6	1.0E-5	2.8E+4	3.0E+5
8.0E-6	4.2E+3	1.0E+4	1.0E-4	1.1E+4	1.0E+6	1.0E-5	2.8E+4	3.0E+5
8.0E-6	4.3E+3	1.0E+4	5.0E-5	1.1E+4	1.0E+6	1.0E-5	2.9E+4	3.0E+5
8.0E-6	4.4E+3	1.0E+4	5.0E-5	1.2E+4	1.0E+6	1.0E-5	2.9E+4	3.0E+5
1.1E-5	4.5E+3	1.0E+4	5.0E-5	1.2E+4	1.0E+6	1.0E-5	3.0E+4	5.0E+5
8.0E-6	4.8E+3	1.0E+4	5.0E-5	1.2E+4	1.0E+6	1.0E-5	3.1E+4	5.0E+5
8.0E-6	5.0E+3	1.0E+4	5.0E-5	1.3E+4	1.0E+6	1.0E-5	3.2E+4	5.0E+5
8.0E-6	5.2E+3	1.0E+4	5.0E-5	1.3E+4	1.0E+6	1.0E-5	3.2E+4	5.0E+5
8.0E-6	5.4E+3	1.0E+4	5.0E-5	1.3E+4	1.0E+6	1.0E-5	3.3E+4	5.0E+5
8.0E-6	5.5E+3	1.0E+4	5.0E-5	1.3E+4	1.0E+6	1.0E-5	3.4E+4	5.0E+5
5.0E-6	5.6E+3	1.5E+4	5.0E-5	1.4E+4	1.0E+6	1.0E-5	3.5E+4	5.0E+5
5.0E-6	5.7E+3	1.5E+4	5.0E-6	1.4E+4	1.0E+6	1.0E-5	3.6E+4	5.0E+5
5.0E-6	5.8E+3	1.5E+4	5.0E-6	1.5E+4	7.0E+4	1.0E-5	3.7E+4	6.0E+5
5.0E-6	6.0E+3	1.5E+4	5.0E-6	1.5E+4	7.0E+4	1.0E-5	3.8E+4	6.0E+5
5.0E-6	6.2E+3	1.5E+4	5.0E-6	1.5E+4	7.0E+4	1.0E-5	3.9E+4	6.0E+5
5.0E-6	6.4E+3	1.5E+4	1.0E-5	1.6E+4	7.0E+4	1.0E-5	4.0E+4	6.0E+5
5.0E-6	6.5E+3	1.5E+4	1.0E-5	1.7E+4	7.0E+4	1.0E-5	4.1E+4	6.0E+5

Table 2.5 list of the Rp_m's, Er_m's and w_m's for 100% ^{235}U continued

Rp_m's	Er_m's	w_m's	Rp_m's	Er_m's	w_m's	Rp_m's	Er_m's	w_m's
5.0E-6	6.8E+3	2.0E+4	7.5E-6	1.8E+4	7.0E+4	5.0E-2	5.0E+4	1.1E+9
5.0E-6	7.0E+3	2.0E+4	7.5E-6	1.9E+4	1.0E+5	5.6E-2	1.5E+5	1.1E+10
5.0E-6	7.3E+3	2.0E+4	7.5E-6	1.9E+4	7.0E+4	7.0E-2	3.0E+5	4.4E+10
5.0E-6	7.4E+3	1.0E+4	1.0E-5	2.0E+4	1.6E+5	1.2E-1	5.0E+5	4.9E+11
5.0E-6	7.5E+3	1.0E+4	1.0E-5	2.0E+4	1.6E+5	6.2E-1	9.0E+5	1.0E+12
5.0E-6	7.7E+3	2.0E+4	1.0E-5	2.1E+4	1.6E+5			

Table 2.6 list of the Rp_n's, Er_n's and w_n's for 100% ^{235}U

Rp_n's	Er_n's	w_n's
1.25E+12	1.00E+6	5.00E+22
6.50E+11	3.00E+6	1.70E+18
1.00E+10	4.00E+6	9.00E+16
2.10E+10	5.00E+6	9.00E+16
1.10E+10	6.00E+6	4.00E+16
1.50E+10	7.00E+6	2.50E+16
9.00E+9	8.00E+6	1.30E+16
8.00E+9	9.00E+6	1.00E+16
5.00E+8	1.00E+7	6.00E+14

References

Bin-Wan, C., & Ring, T. A. (October 2006). Verification of SMOM and QMOM Population Balance Modeling in CFD code Using Analytical Solutions for Batch Particulate Processes. *China Particuology*, 243-249.

Casella, G., & Berger, R. L. (2002). *Statistical Inference 2nd Edition.* Pacific Grove, CA, USA: Wadsworth Group Duxbury.

Chapra, S. C., & Canale, R. P. (2002). *Numerical Methods for Engineers with Software and Programming Applications fourth Edition.* New York: McGraw Hill.

Cho, N. Z. (February 2008). Fundamentals and Recent Developments of Reactor Physics Methods. *Nuclear Engineering and Technology*, 25-78.

Duderstadt, J. J., & Hamilton, L. J. (1976). *Nuclear Reactor Analysis.* United States: John Wiley & Sons, Inc.

Edwards, H. C., & Penney, D. E. (2001). *Differential Equations & Linear Algebra.* Upper Saddle River: Prentice Hall.

Foster, A. R., & Wright, R. L. (1977). *Basic Nuclear Engineering 3rd Edition.* Boston: Allyn and Bacon.

Glasstone, S., & Sesonke, A. (1967). *Nuclear Reactor Engineering.* New York: D. Van Nostrand Company.

INL NEA/NSC DOC(95)03. (September 2009). *International Handbook of Evaluated Criticality Safety Benchmarks.* INL: NEA/NSC.

Institute, K. A. (2000, October 1). *Table of Nuclides*. Retrieved July 5, 2011, from Table of Nuclides: http://atom.kaeri.re.kr/

Kenny, J. F. (1947). *Mathematics of Statistics 2nd Edition.* New York: D. Van Nostrand Company Inc.

Lab, L. A. (2000, July 5). *ENDF/B-VII Incident-Neutron Data*. Retrieved July 5, 2011, from ENDF/B-VII Incident-Neutron Data: http://t2.lanl.gov/data/neutron7.html

Lab, L. A. (2008). *A General Monte Carlo N-Particle Transport Code-Version 5.* Los Alamos: Los Alamos National Lab LA-UR-08-8617.

Lamarsh, J. R. (1966). *Introduction to Nuclear Reactor Theory*. Reading, Massachusetts, USA: Addison-Wesley Publishing Company.
Lamarsh, J. R., & Baratta, A. J. (2001). *Introduction to Nuclear Engineering Third Edition.* Upper Saddle River, New Jersey USA: Prentice Hall.

Lewis, E., & Miller, W. J. (1993). *Computational Methods of Neutron Transport.* La Grange Park, IL USA: American Nuclear Society.

Lockheed Martin/ Knolls Atomic Power Laboratory. (2002). *Chart of the Nuclides and Isotopes 16th Edition.* New York: Lockheed Martin/ Knolls Atomic Power Laboratory.

Marchisio, D. L., Pikturna, J. T., & Fox, R. O. (May 2003). Quadrature Method of Moments for Population-Balance Equations. *AIChE*, 1267-1276.

Marchision, D., Virgil, D. R., & O., F. R. (August 2003). Implementation of the Quadrature Method of Moments in CFD codes for Aggregation-Breakage Problems. *Chemcial Engineering Science*, 3337-3351.

McGraw, R. (1997). Description of Aerosol Dynamics by the Quadrature Method of Moments. *Aerosol Science and Technology*, 255-265.

Morry, S., & Williams, M. (1972). Neutron Flux Perturbations Due to Absorbing Foils. *Journal of Applied Physics*, 6-18.

Sevast'yanov, V., Koshelev, A., & Maslov, G. N. (2000). Representation of the Fission Spectrum of 235U, 239Pu and 252Cf and the Reactor Spectrum as a Superpostition of Five Inelastic Scattering Functions. *Atomic Energy*, 292-299.

Weinberg, A. M., & Wigner, E. P. (1958). *The Physical Theory of Neutron Chain Reactors.* Chicago: The University of Chicago Press.

CHAPTER 3

VALIDATION OF ENERGY MOMENTS FROM THE ONE-DIMENSIONAL ENERGY DEPENDENT NEUTRON DIFFUSION EQUATION, MCNP5 AND ATTILA-7.1.0 WITH THE GODIVA EXPERIMENT

Introduction

This work is focused on validating the method of moments for the EDNDE with GODIVA as well as further the development of the method by investigating the method of moments on a system of more than one isotope. Analytic energy moments derived for a pure 100% sphere of ^{235}U has been verified with MCNP5 and Attila based on the method of moment approach. The derivation for the method of moments for the EDNDE is not discussed here but can be found in literature (Crawford & Ring, submitted 2012). Equation 3.1 is the basis of the normalized moments in this work.

$$\frac{1}{v}\frac{\partial\phi(\vec{r},E,t)}{\partial t} - \nabla D(\vec{r},E)\nabla\phi(\vec{r},E,t) + \Sigma_{\mathrm{t}}(\vec{r},E)\phi(\vec{r},E,t) = \int_0^\infty \Sigma_{\mathrm{s}}\left(\vec{r},E\rightarrow \acute{E}\right)\phi\left(\vec{r},\acute{E},t\right)d\acute{E} + \chi(E)\int_0^\infty \nu\left(\acute{\mathrm{E}}\right)\Sigma_{\mathrm{f}}\left(\vec{r},\acute{\mathrm{E}}\right)\phi\left(\vec{r},\acute{E},t\right)d\acute{E} \qquad \text{Equation 3.1}$$

The method of moments (MOM) approach solves for the moments of a distribution instead of the distribution itself. MOM can be considered to be a deterministic method to find stochastic parameters. The neutron flux can be treated as a

probability density function (PDF), where the normalized moments provide the mean, variance, skewness and kurtosis (Kenny, 1947) of the flux so once the moments are solved for they can be put into the correct PDF or PDF reconstruction method to reproduce the flux. Mathematically the mean, variance, skewness and kurtosis (Casella & Berger, 2002) for the energy variable of the neutron flux are represented here where ϕ in equations 3.2-3.5 represents the energy dependent neutron flux $\phi(\vec{r}, E, t)$:

$$mean = \frac{\int_0^\infty E*\phi dE}{\int_0^\infty \phi dE}, \quad \text{Equation 3.2}$$

$$variance = \frac{\int_0^\infty E^2*\phi dE}{\int_0^\infty \phi dE} \quad \text{Equation 3.3}$$

$$skewness = \frac{\int_0^\infty E^3*\phi dE}{\int_0^\infty \phi dE} \quad \text{Equation 3.4}$$

$$kurtosis = \frac{\int_0^\infty E^4*\phi dE}{\int_0^\infty \phi dE} \quad \text{Equation 3.5}$$

To help determine the proper PDF or PDF reconstruction method, neutron energy moments need to be validated.

This paper compares energy moments from three different numeric methods, with energy moments from the GODIVA experimental data. GODIVA is a well-documented experiment. Two documents were used as the foundation for the details of the computer/mathematical model creation of GODIVA in MCNP5, Attila and the EDNDE. The first document is from the International Handbook of Evaluated Criticality Safety Benchmark Experiments (INL NEA/NSC DOC(95)03, September 2010) and the second is a report outlining experiments done to measure ^{235}U fission spectrum at the core center and on the surface of GODIVA (McElroy, Armani, & Tochilin, 1969). This report is referred to as the McElroy report for the rest of the paper.

A complete comparison of energy moments is achieved from the three different methods: the two well-known computational platforms are; MCNP5 and Attila, the third is energy moments derived from the one-dimensional energy dependent neutron diffusion equation (EDNDE). All three methods are compared to moments from the data in the McElroy report. MCNP5 and Attila are full neutron transport codes. MCNP5 is based on the Monte Carlo numerical method. Attila is a customizable energy group, S_N, P_N, finite element code. EDNDE is based on a moment transformation of equation 3.1. The GODIVA model made in Attila used a 30 group library file named radion5.

Table 3.1 displays the group structure of the flux calculations performed in the Attila-7.1.0-beta software. The group structure in the radion5 file seems suitable for a fast reactor or fast critical assembly calculation, which GODIVA is a fast critical assembly. The greater number of energy groups in the fast region should capture the flux behavior for this situation. 30 energy groups are enough groups to demonstrate a multigroup method sufficiently to make the comparisons with the other two methods.

Table 3.1 Energy Group Structure for GODIVA Model in Attila-7.1.0-beta

Group #	Energy range MeV		Group #	Energy range MeV		Group #	Energy range MeV	
1	20	17	11	7.79	6.87	21	8.21E-1	2.35E-1
2	17	16	12	6.87	6.07	22	2.35E-1	6.74E-2
3	16	15	13	6.07	5.35	23	6.74E-2	1.93E-2
4	15	13.9	14	5.35	4.72	24	1.93E-2	5.53E-3
5	13.9	13.0	15	4.72	3.68	25	5.53E-3	3.54E-4
6	13.0	12.0	16	3.68	2.87	26	3.54E-4	2.26E-5
7	12.0	11.0	17	2.87	2.23	27	2.26E-5	3.47E-6
8	11.0	10.0	18	2.23	1.74	28	3.47E-6	6.25E-7
9	10.0	8.82	19	1.74	1.19	29	6.25E-7	1.24E-8
10	8.82	7.79	20	1.19	8.21E-1	30	1.24E-8	1.0E-11

Simplification of Energy Dependent Neutron Diffusion Equation

Equation 3.1 is solved over the entire fission spectrum; which is well approximated to be from 0 to 10 MeV (Lamarsh, 1966). This analysis assumes steady state so the time dependent term, $\frac{1}{v}\frac{\partial\phi(\vec{r},E)}{\partial t}$ is set equal to zero. GODIVA is assumed to be homogenous so the energy dependent cross sections and diffusion coefficient depend on energy only. The entire population of neutrons is treated as one large energy group E, from 0 to 10MeV. The differential scattering cross section $\left(\Sigma_s\left(\vec{r}, E \rightarrow \acute{E}\right)\right)$ is defined such that integration from 0 to infinity $\left(\int_0^\infty \Sigma_s\left(\vec{r}, E \rightarrow \acute{E}\right) = \Sigma_s(\mathrm{E})\right)$, the probability of scattering into E is unity and yields Σ_s (E) (Duderstadt & Hamilton, 1976). It is assumed that scattering into "E" is unity for this paper. The fission spectrum integrated from 0 to infinity is unity $\left(\int_0^\infty \chi(E)\, dE = 1\right)$. The assumption is that the energy dependence of the cross sections over the range of interest, 0 to 10MeV is retained and the result of the two assumptions yields equation 3.6.

$$-D(E)\nabla^2\phi(\vec{\mathrm{r}},\mathrm{E}) + \Sigma_a(\mathrm{E})\phi(\vec{\mathrm{r}},\mathrm{E}) = \nu(\mathrm{E})\Sigma_f(\mathrm{E})\phi(\vec{\mathrm{r}},\mathrm{E}) \qquad \text{Equation 3.6}$$

We have assumed diffusion theory is applicable and consider only the 1-D analytic solution, for the EDNDE moments based on the shape (sphere) and isotopic concentrations of the GODIVA experiment. Neutron diffusion theory is well documented in literature; (Duderstadt 1976, Foster 1977, Lamarsh 2001, Lewis1993, Weinberg 1958…) and is not discussed in detail here. An average angle of scatter for the neutrons (μ) is also assumed and included in the neutron diffusion coefficient. This method does not assume any distribution to develop the cross sections or a specific spectrum for fission as a weighting value per energy group, which makes this method very unique, the

analysis does cut off at 10MeV since this value captures 100% of the fission spectrum. The neutron flux above that energy is very small and assumed to be negligible. The last assumption is to lump all of the energy dependent cross sections and parameters into one function of energy F(E). Equation 3.7 and 3.8 show the results of the stated assumptions.

$$\nabla^2\phi(\vec{r},\mathrm{E}) + \left(\frac{\nu(\mathrm{E})\Sigma_f(\mathrm{E})-\Sigma_a(\mathrm{E})}{\mathrm{D(E)}}\right)\phi(\vec{r},\mathrm{E}) = 0 \qquad \text{Equation 3.7}$$

$$\mathrm{F(E)} = \frac{\nu(\mathrm{E})\Sigma_f(\mathrm{E})-\Sigma_a(\mathrm{E})}{\mathrm{D(E)}} = 3(\nu(E)\Sigma_f(\mathrm{E}) - \Sigma_a(\mathrm{E}))(\Sigma_t(\mathrm{E}) - \bar{\mu}\Sigma_s(\mathrm{E})) \qquad \text{Equation 3.8}$$

The derivation of the analytic moments from the EDNDE for GODIVA is shown in the next section. An overall energy dependent function F(E) is also derived for the isotopic mix of GODIVA.

Derivation of F(E) and Neutron Energy Moments for GODIVA

An appropriate approximation to the energy dependency of the macroscopic cross sections and the diffusion coefficient is vital for any flux calculation; so a set of functions and constants have been carefully chosen so the energy dependent functionality is retained as much as possible and allow an analytic solution to be found. The macroscopic cross sections may generally be divided into three distinct regions: thermal, resonance and fast, and in this paper the authors consider a 4th region called the transition region and it spans from 2300eV to 1MeV. The reason for the subdivisions is explained in more detail below.

The 1/v or 1/E$^{1/2}$ law is a good approximation to the thermal region of many isotopes and found to be mathematically viable in foil activation (Morry & Williams, 1972). The cross section data referred to and in use for this paper is from the evaluated nuclear data files, ENDF information is found on the web at http://atom.kaeri.re.kr/

(Institute, 2000) and http://t2.lanl.gov/data/neutron7.html) (Lab, ENDF/B-VII Incident-Neutron Data, 2000). In the resonance region, a summation of functions similar to Breit-Wigner single level resonance formulas is used to capture the complicated energy dependence in the resonance region. The functional piece that dominates the Breit-Wigner formulas is this $\left(\frac{\text{Constant}_1}{(E-E_r)^2+\text{Constant}_2}\right)$ term (Lamarsh, Introduction to Nuclear Reactor Theory, 1966, pp. 43-64). The cross sections for many isotopes in the transition region to the fast region generally has a 1/E drop off rate (Weinberg & Wigner, 1958, p. 57) and the fast region (0.1MeV to 10MeV) has a $1/E^{5/2}$ with some broad resonances. The broad resonances give the fast region of $^{235}U\ \Sigma_f\ (E)$ somewhat of a stair step like shape from 1MeV to 20MeV.

It is very difficult to fit an analytic function to the resonance region and the broad resonance region. The number of resonance peaks makes writing a function for each peak a daunting task, but with patience a resonance function can be written for each peak. A resonance peak function has been written for 962 resonances in this work for the GODIVA F(E), see Appendix: Constants for GODIVA. A summation of these single level resonance functions was assembled to provide a functional form, that when integrated over the function would provide correct values when compared to the resonance values from The Chart of the Nuclides and Isotopes 16th Edition (Lockheed Martin/ Knolls Atomic Power Laboratory, 2002). The functional approximations for the energy dependent cross sections are somewhat crude but "if we choose the group constants properly, even one-speed diffusion theory could give an accurate description of nuclear reactor behavior" (Duderstadt & Hamilton, 1976, p. 295).

The general functional relationships for D(E), ν(E), Σ_f (E), Σ_T (E) , Σ_S(E) and Σ_a(E) with energy are incorporated into one function of energy F(E). This work only shows curve fits of F(E) for the isotopic mix in GODIVA. The derived F(E) is fit to ENDF-F(E) with the appropriate function fit for the different energy ranges. The result of the curve fit of F(E) is shown in equation 3.16 and Figures 3.1-3.5.

It is assumed the total macroscopic cross section, the transport cross section, the function ν(E) (the number of prompt neutrons released in fission by an incident neutron of energy E), the neutron diffusion coefficient and the average angle of scatter are:

$$\Sigma_{i,t}(E) = \Sigma_{i,a}(E) + \Sigma_{i,s}(E) \quad \text{Equation 3.9}$$

$$\Sigma_{i,tr}(E) = \Sigma_{i,t}(E) - \bar{\mu}_i \Sigma_{i,s}(E) \quad \text{Equation 3.10}$$

$$D_i(E) = \frac{1}{3\Sigma_{i,tr}(E)} = \frac{1}{3\left(\Sigma_{i,t}(E) - \bar{\mu}_0 \Sigma_{i,s}(E)\right)} \quad \text{Equation 3.11}$$

$$\nu(E) = \nu_s E + \upsilon_{s0} \text{ for } 0 \le E \le 1\text{MeV} \quad \text{Equation 3.12}$$

$$\nu(E) = \nu_f E + \upsilon_{f0} for\ E > 1MeV \quad \text{Equation 3.13}$$

$$\bar{\mu}_0 = \frac{\sum_i^N \omega_i A_i \cdot \bar{\mu}_i}{\sum_i^N \omega_i A_i},\ \bar{\mu}_i = \frac{2}{3A_i},\ \omega_i = \text{atom fraction},\ N = 3 \text{ for GODIVA} \quad \text{Equation 3.14}$$

The parameter, A_i in equation 3.14 is the atomic mass number of isotope, (i), N in equation 3.14 is the total number of isotopes in the reactor, for GODIVA N = 3. The convention for a mix of isotopes is equation 3.15.

$$\Sigma_{system} = \Sigma_j^{^{235}_{92}U} + \Sigma_j^{^{238}_{92}U} + \Sigma_j^{^{234}_{92}U} \quad \text{Equation 3.15}$$

Index j in equation 3.15 is the subscript to represent the specific nuclear reaction: fission (f), scatter (s), absorption (a), etc… This convention is used to calculate the system cross sections for GODIVA. Equation.3.14 is a decent approximation for the average angel of scatter, $\bar{\mu}$ for large atoms, A>16. The function ν(E) is approximated for

the isotopic mix of GODIVA where the ν(E) parameters for ^{235}U is $\nu_s = 0.066$, $\upsilon_{s0} = 2.432$, $\nu_f = 0.15$ and $\upsilon_{f0} = 2.349$ (Duderstadt & Hamilton, 1976, p. 61) if the energy variable is in units of MeV. The parameters of ν(E) for ^{238}U are $\nu_s = 0.16$, $\upsilon_{s0} = 2.3$ for all energies (Lamarsh, Introduction to Nuclear Reactor Theory, 1966, pp. p96 Table 3-5) and for ^{234}U $\nu_s = 0.117$, $\upsilon_{s0} = 2.45$ for all energies. The slope and intercept of ν(E) for ^{234}U are derived from the data provided by Los Alamos National Lab (Lab, ENDF/B-VII Incident-Neutron Data, 2000); the energy variable is in units of MeV. The parameters of ν(E) for the isotope mix of GODIVA are $\nu_s = 0.071$, $\upsilon_{s0} = 2.425$, $\nu_f = 0.15$ and $\upsilon_{f0} = 2.347$.

Figures 3.1 through 3.6 show comparisons of equation 3.16 with the ENDF-F(E). Figure 3.1 shows the thermal region from 1E-5eV to 1eV on a log-log plot. The first term in equation 3.16 is the dominate feature in Figure 3.1. The first resonance for the GODIVA F(E) is also seen in Figure 3.1. Figure 3.2 shows a comparison of ENDF-F(E) to equation 3.16 for GODIVA in the energy range of 1eV to 100eV to show the largest resonance peaks. Figure 3.3 shows the resonance region from 100eV to 1000eV of the cross section for GODIVA. Equation 3.16 is not as sharp as the ENDF-F(E) in the overlap spaces between each resonance peak. Figure 3.4 explicitly shows the difference between the ENDF-F(E) and the derived F(E) by showing the difference in the overlap of the resonance peaks. Figures 3.2-3.5 are not put on log-log plots to point out the negative regions that show up from the $\nu(E)\Sigma(\mathrm{E})_{\mathrm{f}} - \Sigma(\mathrm{E})_{\mathrm{a}}$ term in F(E), where the absorption cross section is greater than the product of $\nu(E)\Sigma(\mathrm{E})_{\mathrm{f}}$. Figure 3.5 (1000eV to 2250eV) and Figure 3.6 (2250eV to 10MeV) show the difference between ENDF-F(E) and the derived F(E) for the end of the energy range of the GODIVA cross sections.

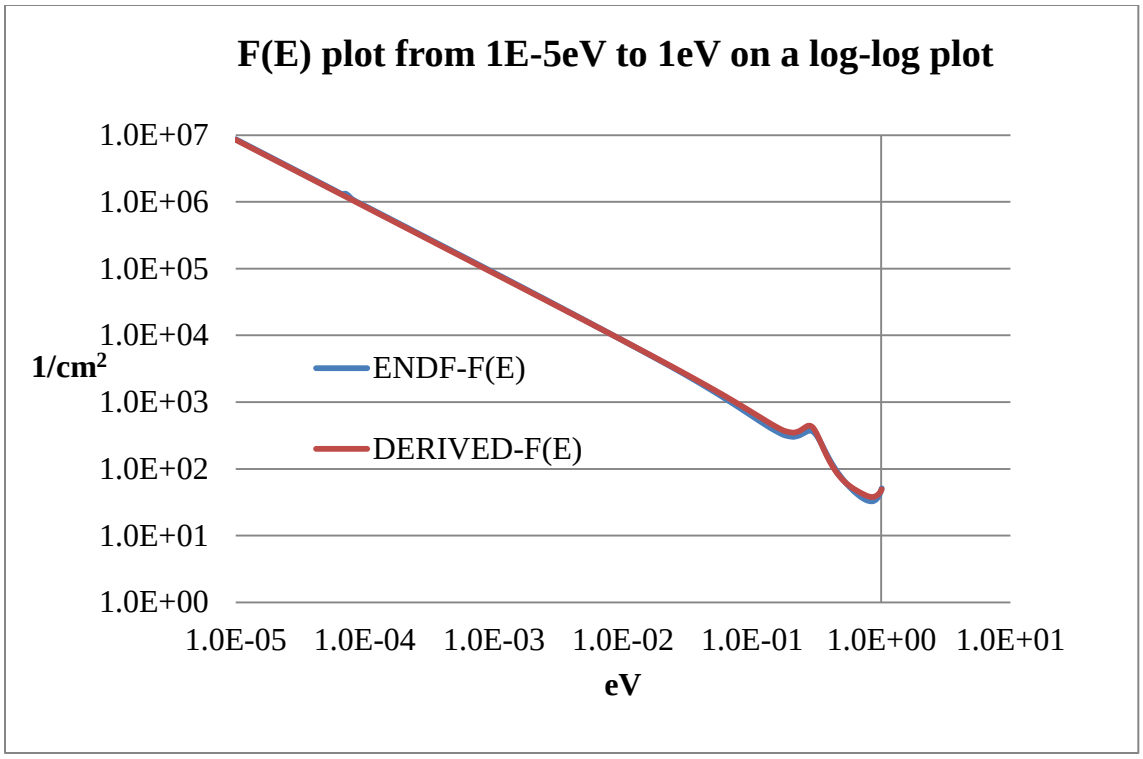

Figure 3.1 Log-log plot of GODIVA F(E) from 1E-5eV to 1eV

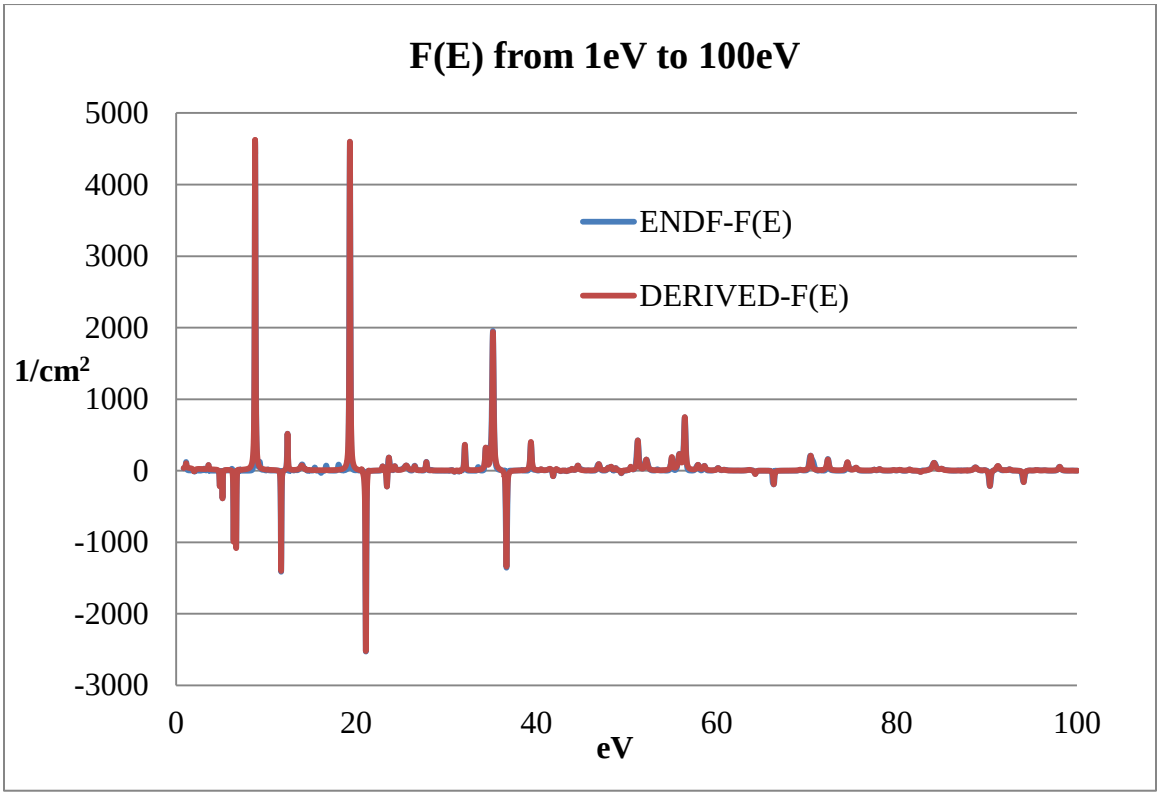

Figure 3.2 Plot of GODIVA F(E) from 1eV to 100eV

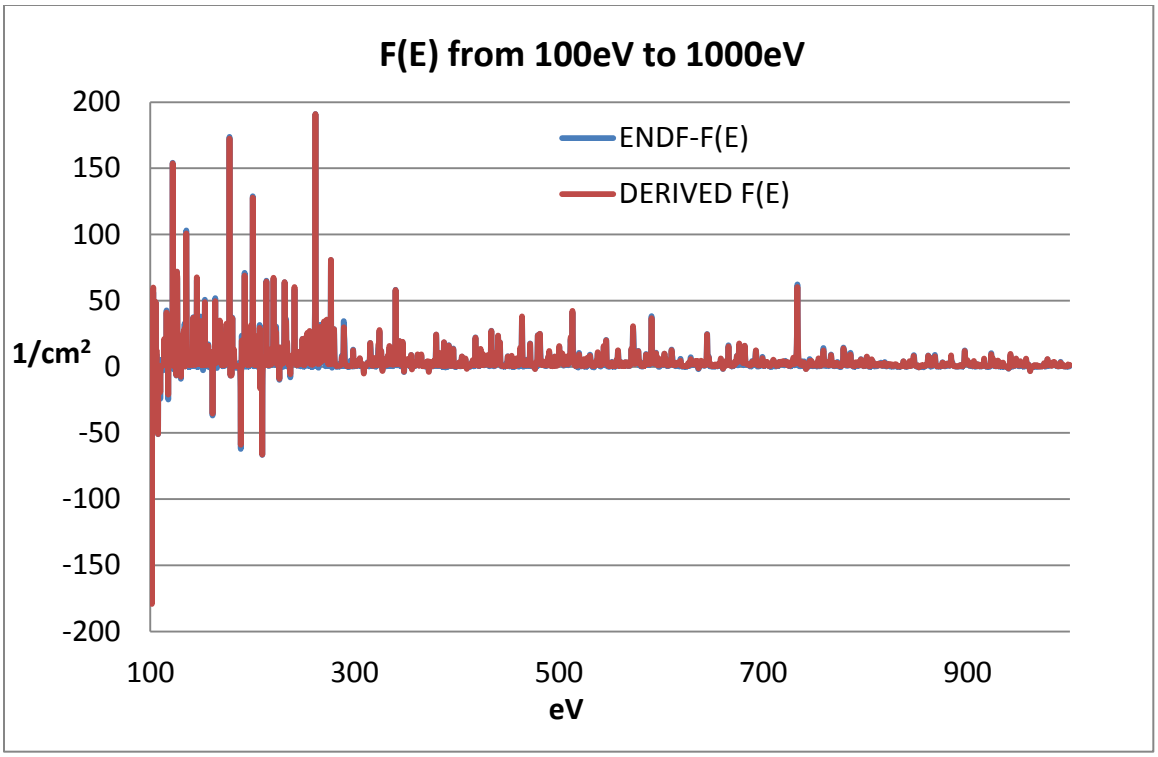

Figure 3.3 Plot of GODIVA F(E) comparison from 100eV to 1000eV

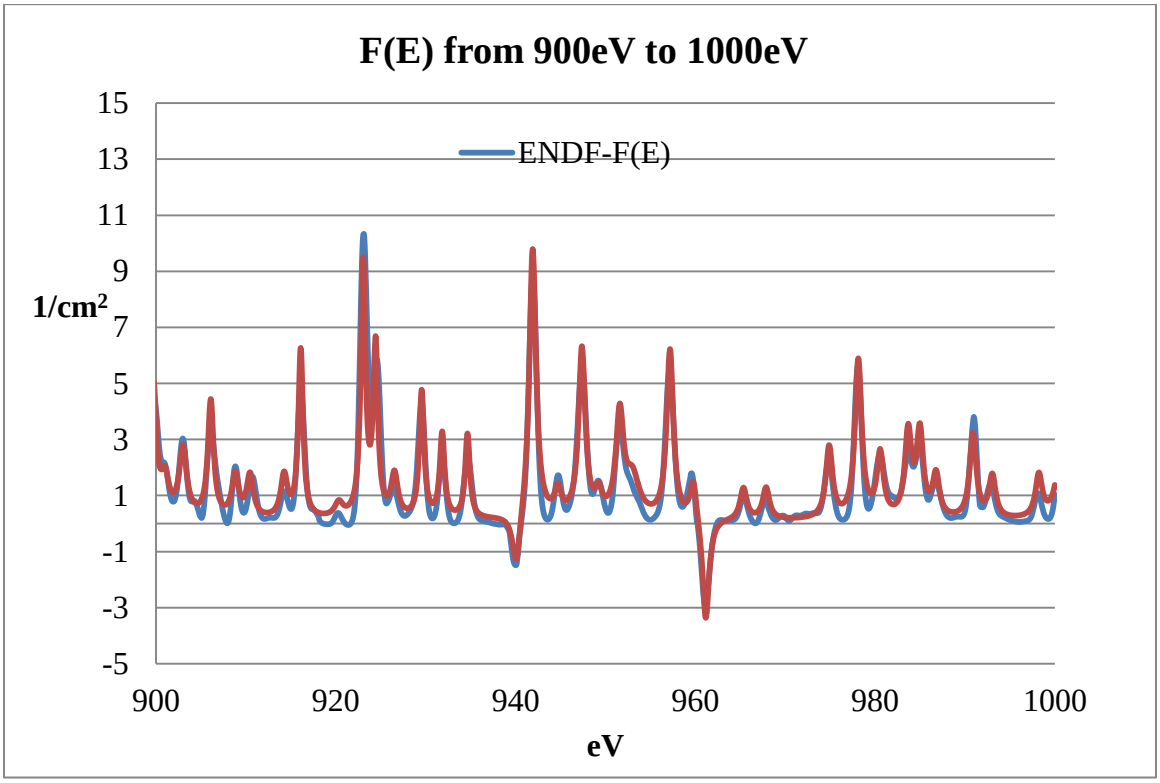

Figure 3.4 Close view of GODIVA F(E) and the overlap between resonance peaks

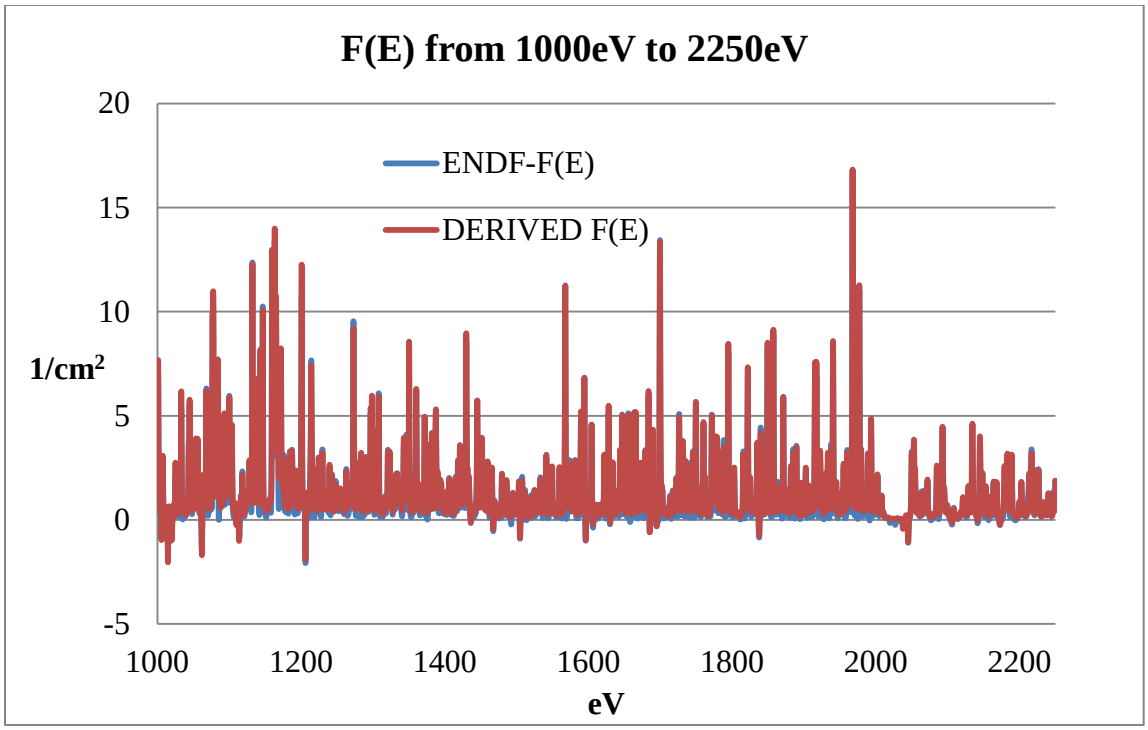

Figure 3.5 Comparison plot of the derived GODIVA F(E) to the ENDF GODIVA F(E) in the energy range of 1000eV to 2250eV

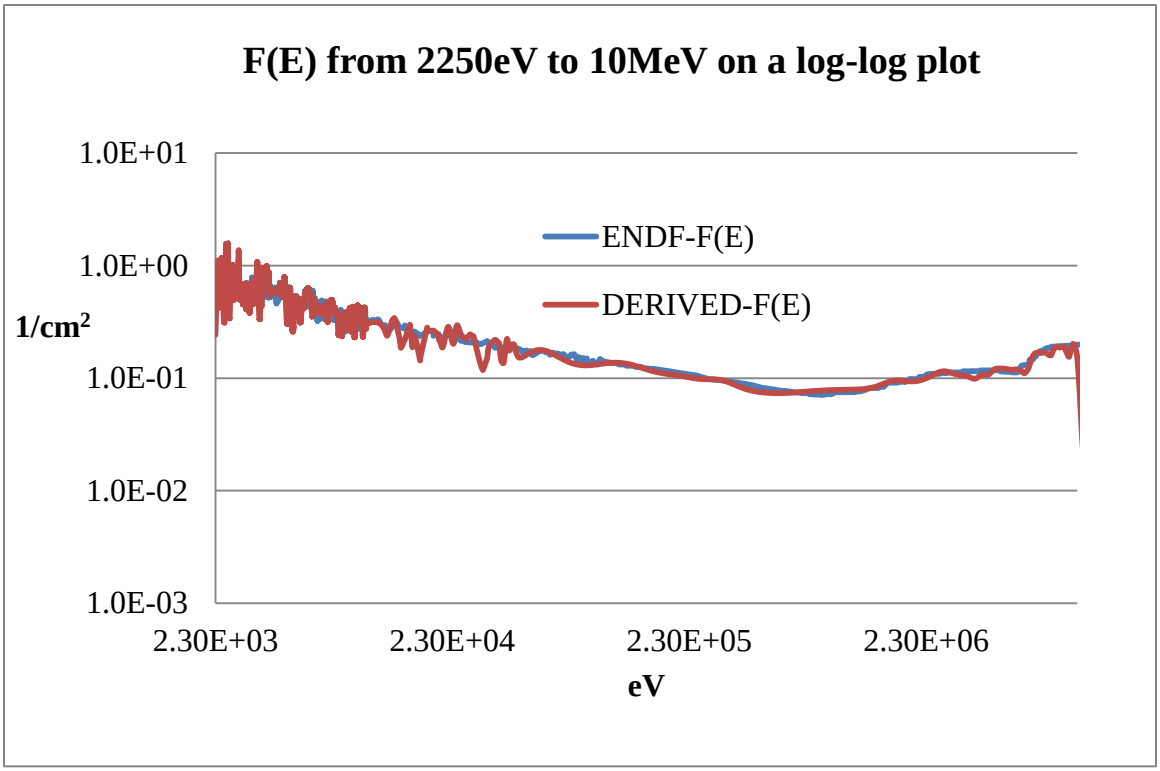

Figure 3.6 Comparison of the two GODIVA F(E) functions from 2250ev to 10MeV

Some of the minor peaks throughout the resonance region were not included into equation 3.16. The reason for doing this is because these small resonance peaks did not add enough value to the resonance integral value. Another reason for not including some small peaks into equation 3.16 is because equation 3.16 over estimates the overlap from resonance peak to resonance peak so the two effects seem to balance each other. The resonance values from The Chart of the Nuclides and Isotopes 16th Edition matched the resonance values from equation 3.16.

$$F(E) = \frac{Rp_0}{E} + \sum_{l=1}^{N} \frac{Rp_l}{(E-Er_l)^2+w_l} + \sum_{m=1}^{N_{TRANS}} \frac{Rp_m \cdot (v_s E + v_{s0})_{2300eV\ to\ 1MeV}}{(E-Er_m)^2+w_m} + \sum_{n=1}^{N_{FAST}} \frac{Rp_n \cdot (v_f E + v_{f0})_{E>1MeV}}{(E-Er_n)^4+w_n \cdot E}$$

Equation 3.16

The constants from equation 3.16 are:

$Rp_0[=]\frac{Energy}{cm^2}$, $Rp_{l,m}'s[=]\frac{Energy^2}{cm^2}$, $Er_{l,m,n}'s[=]Energy$, $w_{l,m}'s[=]Energy^2$, $Rp_n\ 's[=]\frac{Energy^4}{cm^2}$, $w_n's[=]Energy^3$, v_s & $v_f[=]\frac{neutrons}{Energy}$ and v_{s0} & $v_{f0}[=]neutrons$, where N, N_{TRANS} and N_{FAST} are the number of terms included in each sum with indices l, m and n. The $Rp_{l,m}'s$ can be positive or negative because in some energy ranges $(-\Sigma(E)_a)$is greater than $(\nu(E)\Sigma(E)_f)$. The data for each constant is in Appendix 3.A. 832 individual terms, $\left(\frac{Rp_l}{(E-Er_l)^2+w_l}\right)$ are accounted for in the first summation, 120 terms $\left(\frac{Rp_m \cdot (v_s E + v_{s0})_{2300eV\ to\ 1MeV}}{(E-Er_m)^2+w_m}\right)$ in the second summation and 10 individual terms $\left(\frac{Rp_n \cdot (v_f E + v_{f0})_{E>1MeV}}{(E-Er_n)^4+w_n \cdot E}\right)$ are accounted for in the third summation of equation 3.16.

The first term $\frac{Rp_0}{E}$ and the first summation term $\sum_{l=1}^{N} \frac{Rp_l}{(E-Er_l)^2+w_l}$ in equation 3.16 were observable by visual inspection of the ENDF-F(E) plot. The first term comes from

the 1/v portions of the cross sections multiplied together. The first summation term captured ENFD-F(E) in the energy range of 1eV to 2250eV. This range remained visually similar to the resonance region of $^{235}\mathrm{U}\ \Sigma(\mathrm{E})_{\mathrm{t}}$ except for the few negative regions and the height/width of the each resonance peak which is specific to the GODIVA ENDF-F(E) resonance peaks. The height and width of each ENDF-F(E) peak can be matched by equation 3.16 by adjusting Rp_l and w_l respectively.

The second and third summation terms in equation 3.16 account for the linear effect of $\nu(\mathrm{E})$ on F(E). The first and second terms of equation 3.16 are not affected by $\nu(\mathrm{E})$ because the slope is so small, just the constant affects F(E) and it is absorbed into Rp_0 and the $Rp_l's$. The slope of $\nu(\mathrm{E})$ does not change the value of $\nu(\mathrm{E})$ until roughly 46keV and only from 2.43 to 2.44 neutrons produced per incident neutron. It is included in the energy range at 2300eV because of the shape of ENDF-F(E) from 2300eV to 0.9MeV is a rough 1/E function, which $\frac{Rp_m\cdot(\nu_s E+\upsilon_{s0})_{2300eV\ to\ 1MeV}}{(E-Er_m)^2+w_m}$ is approximately a 1/E function. A summation of these terms $\frac{Rp_m\cdot(\nu_s E+\upsilon_{s0})_{2300eV\ to\ 1MeV}}{(E-Er_m)^2+w_m}$ provided a few useful qualities to fit the ENDF-F(E) from 2300eV to 0.9MeV. The first is an ability to shift a 1/E function to this energy range at various places without the sharp discontinuity from these two $\frac{1}{(E-Er_m)}$ or $\frac{(\nu_s E+\upsilon_{s0})}{(E-Er_m)}$ functions or any similar function with an odd order in the denominator, for example a term $\frac{1}{(E-Er_m)^{2n+1}}$ where n=0…∞. The second reason this function is chosen is because it produced a smooth curve (see figure 3.6 from 0.1MeV to 0.9MeV) with a long forward tail which is the 1/E shape desired in this region without the sharp discontinuity. The third reason for this function is small resonance peaks are in

this energy range. The small peaks could be modeled with this function because it can be easily tuned by adjusting Rp_m and $w_m$to have a peak at the resonance energy Er_m.

The energy range 0.9 to 10MeV yielded a different shape. In this energy range ENDF-F(E) increased in a stair step shape (broad resonance) similar to the ^{235}U fission cross section shape from 0.9 to 10MeV. The slope of ν(E) in this energy range is larger and the effect from this linear function is greater. The term inside the third summation, $\frac{Rp_n\cdot(\nu_f E+\upsilon_{f0})_{E>1MeV}}{(E-Er_n)^4+w_n\cdot E}$ is used for similar reasons already mentioned: a smooth curve without sharp discontinuities (no odd ordered denominators), an ability to add an increase or "peak" at a specific energy(Er_n). The denominator $((E-Er_n)^4+w_n\cdot E)$ allowed for a much broader peak and a sharper drop off creating the level stair effect that corresponds to the broad width of the peak. The $w_n\cdot E$ in the denominator along with the 4th order term $(E-Er_n)^4$ restricted any long forward or backward tail that is seen with this these denominator choices $((E-Er_n)^2+E\cdot w_n)$ and $((E-Er_m)^2+w_m)$. The elimination of the long tails in this energy region was necessary to get the correct overlap between resonances. The other function choices investigated could not provide this effect in this energy region and consequently did not match the ENDF-F(E).

These functions included into equation 3.16 allowed for analytic analysis and the development of analytic moments to be created. Table 3.2 is a list of the constants found with equation 3.16 needed for validation of normalized neutron energy moments with the GODIVA experiment. The constants represented in Table 3.2 also allow for verification and comparison of the GODIVA model in MCNP5 and Attila.

Table 3.2 List of the Energy Constants from F(E) Analysis for GODIVA

Constant	Value	Units
CE1	0.052	MeV/cm^2
CE2	0.079	MeV^2/cm^2
CE3	0.310	MeV^3/cm^2
CE4	1.720	MeV^4/cm^2
CE5	12.185	MeV^5/cm^2

Analytic Neutron Moments for GODIVA

The set of analytical energy dependent neutron moments are found from transforming equation 3.7 and 3.8 with the definition of a raw moment. The mathematical definition of a raw moment is $m_k = \int_0^\infty E^k \, \phi(\vec{r}, E) dE$ where k = 0, 1, 2, 3 … N (Casella & Berger, 2002); N is the total number of moments desired. Transformation of equation 3.7 and 3.8 into moment form is not discussed here and can be found in literature (Crawford & Ring, submitted 2012) along with the derivation to obtain the constants in Table 3.2.The derivation and moment transformation of the extrapolated boundary conditions that come from the method of moment's analysis of EDNDE are also found in literature and not reproduced here for briefness of this paper. The extrapolated boundaries for GODIVA are in Table 3.3. All of the other constants (a_1 to a_5, b_1 to b_5, c_2 to c_5, d_3 to d_5, e_4 to e_5 and f_5) that are found in equations 3.17 through 3.22 are derived from the constants reported in Tables 3.2 and 3.3.

Table 3.3 the Extrapolated Boundaries for GODIVA Moment 0-5

$\tilde{R}_0$	$\tilde{R}_1$	$\tilde{R}_2$	$\tilde{R}_3$	$\tilde{R}_4$	$\tilde{R}_5$
11.02cm	11.08cm	11.18cm	11.19cm	11.19cm	11.19cm

The set of moments that are compared are the normalized moments. The moments m_k = 1, 2, 3, 4, 5 are normalized by the 0^{th} moment, m_0. The normalized moments provide information about the population density function i.e. mean energy (m_1/m_0), variance of the energy (m_2/m_0), skewness (m_3/m_0) and kurtosis (m_4/m_0). The normalized energy dependent neutron diffusion moments (NEDNDM) are seen in equation 3.17-3.22, where a_0 = 1. The set of normalized moments, m_k/m_0:

$$\frac{m_0}{m_0} = \frac{a_0\frac{sin(B_{E0}\cdot r)}{r}}{a_0\frac{sin(B_{E0}\cdot r)}{r}} \equiv 1 \qquad \text{Equation 3.17}$$

$$\frac{m_1}{m_0} = \frac{a_1 \sin(B_{E1}\cdot r)}{a_0 \sin(B_{E0}\cdot r)} + \frac{b_1\cdot r\cdot cos(B_{E1}\cdot r)}{a_0 \sin(B_{E0}\cdot r)} \qquad \text{Equation 3.18}$$

$$\frac{m_2}{m_0} = \frac{a_2 sin(B_{E2}\cdot r)}{a_0 sin(B_{E0}\cdot r)} + \frac{b_2 r\, cos(B_{E2}\cdot r)}{a_0 sin(B_{E0}\cdot r)} + \frac{c_2\, r^2 sin(B_{E2}\cdot r)}{a_0 sin(B_{E0}\cdot r)} \qquad \text{Equation 3.19}$$

$$\frac{m_3}{m_0} = \frac{a_3 sin(B_{E3}\cdot r)}{a_0 sin(B_{E0}\cdot r)} + \frac{b_3 r\, cos(B_{E3}\cdot r)}{a_0 sin(B_{E0}\cdot r)} + \frac{c_3 r^2 sin(B_{E3}\cdot r)}{a_0 sin(B_{E0}\cdot r)} + \frac{d_3 r^3 cos(B_{E3}\cdot r)}{a_0 sin(B_{E0}\cdot r)} \qquad \text{Equation 3.20}$$

$$\frac{m_4}{m_0} = \frac{a_4 sin(B_{E4}\cdot r)}{a_0 sin(B_{E0}\cdot r)} + \frac{b_4 r\, cos(B_{E4}\cdot r)}{a_0 sin(B_{E0}\cdot r)} + \frac{c_4\, r^2 sin(B_{E4}\cdot r)}{a_0 sin(B_{E0}\cdot r)} + \frac{d_4\, r^3\, cos(B_{E4}\cdot r)}{a_0 sin(B_{E0}\cdot r)} + \frac{e_4\, r^4 sin(B_{E4}\cdot r)}{a_0 sin(B_{E0}\cdot r)} \qquad \text{Equation 3.21}$$

$$\frac{m_5}{m_0} = \frac{a_5 sin(B_{E5}\cdot r)}{a_0 sin(B_{E0}\cdot r)} + \frac{b_5 r\, cos(B_{E5}\cdot r)}{a_0 sin(B_{E0}\cdot r)} + \frac{c_5 r^2 sin(B_{E5}\cdot r)}{a_0 sin(B_{E0}\cdot r)} + \frac{d_5\, r^3\, cos(B_{E5}\cdot r)}{a_0 sin(B_{E0}\cdot r)} + \frac{e_5\, r^4 sin(B_{E5}\cdot r)}{a_0 sin(B_{E0}\cdot r)} + \frac{f_5\, r^5\, cos(B_{E5}\cdot r)}{a_0 sin(B_{E0}\cdot r)} \qquad \text{Equation 3.22}$$

Results and Discussion

Table 3.4 shows the moment validation results with the three computational methods for the GODIVA experiment. The moments are based on foil activation data from the McElroy report (McElroy, Armani, & Tochilin, 1969) at the center of the sphere. The GODIVA experiment is considered a standard to validate a new method with even though only two locations within the sphere moments can be compared.

Table 3.4 Comparison of GODIVA moments

Energy moments comparison with the GODIVA Experiment						
	m_0 unit less	m_1 [=] MeV	m_2 [=] MeV^2	m_3 [=] MeV^3	m_4 [=] MeV^4	m_5 [=] MeV^5
GODIVA experiment	1+/- 5.6%	1.471+/- 5.6%	4.151+/- 5.6%	16.82+/- 5.6%	86.39+/- 5.6%	526.6+/- 5.6%
NEDNDM	1+/-0%	1.430+/- 2.8%	4.41+/- 6.2%	18.79+/- 10.5%	100.38+/- 16.2%	652.5+/- 23.9%
MCNP5	1+/-0%	1.460+/- 0.7%	4.275+/- 3.0%	18.14+/- 7.8%	96.04+/- 11.2%	588.4+/- 11.7%
Attila	1+/-0%	1.84+/- 25.0%	6.069+/- 46.2%	27.40+/- 62.9%	150.16+/- 73.8%	944.9+/- 79.4%

The best comparison is the remarkable agreement of moment one (m_1) between NEDNDM and the GODIVA experiment. Table 3.5 is the comparison of the time of Flight (T-O-F) measurement for the 1^{st} moment (mean energy) of the leakage neutrons from the surface of the GODIVA experiment. The T-O-F measurement is 1.55MeV+/- 2.9%. The NEDNDM compare very will well with the GODIVA experiment and the two computational platforms: Monte Carlo and Attila. There are two error values in Tables3.4 and 3.5. The first error is the GODIVA experimental measurement error values in both Table 3.4 and Table 3.5. The second error values in Tables 3.4 and 3.5 are the computational methods error with respect to the GODIVA values or relative error,

$$relative\ error = \frac{|experimental\ value - computational\ value|}{experimental\ value} \times 100\%$$

Table 3.5 T-O-F Measurement of m_1

T-O-F measurement of m_1 at sphere surface	
	m_1 [=] MeV
GODIVA experiment	1.55+/-2.9%
NEDNDM	1.64+/-5.8%
MCNP5	1.58+/-2.0%
Attila	1.94+/-25%

The experimental GODIVA moments are not plotted along with the other moments because values for the moments were only measured in two places; at the center of the sphere and at the sphere edge, 8.7407cm. To see a comparison of moments from the computational models of GODIVA, moments were calculated for each of the three computational methods. Moments from MCNP5 were created with an f2 tally on concentric spheres 1 cm radii away from each other including the outermost sphere at 8.7407cm. Moments from Attila are from a custom report created in Attila where a line edit was made to collect the flux in each energy group at approximately 1cm increments up to the system edge to match the MCNP5 sphere surface tallies. The points along the line edit from Attila are not exactly 1cm apart but close enough because each point lined up on a mesh point. The flux data in each energy group are numerically calculated similar to the MCNP5 method where the data was put in an excel spreadsheet and integrated according to the definitions for the mean, variance, skewness, kurtosis and higher order moments.

The f2 tallies in MCNP are broken into 1000 evenly spaced energy bins up to 10MeV. Energy bins from 10MeV to 20 MeV showed large relative errors > 20% and were omitted due to limits in computer power the authors have access to for this work, a

64-bit laptop with a hex core processor and 6 gigabytes of RAM. To get relative errors below 5% for energy bins from 1E-11 to 10MeV 6million particles were tracked in the MCNP model. Computing times for the MCNP5 calculations were roughly a day, 26.3 hours, and Attila computation times were 3-4 hours for a normal mesh of 0.01cm which gave about 100,000 mesh nodes. The reason for the day time frame for MCNP was due to the high number of energy bins and particle histories needed to get in the 5% error range for the 1000 bins in the MCNP case.

The normalized moments from MCNP, Attila and NEDNDM are plotted in Figures 3.7-3.11. There are three curves in Figures 3.7-3.11: in blue the MCNP moment, in red the Attila moment and in green the analytic moment.

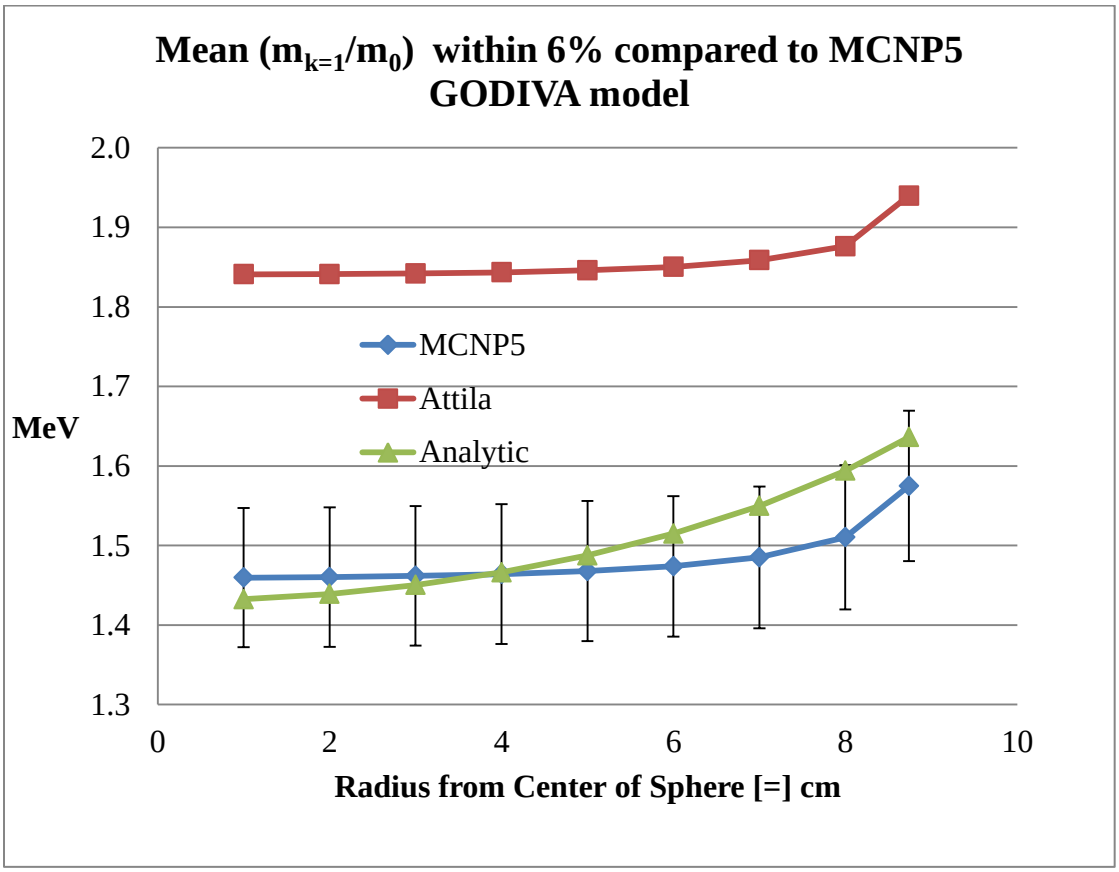

Figure 3.7 Comparison plot of the mean energy for the GODIVA benchmark

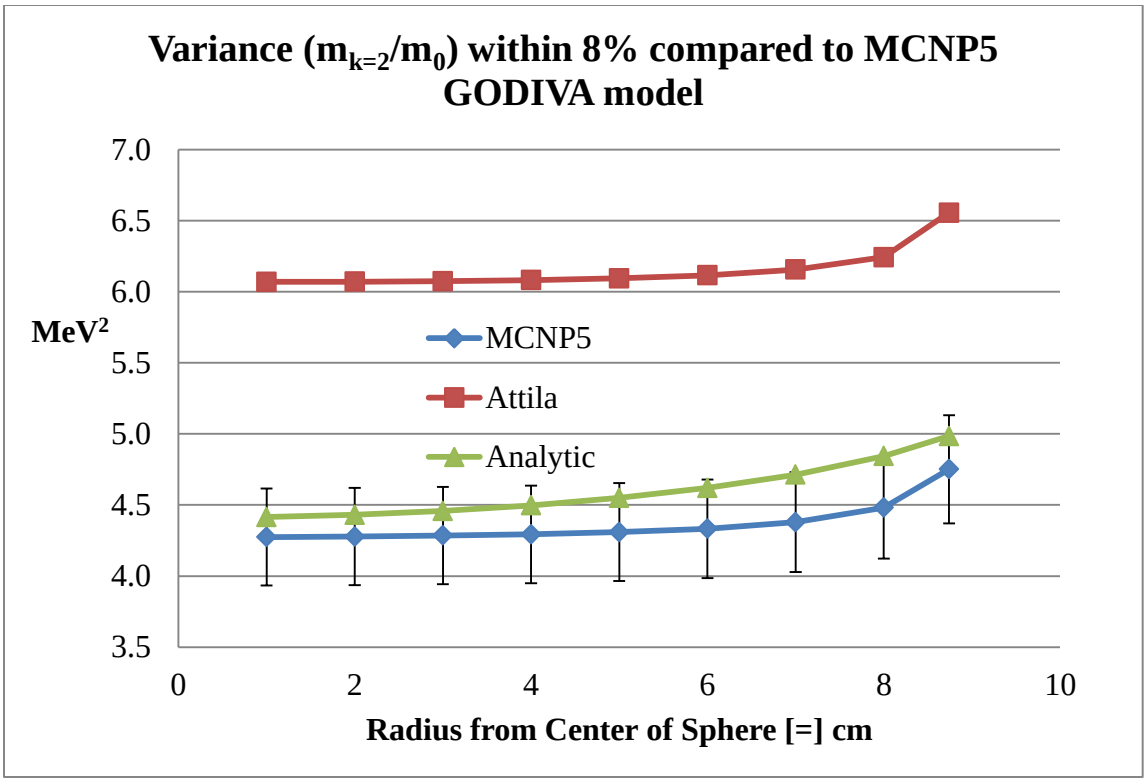

Figure 3.8 Comparison plot of the variance of energy for the GODIVA benchmark

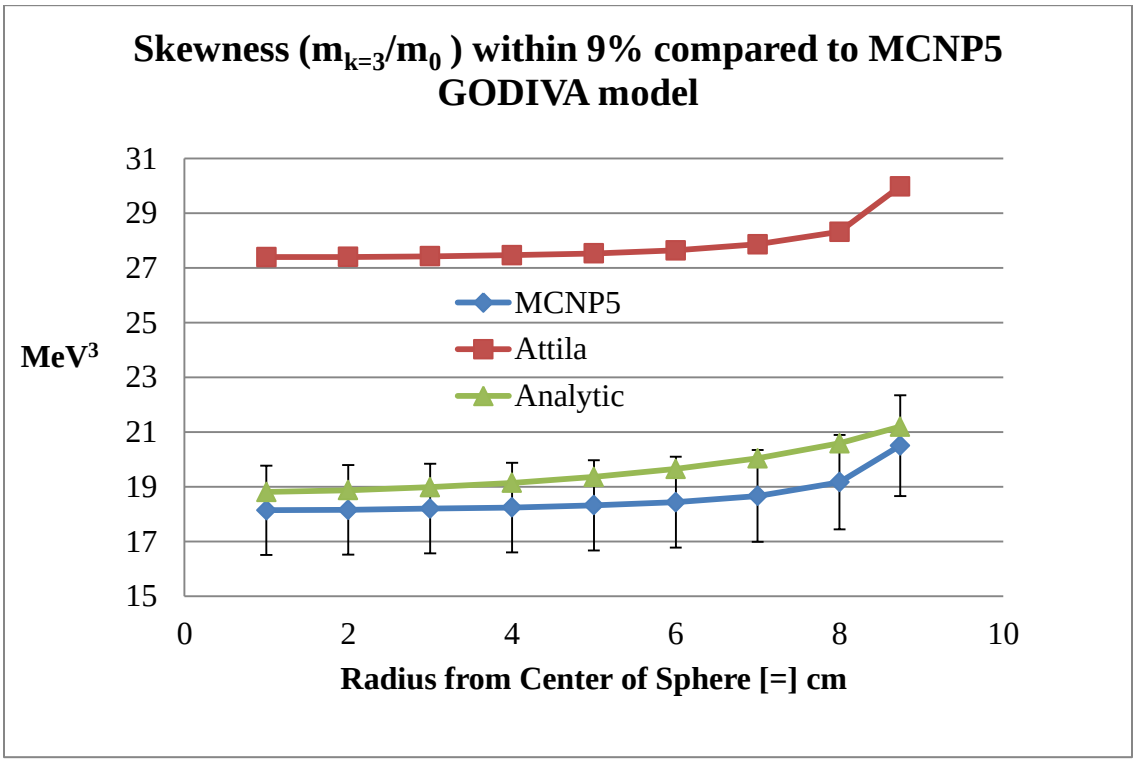

Figure 3.9 Comparison plot of the skewness of energy for the GODIVA benchmark

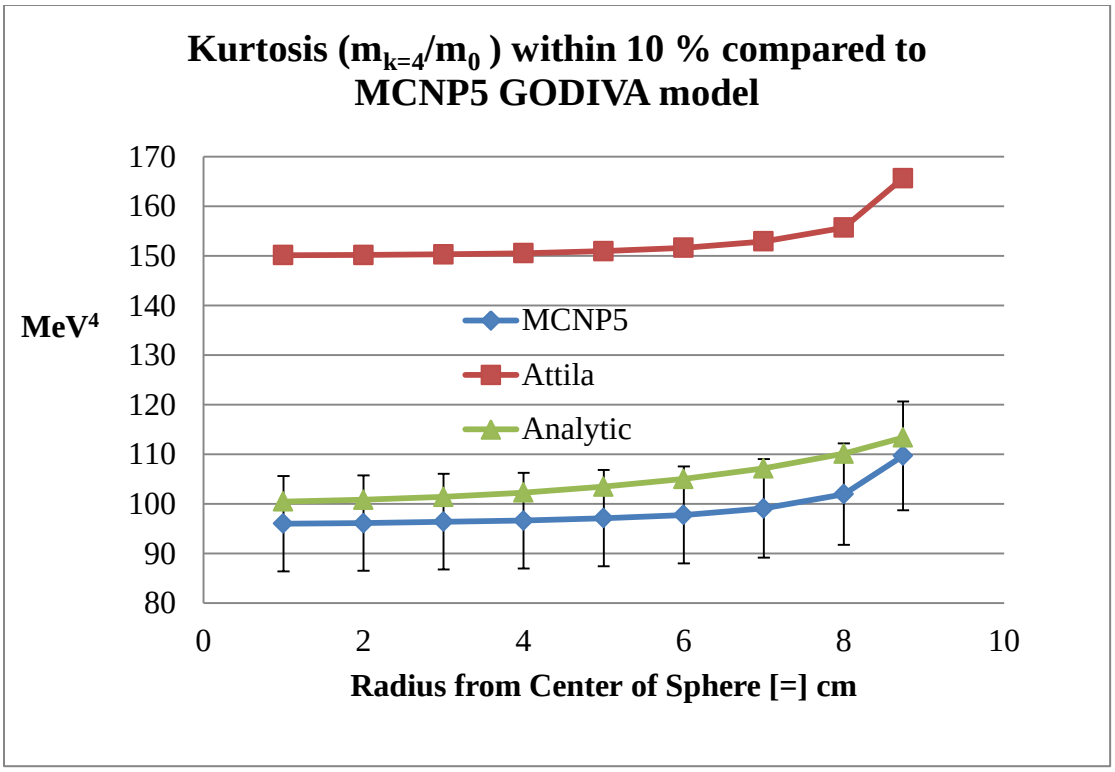

Figure 3.10 Comparison plot of the kurtosis of energy for the GODIVA benchmark

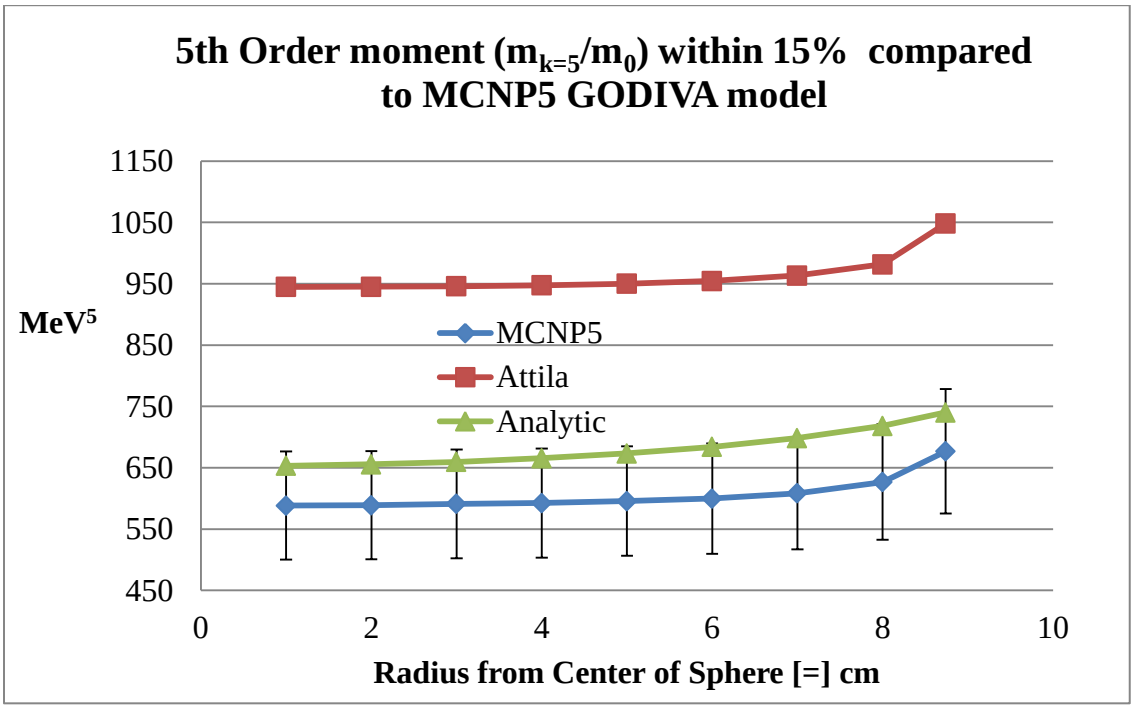

Figure 3.11 Comparison plot of the 5th energy moment for the GODIVA benchmark

The thing that stands out the most in the moment plots is that the Attila moments are higher than the GODIVA moments or the analytic and MCNP moments. The reason the Attila moments are higher is because they are tuned to the fission spectrum which should give an expected mean energy value of about 1.98MeV (Lamarsh & Baratta, 2001, p. 87) for a sphere like GODIVA. The higher order moments should be higher valued than GODIVA because of the fission spectrum weighting. Researchers (Sevast'yanov, Koshelev, & Maslov, 2000) claim that the fission spectrum for ^{235}U could be a superposition of 5 exponential functions and these researchers calculated an average energy value of 1.475MeV+/- 3.77%. Method of neutron energy moments is diffusion based which is not perfect but the bias from the group cross section constants is not seen in the comparison plots. The method of neutron energy moments show a good agreement with the transport codes general shape and the GODIVA experiment, meaning the faster neutrons populate the edges of the system because of the longer diffusion length and the streaming effect of these fast neutrons.

The interesting thing about the NEDNDM is that they start to peel away from the MCNP moments right around 3 mean free paths from the boundary of the sphere, which is about 5 cm (if 1.1cm is taken to be the average mean free path) and then correct back to the boundary value, due to the transport correction factor, r_o. Diffusion theory is valid in finite media at points that are more than a few mean free paths near the edge of the medium (Lamarsh J. R., 1966, p. 129). The limitation of diffusion theory near the boundary of a source is noted and is not valid near the boundary which is why it is transport corrected (Glasstone & Sesonke, 1967, p. 112). Even though diffusion theory has its limits the results agree very well with GODIVA and MCNP. For multiphysics-

engineering type calculations having a continuous energy solution quickly only 24% off in the highest moment (close to engineering limits i.e. 20%) is an excellent benefit that can be very useful to see multiphysics effects on nuclear reactors.

The shape of the functions for MCNP and Attila are very similar, the Attila moment functions have a sharper up turn and less of a parabolic shape which the NEDNDM and MCNP moments have. The reason for this could be the group structure of the radion5 neutron cross section file. The authors do not have control over this file and are thankful for the use of the code from Transpire Inc.

The dominate functional shapes that form the constants, CE's for the moments are from the last two summation terms in F(E), see equation 3.16. If the resonance region was not included it would not have changed the value of the NEDNDM much for this case, because the contribution from the resonance summation was much smaller than the transition and fast region summations in equation 3.16. This makes sense for a fast reactor such as GODIVA. More work still needs to be done to see how reliable the method is for a broader set of reactor types i.e. thermal reactors.

Conclusion

The analytic EDNDE moments (0-5) has been validated with GODIVA. The NEDNDM agrees quite well with the GODIVA moments both at the core center and at the surface of the sphere. NEDNDM, MCNP5 and Attila moments agree with the experiment GODIVA in terms of showing that the higher energy or faster neutrons populate the outer radius of the sphere where they leak out of the system. This is seen by the difference in the value of moment 1 for all three computational moments and

GODIVA at the center and the edge of the sphere. The NEDNDM results fall within the relative error bars associated with GODIVA results for all moments (0 to 5) calculated. The analytical moment results are much more accurate than the 30 energy group Attila simulation because of the reasons stated in the Results and Discussion section of this paper.

Appendix: Constants for GODIVA F(E)

This appendix is the list of constants for each functional piece in the summations that make up F(E), equation 16. The constant Rp_0 equals 85, $units\ \frac{1}{eV}$. The energies, $Er_{l,\ m,\ n}$'s are listed in eV. The $Rp_{l,\ m}$'s are listed in eV/cm^2. The Rp_n's are listed in eV^4/cm^2. The $w_{l,\ m}$'s are listed in eV^2. The w_n's are listed in eV^3.

Table 3.6 List of the Rp_l's, Er_l's and w_l's for GODIVA

Rp_l's	Er_l's	w_l's	Rp_l's	Er_l's	w_l's	Rp_l's	Er_l's	w_l's
-37.5	0.18	0.19	0.9	506.01	0.2	0.3	1254.05	0.25
0.99	0.28	0.0035	0.6	507.89	0.087	0.3	1255.81	0.3
-1.05	0.85	0.065	0.6	510.03	0.087	0.3	1258.17	0.25
0.24	1.12	0.003	1.8	511.48	0.087	1.5	1263.12	0.7
-0.6	2.04	0.015	3.6	513.21	0.087	0.3	1267.02	0.4
0.12	3.6	0.002	0.75	519.66	0.087	0.3	1268.31	0.5
-0.3	4.85	0.0013	0.45	520.6	0.1	0.45	1270	0.5
-0.36	5.16	0.0009	0.54	524.36	0.1	2.25	1273	0.25
1.05	6.3	0.015	0.54	527.85	0.087	0.6	1278.46	0.25
-1.14	6.39	0.0011	2.4	530.33	0.3	0.45	1280.37	0.25
0.3	6.54	0.004	0.24	535.37	0.087	0.75	1283.72	0.25
-1.23	6.68	0.0011	0.3	536.91	0.087	0.15	1287.5	0.5
0.54	6.81	0.012	0.9	537.91	0.087	0.66	1290.61	0.25
12	8.78	0.0026	0.3	539.91	0.2	0.3	1291.89	0.3
-1.2	11.67	0.0009	0.45	542.15	0.087	1.2	1296.89	0.25
0.96	12.38	0.0019	1.5	543.78	0.1	1.35	1298.63	0.25
2.7	13.96	0.04	1.95	546.22	0.1	0.3	1300.78	0.25
13.8	19.3	0.003	0.3	551.8	0.1	0.9	1305.59	0.225
-6	21.07	0.0024	0.45	556.41	0.1	0.9	1308	0.16

Table 3.6 List of the Rp_l's, Er_l's and w_l's for GODIVA continued

Rp_l's	Er_l's	w_l's	Rp_l's	Er_l's	w_l's	Rp_l's	Er_l's	w_l's
0.39	22.94	0.0064	1.2	557.77	0.1	0.15	1311.8	0.25
-0.99	23.41	0.004	0.3	561	0.1	0.06	1315.05	0.25
0.18	20.61	0.005	0.3	564.75	0.1	0.21	1317.07	0.25
0.99	21.32	0.014	0.3	566.74	0.1	0.15	1318.9	0.25
0.99	23.63	0.005	0.6	570.98	0.05	0.75	1320.87	0.25
0.27	24.29	0.0045	3.3	572.51	0.11	0.75	1323.3	0.25
3.3	25.55	0.0475	1.8	575.83	0.2	0.3	1326.05	0.25
0.27	26.5	0.0045	2.19	577.64	0.2	0.45	1329.83	0.25
0.54	27.79	0.0045	0.24	579.51	0.1	0.45	1332.23	0.25
1.26	32.07	0.0035	0.75	585.22	0.1	0.45	1333.8	0.25
-0.06	31.44	0.0035	0.57	585.83	0.1	0.15	1335.5	0.25
-0.06	30.9	0.0035	0.6	587.54	0.1	0.36	1336.99	0.25
2.25	34.38	0.0075	3.6	590.63	0.1	0.3	1338.75	0.25
15	35.18	0.0078	0.6	592.03	0.1	0.9	1343.01	0.25
-4.05	36.68	0.003	0.24	593.47	0.1	2.7	1346.56	0.75
3	39.4	0.0075	0.9	595.02	0.1	0.84	1350.41	0.1
0.15	40.52	0.0095	0.6	595.97	0.1	0.3	1355.6	0.25
1.2	41.51	0.0475	0.51	598.94	0.1	0.3	1358.8	0.25
-0.24	41.86	0.0025	0.42	600.4	0.1	1.5	1360.37	0.25
0.24	42.24	0.0125	2.25	603.22	0.25	0.24	1363.28	0.25
-0.09	42.68	0.01	1.05	604.4	0.25	0.3	1364.07	0.25
-0.09	43.36	0.01	0.54	608.46	0.25	0.3	1367.66	0.25
0.24	43.96	0.01	1.8	610.21	0.15	1.2	1372.05	0.25
1.05	44.61	0.015	0.6	612.9	0.25	0.6	1378.2	0.18
1.35	46.93	0.015	0.6	615.43	0.25	0.45	1380.7	0.3
0.45	47.98	0.015	0.6	616.89	0.25	0.69	1382.1	0.18
0.75	48.3	0.015	1.05	619.02	0.25	2.55	1387.6	0.5
0.24	48.8	0.008	0.6	626.6	0.25	0.45	1390.26	0.25
-0.24	49.43	0.0063	1.05	628.99	0.2	0.6	1393.8	0.4
0.3	50.48	0.0063	0.45	630.8	0.25	0.6	1395.3	0.45
3.45	51.26	0.0083	0.45	631.69	0.25	0.15	1397.37	0.25
3	52.21	0.02	1.05	633.64	0.275	0.15	1400.75	0.25
1.8	55.04	0.01	1.05	635.41	0.25	0.3	1403.45	0.25
5.25	55.88	0.025	-0.6	636.5	0.25	0.45	1406.4	0.25
6.6	56.48	0.009	1.05	639.14	0.25	0.36	1410.5	0.25
1.5	57.95	0.02	0.6	641.17	0.2	0.45	1415.29	0.25
1.2	58.66	0.02	2.4	644.96	0.1	0.63	1418.47	0.25
0.66	60.18	0.02	0.6	646.65	0.1	0.84	1421.17	0.25
0.3	60.84	0.03	0.3	648.83	0.2	0.3	1423.63	0.25
0.84	63.66	0.075	0.3	653.07	0.2	0.3	1425.77	0.25
-0.36	64.3	0.007	0.6	656.4	0.3	0.3	1427.2	0.25
-0.96	66.35	0.005	0.6	658.38	0.1	1.5	1430.07	0.175
0.3	69.29	0.03	-0.3	660.55	0.15	0.6	1431.75	0.35

Table 3.6 List of the Rp_l's, Er_l's and w_l's for GODIVA continued

Rp_l's	Er_l's	w_l's	Rp_l's	Er_l's	w_l's	Rp_l's	Er_l's	w_l's
3.75	70.46	0.018	0.6	663.6	0.15	0.6	1433.53	0.35
2.79	72.36	0.018	1.5	665.92	0.1	-0.15	1436.27	0.35
2.1	74.54	0.018	0.6	672.13	0.2	0.15	1439.5	0.35
1.2	75.49	0.03	1.35	674.11	0.2	0.15	1442.53	0.35
0.3	77.5	0.03	3	676.42	0.2	1.5	1445.29	0.27
0.6	78.11	0.03	7.2	678.07	0.7	0.75	1449.75	0.25
0.3	79.68	0.04	2.25	681.79	0.15	0.9	1451.81	0.25
0.42	80.34	0.04	0.6	683.82	0.5	0.24	1454.09	0.25
0.3	81.42	0.02	0.6	685.53	0.5	0.24	1456.41	0.25
-0.84	82.67	0.04	0.6	689.12	0.2	0.66	1459.68	0.25
4.35	84.15	0.04	0.6	690.45	0.2	0.15	1463.74	0.3
0.9	84.99	0.04	2.4	692.75	0.2	0.6	1465.65	0.25
1.8	88.75	0.04	0.6	696.87	0.2	-0.15	1467.57	0.2
0.3	89.77	0.04	1.2	699.1	0.2	0.15	1469.52	0.2
-1.5	90.35	0.0068	0.6	702.55	0.2	0.15	1472.37	0.25
2.7	91.24	0.04	0.6	703.83	0.2	0.54	1479.7	0.25
0.6	92.54	0.0355	5.1	709.88	1	0.24	1483.01	0.25
-0.9	94.1	0.0055	0.6	715.75	0.2	0.45	1486.02	0.25
0.24	94.77	0.05	0.6	717.13	0.2	0.3	1494.8	0.25
0.3	95.6	0.04	0.6	718.9	0.2	0.24	1498.06	0.25
0.24	96.46	0.05	0.6	719.92	0.2	0.24	1500.95	0.25
1.2	98.1	0.022	0.6	721.59	0.2	0.45	1503.3	0.25
-0.9	101.54	0.0058	0.6	723.53	0.2	-0.3	1504.85	0.25
-0.9	101.7	0.009	0.6	727.41	0.2	0.45	1507.83	0.25
0.9	102.9	0.015	1.2	729.38	0.2	0.3	1511.82	0.25
0.72	105.19	0.015	9	733.36	0.15	0.24	1520.17	0.25
0.24	106.09	0.02	0.6	737.69	0.2	0.33	1524.9	0.25
-0.78	107.62	0.015	0.6	739.95	0.2	0.24	1527.7	0.25
-0.3	109.79	0.015	-1.05	741.74	0.45	0.24	1530.29	0.25
0.3	113.51	0.015	0.6	745.35	0.15	0.45	1533.32	0.25
0.6	115.92	0.015	0.6	747.06	0.15	0.15	1535.37	0.25
-0.39	117.59	0.015	0.6	750	0.35	0.24	1538.43	0.25
0.9	118.18	0.024	0.6	751.22	0.35	0.75	1541.51	0.25
0.45	118.8	0.03	0.6	754.05	0.1	0.15	1546.39	0.5
2.1	121.92	0.0138	3	758.84	0.25	0.6	1549.41	0.25
-0.15	122.92	0.05	0.6	761.71	0.25	0.24	1551.61	0.5
0.66	124.72	0.05	0.6	762.87	0.25	0.24	1553.94	0.4
-0.15	125.46	0.01	2.1	766.31	0.25	0.6	1559.77	0.25
1.5	126.02	0.025	0.15	767.99	0.25	2.79	1567.81	0.25
1.74	126.38	0.03	0.6	770.88	0.25	0.24	1570.94	0.4
0.48	128.1	0.03	0.6	772.63	0.25	0.6	1573.8	0.25
-0.3	130	0.03	1.2	778.46	0.1	0.24	1575.55	0.25
1.05	131.26	0.05	1.8	779.41	0.2	0.45	1579.2	0.25

Table 3.6 List of the Rp_l's, Er_l's and w_l's for GODIVA continued

Rp_l's	Er_l's	w_l's	Rp_l's	Er_l's	w_l's	Rp_l's	Er_l's	w_l's
0.84	132.16	0.05	0.6	782.38	0.2	0.66	1581.44	0.25
1.05	132.72	0.05	1.8	785.3	0.2	0.15	1587.27	0.5
1.35	133.54	0.05	0.6	790.32	0.2	1.26	1589.71	0.25
-1.2	134	0.1	0.6	792.61	0.2	1.35	1594.4	0.2
9	135.25	0.09	0.9	795.5	0.2	-0.39	1596.31	0.25
0.9	142	0.025	0.6	796.28	0.2	0.24	1598.54	0.25
1.5	145.53	0.0225	1.5	801.33	0.2	0.24	1600.54	1
0.3	147.29	0.0225	0.9	806.01	0.2	1.14	1604.4	0.25
0.6	149.06	0.018	1.2	806.95	0.4	-0.15	1606.4	0.25
0.3	149.93	0.025	0.6	810.11	0.4	0.15	1609.25	0.25
0.6	153.42	0.0125	0.6	812.76	0.3	0.15	1612.53	0.25
0.3	154.83	0.05	0.6	815.11	0.3	0.15	1616.18	0.25
0.3	156.75	0.02	0.6	817.9	0.3	0.15	1619.7	0.25
0.45	158.57	0.05	0.6	818.9	0.3	0.75	1622.2	0.25
0.45	159.08	0.05	0.45	821.86	0.3	1.35	1628.13	0.25
-0.33	160.94	0.009	0.45	823.55	0.3	-0.15	1630.18	0.25
1.95	163.6	0.04	0.45	825.51	0.3	0.66	1633.9	0.25
0.3	165.51	0.04	0.45	828.5	0.3	0.03	1637.74	0.25
0.75	166.27	0.04	0.45	830.13	0.3	0.3	1639.98	0.25
1.35	168.02	0.04	0.6	837.15	0.15	0.78	1644.06	0.25
0.36	169.33	0.04	0.6	843.03	0.15	1.2	1647	0.25
0.75	174.09	0.04	2.4	847.2	0.3	0.21	1650	0.25
1.14	174.52	0.04	0.3	851.29	0.3	0.03	1652.5	0.25
0.72	176.54	0.04	-0.3	852.33	0.3	1.23	1655.64	0.25
3	177.54	0.0175	0.3	854.9	0.3	1.2	1663.81	0.25
-0.3	178.45	0.0275	0.3	858.3	0.3	1.2	1665.9	0.25
-0.3	179.5	0.0325	1.5	861.36	0.2	0.33	1671.24	0.25
0.9	180.31	0.025	1.2	862.68	0.2	0.6	1672.77	0.25
0.3	181.99	0.025	0.6	866.17	0.3	0.45	1675.12	0.25
-0.9	188.54	0.015	1.5	867.95	0.2	0.75	1679.47	0.25
0.3	189.53	0.015	0.9	875.45	0.3	0.66	1681.55	0.25
1.5	192.32	0.022	0.6	879.06	0.3	1.2	1683.76	0.2
0.75	194.18	0.0375	0.6	881	0.3	-0.3	1685.43	0.25
3	198.55	0.1	0.6	883.81	0.075	1.05	1690.01	0.25
2.4	200.28	0.019	0.6	884.94	0.3	-0.15	1695	0.25
0.45	203.71	0.02	0.15	886.84	0.3	3.3	1699.63	0.25
0.6	207.02	0.02	0.3	892.69	0.3	0.21	1701.95	0.25
-0.39	207.58	0.02	-0.15	803.71	0.4	0.24	1702.96	0.25
-0.69	209.6	0.01	1.65	897.16	0.145	0.03	1706.86	0.25
0.3	210.72	0.05	0.6	898.5	0.25	0.09	1709.31	0.25
0.3	211.47	0.05	0.6	899.73	0.145	0.24	1713.64	0.25
1.29	213.65	0.02	0.3	901	0.25	0.3	1717.47	0.25
0.3	217.11	0.025	0.6	903	0.25	0.15	1720.12	0.25

Table 3.6 List of the Rp_l's, Er_l's and w_l's for GODIVA continued

Rp_l's	Er_l's	w_l's	Rp_l's	Er_l's	w_l's	Rp_l's	Er_l's	w_l's
3.9	220.62	0.06	0.6	906.09	0.145	0.45	1722.5	0.25
2.4	221.76	0.09	0.3	908.82	0.2	1.2	1726.36	0.25
0.6	223.2	0.025	0.3	910.46	0.2	0.9	1731.66	0.25
-0.3	226.36	0.025	0.3	914.25	0.2	0.66	1735.01	0.25
0.45	226.82	0.03	0.6	916.1	0.1	0.15	1738.22	0.25
0.45	229.12	0.06	0.15	920.34	0.3	0.6	1741.22	0.25
3	231.45	0.048	0.9	923.05	0.1	0.75	1745.56	0.25
1.5	232.95	0.048	0.6	924.42	0.1	1.2	1749.6	0.22
1.2	233.94	0.075	0.3	926.53	0.2	0.3	1751.58	0.25
-0.3	237.09	0.04	0.45	929.56	0.1	0.15	1755.03	0.25
6	239.39	0.75	0.3	931.84	0.1	1.11	1760.23	0.25
1.47	241.16	0.025	0.3	934.66	0.1	0.6	1762.1	0.35
0.3	245.48	0.03	-0.6	940.09	0.3	1.2	1771.82	0.25
0.3	246.36	0.03	1.95	941.91	0.2	0.6	1774.44	0.25
0.3	247.87	0.03	0.18	944.72	0.2	0.9	1777.28	0.25
0.6	248.94	0.03	1.2	947.39	0.2	0.9	1779.3	0.25
0.3	251.56	0.06	0.15	949.25	0.2	0.75	1783.3	0.25
1.2	252.94	0.06	0.9	951.6	0.25	0.84	1788.37	0.25
1.35	253.65	0.06	1.2	953	0.85	0.15	1791.43	0.25
1.35	255.95	0.052	1.2	957.19	0.2	1.5	1794.88	0.18
9.9	261.65	0.052	0.3	959.78	0.2	0.15	1799.53	0.35
1.5	266.35	0.052	-0.75	961.17	0.2	0.6	1803.07	0.25
0.9	268.24	0.095	0.24	965.36	0.2	0.15	1808.12	0.6
3	270.01	0.095	0.24	967.88	0.2	0.75	1815.7	0.25
1.2	270.88	0.1	0.51	974.9	0.2	0.39	1819.56	0.25
2.4	272.78	0.07	1.14	978.14	0.2	1.44	1821.9	0.2
2.4	276.78	0.03	0.45	980.58	0.2	0.45	1825.24	0.25
1.8	279.84	0.065	0.6	983.69	0.2	0.3	1829.04	0.6
0.6	287.47	0.1	0.6	984.99	0.2	0.3	1830.74	0.6
3	289.46	0.1	0.3	986.79	0.2	0.9	1835	0.25
1.2	298.56	0.1	0.6	990.9	0.2	-0.3	1837.8	0.25
0.6	302.79	0.15	0.3	993.05	0.2	0.9	1839.86	0.22
0.6	305.12	0.1	0.3	998.23	0.2	0.3	1843.17	0.6
0.6	307.81	0.3	1.5	1001.05	0.2	2.1	1849.52	0.25
-0.6	308.99	0.1	0.3	1004.5	0.225	1.8	1857.55	0.2
0.6	312.48	0.3	-0.3	1005.67	0.2	0.15	1860.42	0.8
0.15	313.55	0.1	0.6	1007.5	0.2	0.36	1863.3	0.25
1.8	315.3	0.1	0.09	1010.49	0.2	0.3	1865.9	0.25
0.6	319.69	0.1	-0.24	1011.24	0.2	0.15	1868.3	0.25
1.5	323.46	0.1	-0.45	1014.7	0.2	1.02	1871.36	0.175
1.5	324.31	0.06	0.24	1015.91	0.25	0.3	1875.05	0.25
1.8	325.97	0.165	-0.3	1017.62	0.25	0.24	1877.8	0.25
-0.3	327.25	0.06	0.15	1019.08	0.25	0.6	1881.95	0.25

Table 3.6 List of the Rp_l's, Er_l's and w_l's for GODIVA continued

Rp_l's	Er_l's	w_l's	Rp_l's	Er_l's	w_l's	Rp_l's	Er_l's	w_l's
0.3	329.07	0.06	-0.3	1020.1	0.25	0.75	1885.1	0.25
0.3	330.53	0.075	0.15	1022.77	0.25	0.84	1889.61	0.25
0.45	332.51	0.06	0.54	1025.15	0.2	0.03	1893.33	0.25
1.5	334.05	0.1	0.3	1030.53	0.2	0.42	1897.04	0.25
0.75	336.61	0.06	1.2	1033.27	0.2	0.6	1902.6	0.25
3.45	340.07	0.06	0.15	1036.5	0.2	0.54	1906.65	0.35
0.15	342.32	0.075	0.9	1043.75	0.3	0.3	1910.42	0.35
1.14	343.95	0.06	0.75	1044.82	0.15	2.1	1915.5	0.3
1.11	346.98	0.06	0.6	1049.66	0.25	0.6	1902.6	0.25
-0.3	348.33	0.06	0.9	1053.64	0.25	0.54	1906.65	0.35
0.24	349.37	0.1	0.9	1056.08	0.25	0.3	1910.42	0.35
0.24	350.63	0.1	0.15	1059.8	0.25	2.1	1915.5	0.3
0.3	351.54	0.06	-0.42	1061.87	0.2	2.1	1917.54	0.3
0.3	353.02	0.06	0.6	1064.03	0.3	0.9	1922.7	0.3
0.54	355.33	0.06	1.8	1068.19	0.3	0.45	1924.5	0.3
-0.24	356.06	0.06	0.15	1071.4	0.3	0.6	1930.37	0.3
0.3	356.67	0.1	0.15	1074.62	0.3	0.9	1933.32	0.3
0.3	359.59	0.1	1.8	1076.83	0.225	0.9	1937.95	0.3
0.3	360.43	0.1	1.8	1077.74	0.2	1.5	1940.64	0.18
0.54	361.6	0.06	0.3	1080.06	0.2	0.9	1945.2	0.55
0.3	364.31	0.1	0.75	1082.56	0.3	0.6	1952.2	0.55
0.54	365.28	0.06	1.8	1084.2	0.25	0.75	1955.3	0.3
0.3	370.45	0.1	0.15	1086.75	0.25	0.9	1960.3	0.3
0.3	371.37	0.08	0.6	1089.92	0.4	0.66	1963.67	0.3
-0.3	372.6	0.06	1.2	1093.28	0.25	3	1967.8	0.18
0.3	373.32	0.075	0.3	1095.59	0.225	0.45	1972.71	0.5
0.3	377.78	0.075	0.6	1097.5	0.3	1.65	1977.16	0.15
1.8	379.81	0.075	1.65	1100.16	0.3	0.9	1979.7	0.3
0.75	383.32	0.075	1.5	1103.44	0.35	0.3	1983.8	0.75
1.05	387.47	0.0575	0.24	1108.42	0.35	0.3	1985.8	0.75
0.9	392.17	0.0575	-0.12	1110	0.2	0.9	1989.29	0.3
0.75	396.58	0.0575	0.21	1111.2	0.3	1.05	1993.6	0.22
0.3	402.3	0.1	-0.39	1113.7	0.3	0.3	1997.85	0.75
0.75	405	0.1	0.3	1116.08	0.3	0.54	1999.84	0.75
0.6	408.45	0.1	0.6	1118.3	0.3	0.6	2002.45	0.3
-0.15	409.79	0.0575	0.6	1123.6	0.5	0.24	2006.36	0.3
0.3	410.63	0.2	0.3	1125.22	0.5	0.3	2008.22	0.3
0.3	414.18	0.2	0.3	1116.08	0.3	0.09	2010.9	0.3
0.9	415.61	0.2	0.6	1118.3	0.3	-0.15	2037.9	0.3
0.75	418.26	0.035	0.6	1123.6	0.5	0.15	2042.43	0.75
0.45	419.83	0.0575	0.3	1125.22	0.5	-0.36	2045.17	0.3
0.75	423.25	0.0575	0.3	1126.11	0.5	0.9	2050.17	0.3
0.84	425.46	0.09	0.75	1128.2	0.3	1.05	2053.18	0.3

Table 3.6 List of the Rp_l's, Er_l's and w_l's for GODIVA continued

Rp_l's	Er_l's	w_l's	Rp_l's	Er_l's	w_l's	Rp_l's	Er_l's	w_l's
0.3	427.54	0.08	2.1	1132.3	0.175	0.6	2054.84	0.3
0.3	428.76	0.07	0.15	1134.39	0.3	0.3	2058.85	0.75
0.75	430.53	0.09	0.3	1136.48	0.2	0.36	2063.75	0.3
1.5	433.81	0.0575	1.95	1139.08	0.3	0.36	2067.31	0.3
0.75	434.88	0.08	0.9	1143.43	0.115	0.3	2069.75	0.3
0.75	439.11	0.1	1.14	1146.66	0.115	0.54	2072.1	0.3
1.8	440.4	0.08	0.15	1149.9	0.3	0.15	2081.23	0.75
1.2	442.19	0.068	0.15	1152.79	0.3	0.75	2085.12	0.3
1.5	449.89	0.2	0.6	1156.1	1	0.54	2090.43	0.3
0.6	453.7	0.075	1.2	1159.65	0.1	1.26	2093.07	0.3
0.45	458.79	0.08	1.5	1161.5	0.2	0.6	2095.29	0.5
0.3	459.57	0.08	3.81	1163.3	0.3	0.6	2099.65	1
0.9	462.02	0.068	1.8	1165.23	0.2	-0.24	2106.22	1
2.55	463.8	0.068	3	1167.55	0.7	0.15	2108.78	0.3
0.75	2207.17	0.7	0.6	1170.27	0.1	0.15	2118.2	0.5
12	2213.88	2	1.5	1172	0.2	0.3	2121.42	0.3
10.95	2216.99	1	0.6	1174	0.3	0.15	2124.65	0.3
3.45	2223.71	0.45	0.6	1175.99	0.25	0.6	2129.05	0.4
3.45	2226.61	0.45	0.15	1178.6	0.3	1.8	2134.61	0.4
0.9	2233.24	0.45	0.3	1180.7	0.3	0.15	2137.75	0.3
0.9	2236.21	0.75	0.9	1184.41	0.3	-0.24	2141.9	0.75
3.6	2240.52	0.9	0.9	1187.46	0.3	1.95	2145.14	0.5
1.5	2247.9	0.35	0.3	1190.1	0.3	0.6	2148.5	0.3
0.6	2250	0.1	0.6	1192.67	0.3	0.6	2153.21	0.4
0.45	458.79	0.08	0.3	1194.18	0.3	0.3	2160.8	0.3
0.3	459.57	0.08	0.9	1198	1	0.6	2164.15	0.35
0.9	462.02	0.068	1.8	1200.8	0.15	0.6	2168.27	0.35
2.55	463.8	0.068	0.3	1204.56	0.3	-0.3	2172.9	0.75
0.3	466.61	0.1	-0.3	1206.15	0.125	1.8	2179.37	0.75
0.9	469	0.2	0.3	1207.49	0.25	2.25	2183.35	0.75
1.17	471.77	0.068	3.6	1214.2	0.5	0.9	2189.31	0.3
-0.24	476.6	0.068	0.3	1216.1	0.25	0.3	2199.99	0.4
0.6	477.25	0.2	0.54	1220.19	0.25	0.51	2202.8	0.3
1.56	479.28	0.068	0.66	1224.59	0.25	0.15	2207.17	0.3
1.65	481.33	0.068	0.3	1225.88	0.25	1.2	2213.88	0.6
0.3	483.56	0.09	0.75	1229.7	0.25	1.8	2216.99	0.6
0.3	485.29	0.09	0.3	1232.86	0.3	0.66	2223.71	0.3
0.3	487.1	0.09	0.3	1235.6	0.3	0.66	2226.61	0.3
0.6	489.55	0.09	0.3	1237.34	0.3	0.24	2233.24	0.3
0.75	490.47	0.068	0.6	1239.65	0.25	0.12	2236.21	0.3
0.66	495.7	0.087	0.6	1243.2	0.3	1.2	2240.52	1
1.5	500.28	0.1	1.2	1248.2	0.8	0.45	2247.9	0.4
0.9	502.01	0.1	0.3	1251.71	0.25	0.18	2250	0.1

Table 3.7 list of the Rp_m's, Er_m's and w_m's for GODIVA

Rp_m's	Er_m's	w_m's	Rp_m's	Er_m's	w_m's	Rp_m's	Er_m's	w_m's
3.00E-6	2350	5.00E+2	3.00E-6	7100	6.0E+3	7.50E-6	20500	1.6E+5
3.00E-6	2447	5.00E+2	3.00E-6	7200	7.0E+3	7.50E-6	21000	1.6E+5
7.50E-7	2548	1.00E+2	3.00E-6	7350	7.0E+3	1.50E-5	22100	1.2E+5
7.50E-7	2598	1.00E+2	3.00E-6	7500	7.0E+3	7.50E-6	23200	2.6E+5
7.50E-7	2672	2.00E+2	3.00E-6	7750	7.0E+3	1.20E-5	23700	2.6E+5
7.50E-7	2718	2.00E+2	3.00E-6	8000	7.0E+3	6.00E-6	24000	2.6E+5
6.75E-6	2800	2.50E+3	3.00E-6	8200	7.0E+3	1.20E-5	24200	2.6E+5
1.05E-6	2883	2.00E+2	1.50E-6	8400	7.0E+3	1.20E-5	24600	3.5E+5
2.25E-6	2960	1.00E+3	3.00E-6	8500	7.0E+3	1.20E-5	25000	3.5E+5
2.25E-6	3050	1.00E+3	3.00E-6	8750	6.0E+3	1.05E-5	25700	3.0E+5
2.25E-6	3150	1.00E+3	1.50E-6	9000	8.0E+3	1.05E-5	26200	3.0E+5
2.25E-6	3260	1.00E+3	3.45E-6	9150	8.5E+3	1.05E-5	27200	3.0E+5
2.25E-6	3356	1.00E+3	3.00E-6	9300	8.5E+3	1.05E-5	27500	3.0E+5
3.75E-6	3458	1.00E+3	3.00E-6	9500	8.5E+3	1.05E-5	28300	3.0E+5
3.75E-7	3574	1.50E+2	3.00E-6	9800	7.0E+3	1.05E-5	28800	3.0E+5
3.84E-7	3630	1.50E+2	1.20E-6	10000	6.0E+3	1.05E-5	29300	3.0E+5
3.00E-6	3700	1.50E+3	1.05E-5	10400	7.0E+4	1.05E-5	30000	3.0E+6
3.00E-6	3785	1.15E+3	1.05E-5	10650	7.0E+4	1.05E-5	31100	3.0E+6
1.50E-6	3858	8.00E+2	9.00E-6	10850	7.0E+4	9.90E-6	31800	3.0E+6
3.00E-6	3950	3.00E+3	1.35E-5	11200	7.0E+4	9.90E-6	32100	3.0E+6
9.00E-6	4050	7.50E+3	1.20E-5	11650	7.0E+4	9.90E-6	32800	3.0E+5
3.00E-6	4150	3.50E+3	7.50E-6	12000	7.0E+4	9.90E-6	34200	3.0E+5
3.60E-6	4250	3.50E+3	7.50E-6	12400	7.0E+4	9.90E-6	35000	3.0E+5
4.80E-6	4350	3.50E+3	9.00E-6	12800	7.0E+4	9.90E-6	36200	3.0E+5
6.75E-6	4500	3.50E+3	3.00E-6	12900	7.0E+4	9.90E-6	37000	3.0E+5
5.25E-6	4750	3.50E+3	9.00E-6	13100	8.0E+4	9.90E-6	37900	3.0E+5
3.75E-6	5000	3.50E+3	7.50E-6	13250	7.0E+4	9.90E-6	39100	3.0E+5
3.75E-6	5150	4.00E+3	7.50E-6	13700	7.0E+4	1.20E-5	40000	3.0E+6
3.75E-6	5350	5.00E+3	7.50E-6	14300	7.0E+4	1.20E-5	41000	8.0E+5
3.75E-6	5500	5.00E+3	7.50E-6	14800	7.0E+4	1.20E-5	42000	8.0E+5
3.75E-6	5600	5.00E+3	7.50E-6	15000	7.0E+4	0.0112	50000	9.0E+8
3.75E-6	5700	5.00E+3	9.00E-6	15300	7.0E+4	0.045	100000	1.8E+10
3.75E-6	5800	5.00E+3	9.00E-6	16000	7.0E+4	0.01	200000	7.5E+10
3.75E-6	6000	5.00E+3	1.20E-5	17200	7.5E+4	0.01	300000	8.0E+10
3.30E-6	6150	6.00E+3	9.00E-6	17900	7.0E+4	0.025	400000	5.5E+11
3.30E-6	6300	6.00E+3	9.00E-6	18400	7.0E+4	0.01	500000	1.0E+12
3.00E-6	6450	6.00E+3	7.50E-6	18900	7.0E+4	0.01	600000	1.0E+12
3.00E-6	6600	6.00E+3	7.50E-6	19400	7.0E+4	0.01	700000	9.0E+11
3.00E-6	6750	5.00E+3	7.50E-6	19800	1.6E+5	0.2	800000	2.4E+12
3.00E-6	6950	5.00E+3	7.50E-6	20000	1.6E+5	0.39	900000	4.0E+12

Table 3.8 List of Rp_n's, Er_n's and w_n's for GODIVA

Rp_n's	Er_n's	w_n's
1.52E+12	1.00E+06	1.00E+20
1.00E+10	2.00E+06	6.00E+16
3.80E+10	3.00E+06	8.00E+16
3.00E+09	4.00E+06	1.00E+16
5.10E+10	5.15E+06	8.00E+16
6.00E+10	7.00E+06	6.10E+16
1.50E+10	8.40E+06	1.50E+16
9.00E+09	9.40E+06	1.50E+16
1.20E+09	9.70E+06	3.00E+15

References

Casella, G., & Berger, R. L. (2002). *Statistical Inference 2nd Edition.* Pacific Grove, CA, USA: Wadsworth Group Duxbury.

Chapra, S. C., & Canale, R. P. (2002). *Numerical Methods for Engineers with Software and Programming Applications fourth Edition.* New York: McGraw Hill.

Cho, N. Z. (February 2008). Fundamentals and Recent Developments of Reactor Physics Methods. *Nuclear Engineering and Technology* , 25-78.

Crawford, D. S., & Ring, T. A. (submitted 2012). Verification of Analytic Energy Moments for the One-Dimensional Energy Dependent Neutron Diffusion Equation with MCNP5 and Attila-7.1.0. *Annals of Nuclear Energy* , unknown.

Duderstadt, J. J., & Hamilton, L. J. (1976). *Nuclear Reactor Analysis.* United States: John Wiley & Sons, Inc.

Foster, A. R., & Wright, R. L. (1977). *Basic Nuclear Engineering 3rd Edition.* Boston: Allyn and Bacon.

Glasstone, S., & Sesonke, A. (1967). *Nuclear Reactor Engineering.* New York: D. Van Nostrand Company.

INL NEA/NSC DOC(95)03. (September 2010). *International Handbook of Evaluated Criticality Safety Benchmarks.* INL: NEA/NSC.

Institute, K. A. (2000, October 1). *Table of Nuclides*. Retrieved July 5, 2011, from Table of Nuclides: http://atom.kaeri.re.kr/

Kenny, J. F. (1947). *Mathematics of Statistics 2nd Edition.* New York: D. Van Nostrand Company Inc.

Lab, L. A. (2008). *A General Monte Carlo N-Particle Transport Code-Version 5.* Los Alamos: Los Alamos National Lab LA-UR-08-8617.

Lab, L. A. (2000, July 5). *ENDF/B-VII Incident-Neutron Data*. Retrieved July 5, 2011, from ENDF/B-VII Incident-Neutron Data: http://t2.lanl.gov/data/neutron7.html

Lamarsh, J. R. (1966). *Introduction to Nuclear Reactor Theory.* Reading, Massachusetts, USA: Addison-Wesley Publishing Company.

Lamarsh, J. R., & Baratta, A. J. (2001). *Introduction to Nuclear Engineering Third Edition.* Upper Saddle River, New Jersey USA: Prentice Hall.

Lewis, E., & Miller, W. J. (1993). *Computational Methods of Neutron Transport.* La Grange Park, IL USA: American Nuclear Society.

Lockheed Martin/ Knolls Atomic Power Laboratory. (2002). *Chart of the Nuclides and Isotopes 16th Edition.* New York: Lockheed Martin/ Knolls Atomic Power Laboratory.

McElroy, W., Armani, R., & Tochilin, E. (1969). *Fast-Resctor Neutron Spectra and Foil-Activation Cross Section.* Richland, WA: Pacific Northwest National Laboratory.

Morry, S., & Williams, M. (1972). Neutron Flux Perturbations Due to Absorbing Foils. *Journal of Applied Physics* , 6-18.

Sevast'yanov, V., Koshelev, A., & Maslov, G. N. (2000). Representation of the Fission Spectrum of 235U, 239Pu and 252Cf and the Reactor Spectrum as a Superpostition of Five Inelastic Scattering Functions. *Atomic Energy* , 292-299.

Weinberg, A. M., & Wigner, E. P. (1958). *The Physical Theory of Neutron Chain Reactors.* Chicago: The University of Chicago Press.

CHAPTER 4

VERIFICATION AND VALIDATION OF THE MAXIMUM ENTROPY METHOD FOR RECONSTRUCTING NEUTRON FLUX, WITH MCNP5, ATTILA-7.1.0 AND THE GODIVA EXPERIMENT

Introduction

The method of moments is a very useful approach in the solution of transport equations for density distributions (Marchisio, Pikturna, & Fox, May 2003). This procedure however dampens much of the information contained in the continuous distribution. The resulting moments are useful for inferring integral information about a distribution such as the mean number of particles and their mean size, in the case of neutron flux the average number of neutrons and their average energy. For neutron flux it is desirable to calculate the continuous distribution itself (the neutron flux spectrum), which provides useful information for finding collision densities across the entire energy range, 0 to 10MeV (Duderstadt & Hamilton, 1976) for most nuclear reactors.

The maximum entropy method provides an elegant means of reconstructing a density distribution given a finite number of moments. Neutron energy moments have been verified for a 100% ^{235}U critical assembly (Crawford & Ring, submitted 2012) and validated with the GODIVA experiment (Crawford & Ring, submitted 2012); both can be

found in literature. In general, there are infinitely many continuous distributions whose moments match the known moments. This is commonly known as the moment's problem (Bandyopadhyay, Bhattacharya, Biswas, & Drabold, may 2005). The precise statement of this problem is as follows: given a finite number of moments, is it possible to find a unique distribution that gives rise to these moments? Additional constraints are then required to guide the process of finding a continuous distribution that fits the known moments. The maximum entropy method is one such constraint.

Overview of the Maximum Entropy Method for Reconstruction of Density Distributions

The maximum entropy method is based on the concept that the distribution that maximizes the information entropy is the statistically most likely to occur. In the context of information theory, the information entropy S, of a distribution p(x), is given by the integral in equation 4.1, where Ω is the support of the distribution.

$$S = -\int_{\Omega} p(x)\, ln\, p(x) dx \qquad \text{Equation 4.1}$$

The problem becomes a search to find a p(x) that maximizes the information entropy S subject to the known moments (equation 4.2), where the number of known moments is (N + 1).

$$\mu_k = \int_{\Omega} x^k p(x) dx\,, k = 0,1,2 \ldots N \qquad \text{Equation 4.2}$$

This is accomplished by multiplying the definition of the entropy functional (equation 4.3) with Lagrangian multipliers, λ_k and finding the maximum of this function.

$$H \equiv S + \sum \lambda_k \left(\int_{\Omega} x^k p(x) dx\right) = -\int_{\Omega} p(x)\, ln\, p(x) dx + \sum \lambda_k \left(\int_{\Omega} x^k p(x) dx - \mu_k\right)$$

Equation 4.3

The maximum of equation 4.3 is when the derivatives (equation 4.4 and 4.5) are zero.

$$\frac{\partial H}{\partial \lambda_k} = 0 \qquad \text{Equation 4.4}$$

$$\frac{\partial H}{\partial p(x)} = 0 \qquad \text{Equation 4.5}$$

The derivative of equation 4.4 gives the moment constraint back, equation 4.2. The results of the derivative of equation 4.5 are equation 4.6.

$$\frac{\partial H}{\partial p(x)} = -\int_{\Omega} (\ln p(x) + 1)dx + \sum_{k=0}^{N} \lambda_k \int_{\Omega} x^k dx = 0 \qquad \text{Equation 4.6}$$

The integrals in equation 6 must be valid on an arbitrary domain Ω, so the integrand must be zero. The result is equation 4.7.

$$-\ln p(x) - 1 + \sum_{k=0}^{N} \lambda_k x^k = 0 \qquad \text{Equation 4.7}$$

Equation 8 gives the general solution.

$$p(x) = \exp(-1 + \sum_{k=0}^{N} \lambda_k x^k) \qquad \text{Equation 4.8}$$

The maximum entropy solution is found by solving for the Lagrangian multipliers λ_k with a system of nonlinear equations based on finding λ_k such that $(\tilde{\mu}_k - \mu_k)$is below a certain specified precision. The moments based on the reconstructed distribution are $\tilde{\mu}_k$.

$$\tilde{\mu}_k = \int_{\Omega} x^k \exp(-1 + \sum_{k=0}^{N} \lambda_k x^k)\, dx\,, k = 0,1,2 \ldots N \qquad \text{Equation 4.9}$$

The moments based on the distribution (μ_k) are known via the method of moments. Gauss quadrature coupled with Newton's method can be used to solve this system of nonlinear equations for $(\tilde{\mu}_k - \mu_k) < tolerance\ value$.

The maximum entropy method is applied to the reconstruction of neutron flux spectrum within a 100% enriched ^{235}U critical assembly and to the GODIVA experiment. Neutron moments are obtained from the method of neutron energy moments. Neutron energy moments have been verified (Crawford & Ring, submitted 2012) and validated

(Crawford & Ring, submitted 2012) for the cases in this paper, GODIVA and the critical assembly. The maximum entropy reconstruction method is verified for neutron flux with the spherical 100% ^{235}U critical assembly modeled in Monte Carlo N Particle 5 version 1.40 (MCNP5) and Attila-7.1.0-beta version (Attila) and validated with neutron flux calculated from foil activation measurements (McElroy, Armani, & Tochilin, 1969) from the GODIVA experiment (INL NEA/NSC DOC(95)03, September 2010).

Application of the Maximum Entropy Method to Reconstruct Neutron Flux Spectrum

Equations 4.1 to 4.9 can be quickly rewritten in the terms of energy dependent neutron moments following the same mathematical approach. Energy dependent neutron flux $\phi(\vec{r}, E)$ is taken to be the density distribution sought after i.e. $p(x)$ is replaced with $\phi(\vec{r}, E)$ as the distribution to solve for at a specific distance $\vec{r}$. The moments are known functions of $\vec{r}$ so for any given $\vec{r}$ the flux spectrum can be determined, (Crawford & Ring, Verification of Analytic Energy Moments for the One-Dimensional Energy Dependent Neutron Diffusion Equation with MCNP5 and Attila-7.1.0, submitted 2012).

$$S = -\int_{\Omega} \phi(\vec{r}, E)\, ln\, \phi(\vec{r}, E) dE \qquad \text{Equation 4.10}$$

The moments, μ_k are replaced with m_k, which can be found by the method of neutron energy moments previously mentioned.

$$m_k = \int_{\Omega} E^k \phi(\vec{r}, E) dE\,, k = 0,1,2 \ldots N \qquad \text{Equation 4.11}$$

$$H = -\int_{\Omega} \phi(\vec{r}, E) \ln \phi(\vec{r}, E)\, dE + \sum \lambda_k \left(\int_0^{\infty} E^k \phi(\vec{r}, E) dE - m_k \right) \qquad \text{Equation 4.12}$$

$$\frac{\partial H}{\partial \lambda_k} = 0 \qquad \text{Equation 4.13}$$

$$\frac{\partial H}{\partial \phi(\vec{r},E)} = 0 \qquad \text{Equation 4.14}$$

$$\frac{\partial H}{\partial \phi(\vec{r},E)} = -\int_{\Omega} (\ln \phi(\vec{r},E) + 1)dE + \sum_{k=0}^{N} \lambda_k \int_{\Omega} E^k dE = 0 \qquad \text{Equation 4.15}$$

$$-\ln \phi(\vec{r},E) - 1 + \sum \lambda_k E^k = 0 \qquad \text{Equation 4.16}$$

Equation 4.17 gives the general solution.

$$\phi(\vec{r},E) = \exp(-1 + \sum_{k=0}^{N} \lambda_k E^k) \qquad \text{Equation 4.17}$$

The same method can be used to solve $(\widetilde{m}_k - m_k)$for the Lagrangian multipliers. The reconstructed moments, $\widetilde{m}_k$ are the moments based on reconstructed flux from the maximum entropy method.

$$\widetilde{m}_k = \int_{\Omega} E^k \exp(-1 + \sum_{k=0}^{N} \lambda_k E^k)\, dE\,, k = 0,1,2 \ldots N \qquad \text{Equation 4.18}$$

Gauss Quadrature was used for integrating the moments in conjunction with Newton's Method to solve for the Lagrangian multipliers. The tolerance for the Newton solver is 1E-6 and it is extremely sensitive to the initial guesses. The initial guesses ranged from -1.5 to 0 for λ_0; -1 to 0 for λ_1; -1 to 0 for λ_3, λ_4 and λ_5.

Results and Discussion

The reconstructed neutron flux is compared to the MCNP5 and Attila neutron flux spectrum at the different radial positions within the spherical critical assembly for the 100% ^{235}U sphere. The different radial positions within the spherical critical assembly are: 1cm, 2cm, 3cm… 8cm and 8.35cm.The energy range for the spectrum plots is 0 to 10MeV. The MCNP5 spectrum has 1000 data points, based on the energy bins used in conjunction with an f2 tally. MCNP5 (Los Alamos National Lab, April 24, 2003) has

become the gold standard for comparison so the relative errors were based on the MCNP5 continuous flux spectrum.

Error bars are not explicitly shown on every data point in Figures 4.1 and 4.2 to keep the figures clean and readable. The relative error listed in the titles of Figure 4.1 and 4.2 is the error comparison of the maximum entropy method with MCNP5 computation. Only figures at 1cm and at the sphere edge (8.35cm) were plotted. Figures at the other radii within the spherical critical assembly look extremely similar to Figures 4.1 and 4.2, and were omitted. The neutron moments did not change significantly enough from the center to the outer edge to change the flux spectrum shape, only the relative error.

The overall results shown by figures 4.1-4.2 show the maximum entropy method produces a general 1/E shape which is consistent with the 1/E theoretical spectrum that is expected from a fast critical assembly or reactor (Duderstadt & Hamilton, 1976).

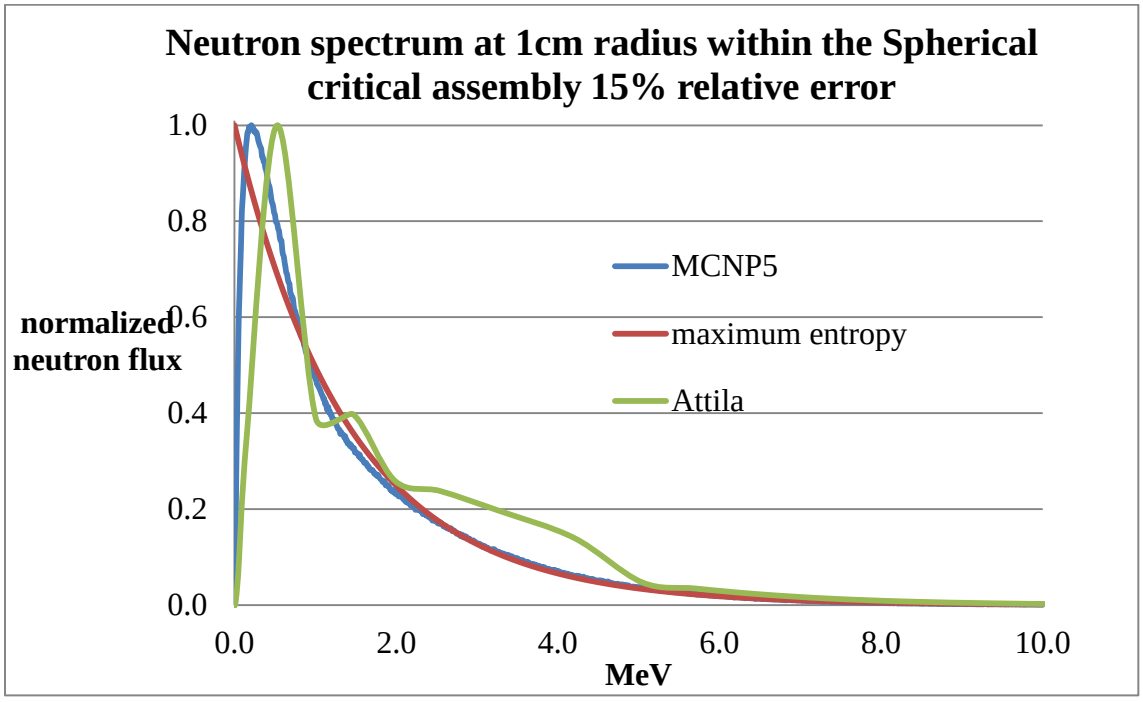

Figure 4.1 Comparison plot of the three computational methods flux spectrum at 1cm radius within the spherical critical assembly

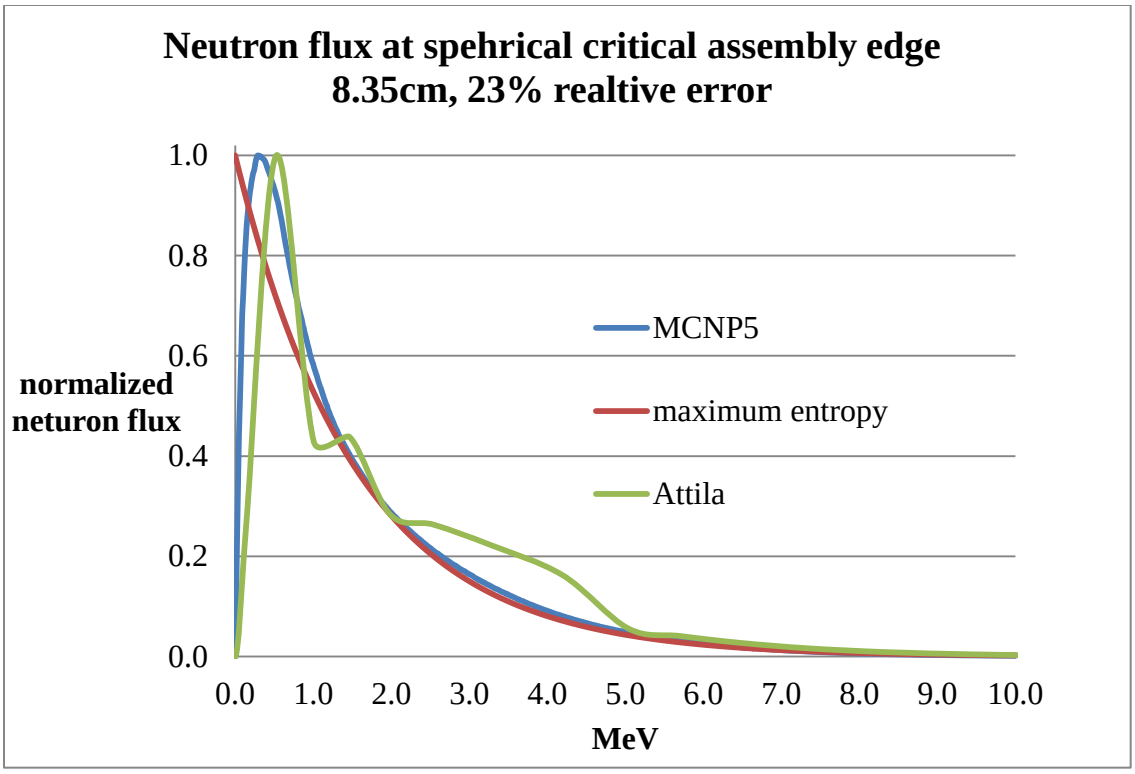

Figure 4.2 plot of the neutron spectrum for the three computation methods at the edge of the spherical critical assembly

Table 4.1 shows the relative error of the maximum entropy method with MCNP5 at each radius from the center of the spherical critical assembly. The % relative error in the maximum entropy reconstruction method is likely from the higher order neutron energy moments, specifically 4 and 5 which are 10% and 14% off of the MCNP5 moments (Crawford & Ring, submitted 2012). The higher relative error towards the critical assembly edge is because neutron diffusion theory starts to break down at 3 mean free paths near a system boundary (Lamarsh J. R., 1966). The neutron diffusion theory limitation was observed in the comparison of the neutron energy moments as well. The system edge for both the 100% ^{235}U sphere and the GODIVA is where the error is greatest. The error is within a reasonable range for practical engineering purposes and could be implemented in a multiphysics calculation involving other transport phenomena.

Table 4.1 Relative Error of the Maximum Entropy Method with Respect to MCNP5

Radius from center within spherical critical assembly	% relative error with respect to MCNP5
1cm	15%
2cm	15%
3cm	15%
4cm	15%
5cm	16%
6cm	18%
7cm	20%
8cm	21%
8.35cm	23%

The flux spectrum at the center of the GODIVA experiment was determined with foil activation measurements (McElroy, Armani, & Tochilin, 1969). The data for the GODIVA spectrum can be found in the McElroy reference in the reference section in this paper. Figure 4.3 compares the neutron flux spectrum from the three computational methods with the flux spectrum from the GODIVA experiment. Figure 4.3 shows the maximum entropy spectrum is in good agreement with the GODIVA spectrum, the relative error range is 0% to 10% from reported values, (see McElroy, Armani, & Tochilin reference). MCNP5 flux spectrum relative error range is 0% to 20% from GODIVA data and the Attila relative error range is 0% to 35% from GODIVA. The GODIVA spectrum has a very strong 1/E shape. In the energy range from 0 to roughly 1eV the maximum entropy flux spectrum is within a 5% of the GODIVA spectrum while the other two methods are in the 10% to 30% range.

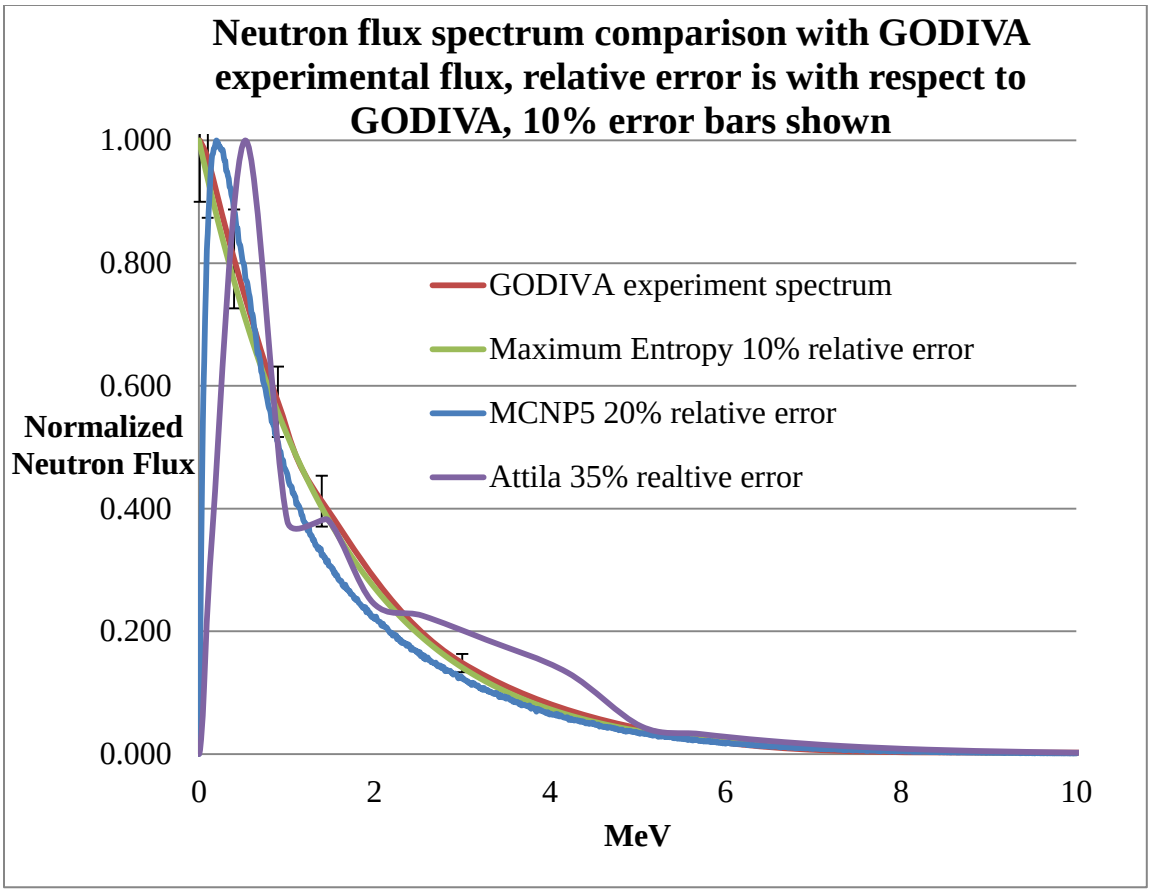

Figure 4.3 Comparison plot of the three computational methods with the neutron spectrum from GODIVA

The major difference between maximum entropy flux spectrum and the other two methods as well as GODIVA is the lack of a turnover point i.e. there is not a maximum peak in the curve. The maximum point in the maximum entropy flux spectrum is at $E=1x10^{-10}$MeV. A measurement of neutron flux near $1x10^{-10}$MeV was not made for GODIVA so there is not a real comparison at this energy. The neutron flux at a very narrow energy region i.e. 0 to $1x10^{-10}$ is not easily calculated in MCNP5 either. A calculation was attempted in MCNP5 for an energy bin of $1x10^{-16}$ to $1x10^{-10}$ and the relative error for this was 58%, and a value of 0, which means that the value is not meaningful (Los Alamos National Lab, April 24, 2003, p. 1.7). Thermal neutrons will

come to some equilibrium at some temperature (Weinberg & Wigner, 1958) and populate the thermal region of the neutron spectrum at this temperature not 0, which is what MCNP5 and Attila predict. More work needs to be done to include this into the maximum entropy reconstruction method, but the general 1/E shape is promising and does capture the neutron physics of the fast spherical 100% ^{235}U critical assembly and the GODIVA experiment. Even though the peak of the maximum entropy flux is not around 0.4MeV the value is still within 20% of the MCNP5 flux spectrum at that point.

Conclusion

Overall the maximum entropy method applied to reconstruct a neutron flux spectrum from known neutron energy moments compares well to standard computational methods and the GODIVA experiment. The neutron flux spectrum calculated from the maximum entropy method has a relative error range of 0% to 10% with respect to GODIVA and a relative error range with respect to MCNP5 of 15% to 23%. The maximum entropy method as a way to reconstruct neutron flux spectrums shows great promise. The maximum entropy method is a computationally fast reliable method to calculate a full energy neutron flux spectrum.

References

Bandyopadhyay, K., Bhattacharya, A., Biswas, P., & Drabold, D. (may 2005). Maximum Entropy and the Problem of MOments: A Stable Algorithm. *Physical Review*, 57-71.

Bin-Wan, C., & Ring, T. A. (October 2006). Verification of SMOM and QMOM Population Balance Modeling in CFD code Using Analytical Solutions for Batch Particulate Processes. *China Particuology*, 243-249.

Casella, G., & Berger, R. L. (2002). *Statistical Inference 2nd Edition.* Pacific Grove, CA, USA: Wadsworth Group Duxbury.

Crawford, D. S., & Ring, T. A. (submitted 2012). Validation of Energy Moments from the One-Dimensional Energy Dependent Neutron Diffusion Equation, MCNP5 and Attila-7.1.0 with the GODIVA Experiment. *Annals of Nuclear Energy,* unknown.

Crawford, D. S., & Ring, T. A. (submitted 2012). Verification of Analytic Energy Moments for the One-Dimensional Energy Dependent Neutron Diffusion Equation with MCNP5 and Attila-7.1.0. *Annals of Nuclear Energy,* unknown.

Duderstadt, J. J., & Hamilton, L. J. (1976). *Nuclear Reactor Analysis.* United States: John Wiley & Sons, Inc.

INL NEA/NSC DOC(95)03. (September 2010). *International Handbook of Evaluated Criticality Safety Benchmarks.* INL: NEA/NSC.

Kenny, J. F. (1947). *Mathematics of Statistics 2nd Edition.* New York: D. Van Nostrand Company Inc.

Los Alamos National Lab. (April 24, 2003). *MCNP-A General Monte Carlo N-Particle Transport Code, Version 5.* Los Alamos: Los Alamos National Laboratory.

Marchisio, D. L., Pikturna, J. T., & Fox, R. O. (May 2003). Quadrature Method of Moments for Population-Balance Equations. *AIChE,* 1267-1276.

Marchisio, D., Virgil, D. R., & O., F. R. (August 2003). Implementation of the Quadrature Method of Moments in CFD codes for Aggregation-Breakage Problems. *Chemcial Engineering Science,* 3337-3351.

McElroy, W., Armani, R., & Tochilin, E. (1969). *Fast-Resctor Neutron Spectra and Foil-Activation Cross Section.* Richland, WA: Pacific Northwest National Laboratory.

McGraw, R. (1997). Description of Aerosol Dynamics by the Quadrature Method of Moments. *Aerosol Science and Technology,* 255-265.

CHAPTER 5

SUMMARY, CONCLUSION AND FUTURE WORK

The results of the research show the beginnings of a fast reliable new approach to solving neutron transport phenomena. Converting the EDNDE into moment form via the method of moments produced normalized energy dependent neutron moments, NEDNM. The NEDNM are used to reconstruct a continuous energy spectrum neutron flux with the maximum entropy method. The NEDNM are verified and validated for two bare spherical critical assemblies: a 100% enriched ^{235}U theoretical case and the GODIVA experiment. The NEDNM and the reconstructed neuron flux spectrum is verified and validated with MCNP5, Attila and GODIVA with great results.

The relative error of the neutron diffusion NEDNM based on MCNP5 as the standard is 0% to 14%. The relative error of neutron diffusion NEDNM based on GODIVA values as the standard is 0% to 24%. The estimated experimental error in the values from the GODIVA experiment is 5.6%. The relative error of the reconstructed neutron flux with respect to GODIVA is 0 to 10% and the reconstructed neutron flux relative error with respect to MCNP5 is 15% to 23%. The low relative error is very encouraging to continue to pursue developing the method of moments applied to neutron transport and to continue working on reconstructing neutron flux spectrum for other critical assemblies and isotope blends. The relative error with respect to GODIVA for the

reconstructed neutron flux shows the overall method is reliable and accurate. The reconstructed flux has the highest amount of error between 0 and 0.5MeV. This error is because the exponential function that satisfies the conditions of the maximum entropy method is a maximum at E = 0 instead of a value of 0. The maximum entropy method could be reformulated to maximize the log normal of the distribution to provide a better solution and a flux value of zero at E = 0. The reconstructed neutron flux captures the general expected theoretical functional shape, 1/E. Other limits of the method are due to the neutron diffusion approximation used as well as the assumed value for the average angle of scatter ($\mu=2/3*A$). The limits of neutron diffusion theory can be seen in the moment plots in Figures 2.7 through 2.11, 3.7 through 3.11, and in the higher relative error of the reconstructed neutron flux towards the sphere edges, see Table 4.1 and Figure 4.2. The diffusion approximation is where the method could be improved first to increase its accuracy by adding in a better approximation to the average angle of scatter and including more terms to the energy dependent diffusion coefficient.

The method could be extended to a reflected critical assembly that has a reflector i.e. graphite or beryllium surrounding a critical assembly. A reflected boundary and the neutron physics from a reflected boundary could be investigated instead of a bare boundary which is what this research presented. This would add a crucial next step to broaden the maximum entropy method of moments towards a full neutron spectrum heterogeneous nuclear reactor type calculation. All nuclear reactors are composed of fuel, cladding, moderator and structure materials that are exposed to a harsh neutron rich radiation environment. All nuclear reactors are extremely affected by more than neutron-isotope interactions alone.

There are many opportunities of expanding this method to capture the effect other transport phenomena (specifically momentum and heat) have on neutron transport in a nuclear reactor or the multiphysics effects on nuclear reactors. A full neutron spectrum solution allows for the inclusion of temperature effects (Doppler Broadening) across the entire resonance region in any isotope or mix of isotopes cross sections. Temperature effects on nuclear reactivity could be computed and modeled. Void coefficients could also be modeled in a multiphysics environment by solving for the neutron flux and simultaneously solving the heat and momentum equations which would provide the temperatures and velocities to determine: density changes and velocities of a fluid. Film and nucleate boiling that incorporates a full neutron spectrum could be modeled for a fuel pin which would provide insight into the moderator voids and where departure from nucleate boiling (DNB) takes place. The temperature effects from Doppler Broadening and void coefficients can be directly coupled to the reactivity changes and allow for transient calculations to be made.

Isotope changes in the fuel, moderator or cladding could be computed by adding in the nuclear reaction sets of interest. Adding in nuclear reaction sets would provide a way to calculate fuel burn-up, i.e., the fission products created in fission events which change the isotopic concentrations within a fuel matrix and the fuels performance. Possible neutron damage calculations could be made for the cladding matrix from the entire neutron spectrum with the right nuclear reaction set. Activation analysis and activation of the moderator/support structures could be performed as well for many neutron transport problems including the constantly changing isotope inventory inside of a nuclear reactor fuel pin.

A great challenge for many operating nuclear power plants is to keep an up-to-date record of the isotopes in the fuel and in the fuel inventory. Currently there are a only a few method to do this and all are multigroup methods and are not calculated in a multiphysics environment. This means that there is a great opportunity and the maximum entropy method of moment reconstruction of neutron flux could provide a way to determine an isotopic inventory.

Overall the method of moments in conjunction with maximum entropy method applied to the energy dependent neutron diffusion equation for simple bare critical assemblies is computationally fast, reliable and accurate. The method of moments and the maximum entropy method show great promise as a technique to solve neutron transport phenomena and worth further research efforts.